

A Kriging Model for Dynamics of Mechanical Systems With Revolute Joint Clearances

Zhenhua Zhang

Department of Mechanical Engineering,
Wichita State University,
Wichita, KS 67260
e-mail: zxzhang1@wichita.edu

Liang Xu

Department of Mechanical Engineering,
Wichita State University,
Wichita, KS 67260
e-mail: lxu3@wichita.edu

Paulo Flores

Departamento de Engenharia Mecânica,
Universidade do Minho,
Campus de Azurém,
Guimarães 4800-058, Portugal
e-mail: pflores@dem.uminho.pt

Hamid M. Lankarani

Department of Mechanical Engineering,
Wichita State University,
Wichita, KS 67260
e-mail: hamid.lankarani@wichita.edu

Over the past two decades, extensive work has been conducted on the dynamic effect of joint clearances in multibody mechanical systems. In contrast, little work has been devoted to optimizing the performance of these systems. In this study, the analysis of revolute joint clearance is formulated in terms of a Hertzian-based contact force model. For illustration, the classical slider-crank mechanism with a revolute clearance joint at the piston pin is presented and a simulation model is developed using the analysis/design software MSC.ADAMS. The clearance is modeled as a pin-in-a-hole surface-to-surface dry contact, with an appropriate contact force model between the joint and bearing surfaces. Different simulations are performed to demonstrate the influence of the joint clearance size and the input crank speed on the dynamic behavior of the system with the joint clearance. In the modeling and simulation of the experimental setup and in the followed parametric study with a slightly revised system, both the Hertzian normal contact force model and a Coulomb-type friction force model were utilized. The kinetic coefficient of friction was chosen as constant throughout the study. An innovative design-of-experiment (DOE)-based method for optimizing the performance of a mechanical system with the revolute joint clearance for different ranges of design parameters is then proposed. Based on the simulation model results from sample points, which are selected by a Latin hypercube sampling (LHS) method, a polynomial function Kriging meta-model is established instead of the actual simulation model. The reason for the development and use of the meta-model is to bypass computationally intensive simulations of a computer model for different design parameter values in place of a more efficient and cost-effective mathematical model. Finally, numerical results obtained from two application examples with different design parameters, including the joint clearance size, crank speed, and contact stiffness, are presented for the further analysis of the dynamics of the revolute clearance joint in a mechanical system. This allows for predicting the influence of design parameter changes, in order to minimize contact forces, accelerations, and power requirements due to the existence of joint clearance. [DOI: 10.1115/1.4026233]

Keywords: Revolute joint clearance, contact forces, multibody dynamics, Kriging meta-model, genetic algorithms

1 Introduction

In the past decade, many researchers have examined the optimal dynamical solution of different mechanical systems and mechanisms [1–3]. Additionally, different optimization methods have been implemented to obtain optimal solutions. In the study by Laribi et al. [2], a solution for the path generation problem in mechanisms was presented using the generic algorithm-fuzzy logic method. Selcuk et al. [3] proposed a neural-genetic method to investigate the effects of joints with clearance on its path generation and kinematic transmission quality. In order to reduce the computational complexity, the neural network has been used as a surrogate model in this study. The Genetic algorithm, as a global optimization method, has been widely used in many research fields, but its associated computational cost dramatically increases, especially for expensive model functions.

As a result of manufacturing tolerances, material deformations, and wear after a certain working period, clearances between mechanical components of mechanical systems occur in most kinematic joints. Excessive clearance values result in large contact forces at the joints, especially during high-speed mechanical operations. The presence of clearances leads to a decrease in the sys-

tem reliability and durability of the system's components and machines [4,5]. Over the past decades, advances, mainly due to the development of intercross applications between computer-aided analysis of mechanical systems and optimization methodologies, have been achieved. These results could be utilized for the application of different mathematical programming techniques to the parametrical and topological syntheses and analyses of mechanical systems [6]. The optimization of mechanical system modeling with clearances can be used to bypass the computationally intensive simulation of the computer dynamic model. It also helps in the analysis, design, and control of the dynamic performance of a complex mechanical system and in quantifying the influence of clearance parameters.

During the past two decades, many studies on the influence of the joint clearance in planar and spatial multibody mechanical systems have been conducted. Dubowsky and Freudenstein developed the impact ring model, which is a simple model to demonstrate the effects of joint clearance in planar mechanisms [7]. Springs and dashpots were arranged in their model to predict the dynamics response of the mechanical system. Dubowsky and Moening quantified the interaction between the clearance joints and the mechanical system elasticity using a Scotch-Yoke simulation model [8]. Large impact forces developed at the clearance joints caused a failure in the Scotch-Yoke model. Furubashi and Morita presented a four-bar mechanism with multiple clearance revolute joints [9]. They analyzed and compared the results for

Contributed by the Design Engineering Division of ASME for publication in the JOURNAL OF COMPUTATIONAL AND NONLINEAR DYNAMICS. Manuscript received August 1, 2013; final manuscript received December 10, 2013; published online February 13, 2014. Assoc. Editor: Ahmet S. Yigit.

different numbers and various combinations of clearance joints and demonstrated the effect of clearances on the performance of the four-bar mechanism system.

Lankarani and Nikravesh extended the Hertz contact law to include a hysteresis damping function and represent the dissipated energy during impact [10]. A nonlinear continuous force acted on the model and the local indentation and relative penetration velocity was related to the contact force. Flores and his coworkers developed a precise model for the dynamic analysis of a mechanical system with dry and lubricated revolute joints [11–13]. The influences of the selected parameters on the dynamic response of mechanical systems with multiple clearance joints, including the clearance size, input crank speed, and number of joints modeled as clearance joints, were quantified in this study.

Mahrus designed a set of experimental investigations to show the performance of the journal bearing and the effect of the load diagram on hydrodynamic lubrication [14]. Different loads were applied to the test journal-bearing joint and both steady and varying unidirectional and full two-component dynamic loading were considered in the study. Wilson and Fawcett modeled a slider-crank mechanism with a clearance in the sliding bearing to measure the transverse motion of the slider [15]. They tested a number of parameters such as the geometry, speed, and mass distribution of the mechanical system, which influence the transverse motion and they derived the equation of motion with these parameters based on the results. Haines derived the equations of motion for a multibody mechanical system that describes the contributions at a revolute clearance joint with no lubrication present [16]. The study also included an experimental investigation on the dynamic response of revolute clearance joints. Under static loading, the deflection associated with contact elasticity in the dry journal-bearing joint was found to be much greater and linear than predicted [17]. Bengisu et al. developed a four-bar mechanism based on zero-clearance analysis to compare the theoretical results with the experimental results [18]. A model with multiple joints was used in clearances to study contact energy loss in the mechanical system.

Feng et al. developed a method for optimizing the mass distribution of planar linkage with clearance joints to control the change of inertia forces [19]. Tsai and Lai investigated the kinematic sensitivity of the transmission performance of linkages with joint clearances [20]. In their study, loop-closure equations were used in the position analysis of a four-bar mechanism in which all joints have clearances. Yildirim et al. predicted the transmission angle of a slider-crank mechanism with an eccentric connector based on neural networks [21]. The neural network structure was a feed-forward network and the best approximation was obtained with five types of algorithms. Erkaya and Uzmay studied the effects of joint clearances on the performance of a mechanism in terms of path generation and transmission angle, using neural networks and genetic algorithms (GAs), respectively [3,21].

A computer-aided analysis of multibody mechanical systems is utilized in this study as a simulation model. The goal of this study is to use the Kriging mathematical model as a design-of-experiments optimization tool, in order to demonstrate the influence of the design variables on the dynamic performance of mechanical systems with revolute clearance joints. The reason the Kriging model was used in this research is that the computer simulation for a given set of design parameters is usually quite computationally intensive and each simulation for a given set of design variables could take extensive computation time. Because there are wide ranges of values in the design variables such as the clearance sizes, ratios of length, material properties, contact stiffnesses, and speeds of operation, studying the effects of each of these variables would take enormous computational time and effort.

In the present study, the mathematical formulation of the revolute clearance joint is fully described and the relationship between the design parameters and contact forces in joints is examined. First, the classical slider-crank mechanical system is modeled and simulated in MSC.ADAMS and the performance of the system with different sets of parameters is examined. Next, the theoretical basis of the methods are stated, illustrating the framework for the DOE methods of the Latin hypercube sampling, Kriging metamodel, and genetic algorithm. Next, two simple examples are presented using these previous methods to further expand the analysis of the dynamic behavior of the mechanism with the revolute clearance joint at different ranges of the design parameters.

2 Modeling Revolute Joints With Clearance

A revolute joint with clearance, as shown in Fig. 1, can be described as a movable journal assembled inside a bearing, with the journal's and bearing's radii of R_J and R_B , respectively. In reality, there is a clearance between the journal and the bearing in mechanical systems in order to cause a relative motion between the two. The journal can move inside the bearing and this will add some degrees of freedom to the system. The difference between the radius of the bearing and the radius of the journal is the radial clearance size c . The penetration between the bearing and journal appears when they are in contact.

The indentation depth due to the contact impact between the journal and the bearing can be defined as

$$\delta = e - c \quad (1)$$

where e is the magnitude of the eccentricity and c is the radial clearance. The eccentricity is evaluated as

$$e = \sqrt{\Delta X^2 + \Delta Y^2} \quad (2)$$

where ΔX and ΔY are the horizontal and vertical displacements, respectively, measured from the state when the centers of the

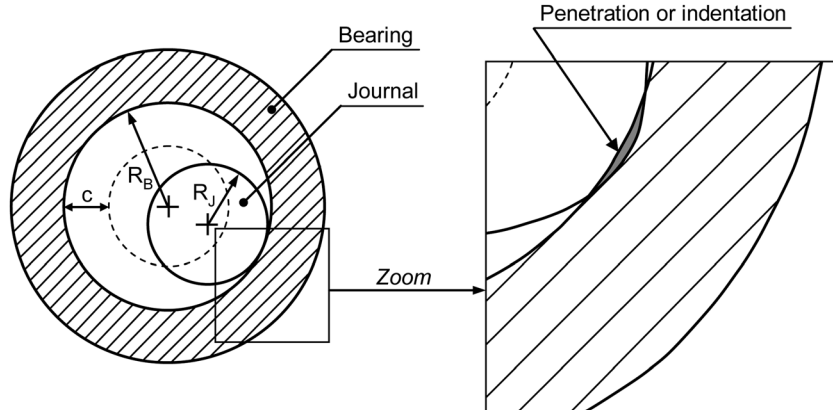


Fig. 1 Revolute joint with clearance (clearance exaggerated for clarity)

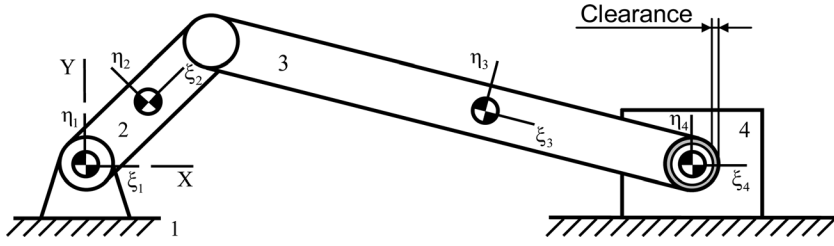


Fig. 2 Slider-crank mechanism with clearance joint

Table 1 Geometric and inertial properties of mechanism

Body number	Length (m)	Mass (kg)	Moment of inertia (kg m^2)
2	0.05	0.30	0.00010
3	0.12	0.21	0.00025
4	0.06	0.14	0.00010

journal and the bearing coincide. In turn, the radial clearance is defined as

$$c = R_B - R_J \quad (3)$$

Two situations can occur at the joint. In the first case, when the journal does not make contact with the bearing and the penetration depth is a negative value, the journal has a free-flight motion inside the bearing and, thus, there is no contact-impact force developed at the joint. In the second case, when the journal contacts with the bearing wall, a contact force between the journal and the bearing is developed in the direction of the centers of the bearing and the journal [4] and the indentation depth value will be greater than zero.

The contact-impact force F_N , in relation to the penetration indentation, can be modeled by the Hertz law as [10]

$$F_N = K\delta^n \quad (4)$$

where K is the stiffness coefficient and δ is the indentation depth given by Eq. (1). The exponent n is usually set for analysis in the range of 1.5–2.5 for most metal-to-metal contact. The stiffness coefficient K depends on the material properties and the contacting surface and is defined as

$$K = \frac{4}{3(\sigma_B + \sigma_J)} \left[\frac{R_B R_J}{R_B - R_J} \right]^{1/2} \quad (5)$$

The material parameters σ_B and σ_J are defined as

$$\sigma_k = \frac{1 - \nu_k^2}{E_k} \quad (k = B, J) \quad (6)$$

where the variables ν_k and E_k are Poisson's ratio and Young's modulus, respectively, for the journal and the bearing.

The Hertz law given by Eq. (4) does not include any energy dissipation. Lankarani and Nikravesh [10] extended the Hertz model to include a hysteresis damping function as follows:

$$F_N = K\delta^n \left[1 + \frac{3(1 - c_e^2)}{4} \frac{\dot{\delta}}{\dot{\delta}^{(-)}} \right] \quad (7)$$

where the stiffness coefficient K can be obtained from Eqs. (5) and (6), c_e is the restitution coefficient, $\dot{\delta}$ is the relative penetration velocity, and $\dot{\delta}^{(-)}$ is the initial impact velocity.

3 A Multibody System With Joint Clearance

In this section, a computer model for the classic slider-crank mechanism with one revolute clearance joint is considered in order to analyze the dynamic behavior of the mechanical system. Figure 2 shows the configuration of the slider-crank mechanism, which comprises four bodies that represent the crank, connecting rod, slider, and ground. In this case, the multibody model has only one clearance joint. There are four joints: two ideal revolute joints between the ground and the crank and the crank and the connecting rod; one ideal translational joint between the slider and ground; and one nonideal revolute joint clearance between the connecting rod and slider. The geometric and inertia properties of each body in this system are shown in Table 1 [17]. The moment of inertia is taken with respect to the center of gravity of the body.

A model of the slider-crank mechanism is constructed in MSC.ADAMS, as shown in Fig. 3. In the model, all bodies are considered to be rigid. The initial crank angle and velocity of the journal

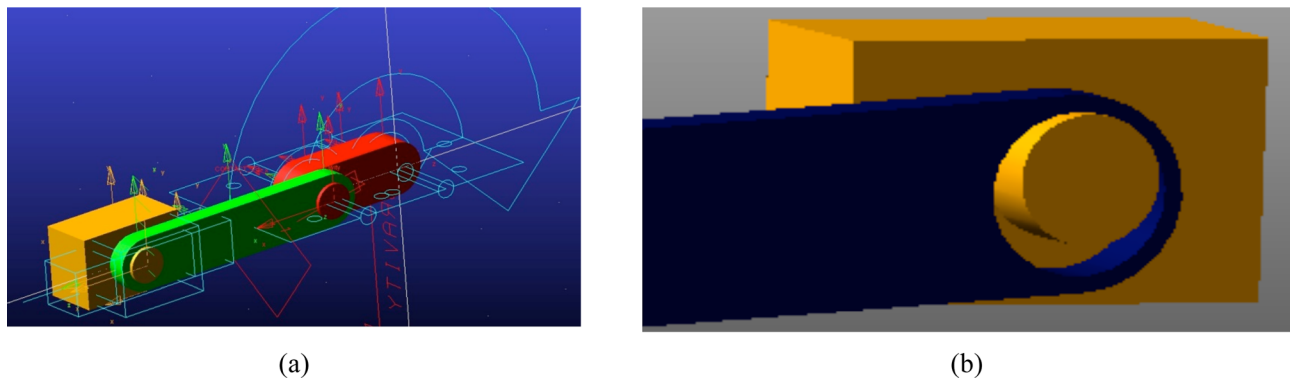


Fig. 3 (a) Model of the slider-crank mechanism developed in MSC. ADAMS, and (b) exaggerated joint clearance at the piston pin

Table 2 Parameters used in dynamic simulation of slider-crank mechanism with clearance joint

Nominal-bearing radius	10.0 mm
Journal-bearing width	40.0 mm
Restitution coefficient	0.9
Friction coefficient	0.0
Young's modulus	207 GPa
Poisson's ratio	0.3
Baumgarte α, β	5
Total simulation time	0.24 s
Total steps	50,000

center are set to zero and the journal and bearing centers are coincident. The dynamic parameters used in the simulation are listed in Table 2.

Comparing the results from this MSC.ADAMS computer simulation model (Fig. 4) with the experimental results of the slider-crank mechanism obtained by Flores et al. [22] (see Fig. 5) indicates a similar pattern between the computer model in this study and the experimental results. Hence, the slider-crank mechanism model from this study can simulate the dynamic behavior of the system with reasonable accuracy. This simulation model will be utilized here. The values for the radial clearance size and the input crank speed are used for investigating the impact of the revolution clearance joint in the slider-crank mechanical system.

As shown in Figs. 6–8, the results of the slider acceleration, contact force at the clearance, and crank reaction force demonstrate different dynamic behaviors of the slider-crank mechanism with different values of the radial clearance; namely, 0.05 mm, 0.1 mm, 0.2 mm, and 0.5 mm. The crank rotates with a 2000 rpm constant angular speed. The results indicate that when the clearance size is increased, the curves become noisier and the dynamic behavior tends to be nonperiodic. As the clearance size decreases, the dynamic behavior tends to be closer to ideal. Those plots typically reach the highest value when the crank angle is at multiples of 180 deg rotation, which is when the slider is in the critical position. These observations can also be confirmed in the plots of the joint reaction forces shown in Figs. 7 and 8. As can be seen, when the clearance size is increased, the contact force and required crank input power are significantly increased.

Figures 9–11 show the influence of the crank angular speed. The values chosen for the crank speed are 200 rpm, 1000 rpm, 2000 rpm, and 5000 rpm. In this set, the clearance size is set to 0.1 mm. The different behaviors of the slider acceleration and the joint reaction force are displayed in these plots. The decrease in crank speed results in the curves having more noise and higher peak values for the slider acceleration.

4 Kriging Model-Based Optimization

This section presents a procedure for constructing an objective function using the Kriging model. In the first part, the Latin

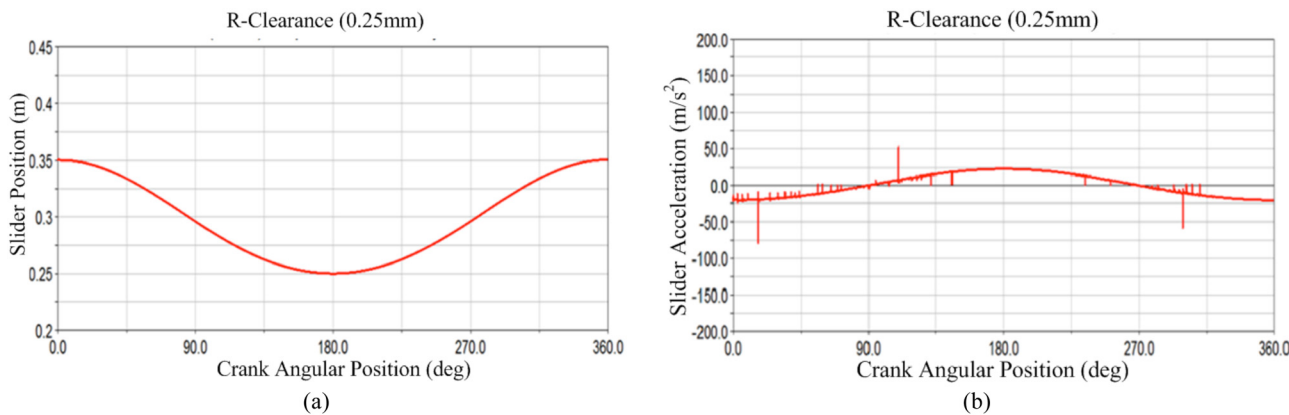


Fig. 4 Dynamic response of the slider-crank from MCS.ADAMS modeling with a crank speed of 200 rpm: (a) slider position for a clearance of 0.25 mm, and (b) slider acceleration for a clearance of 0.25 mm

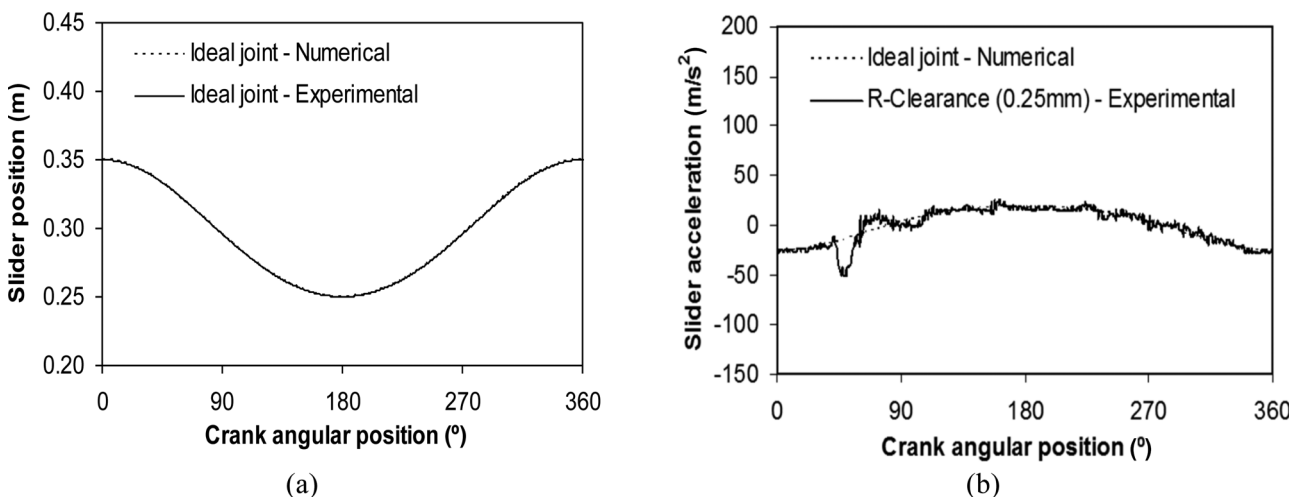


Fig. 5 Dynamic response of the experimental slider-crank from Ref. [22] with a crank speed of 200 rpm: (a) slider position for a clearance of 0.25 mm, and (b) slider acceleration for a clearance of 0.25 mm

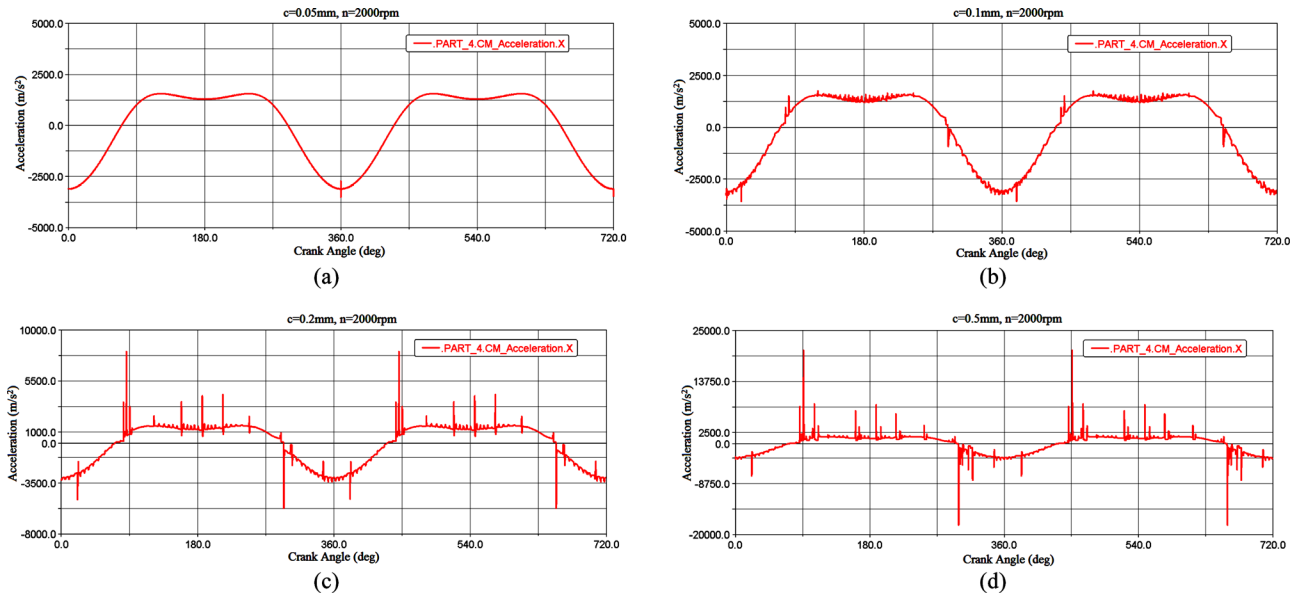


Fig. 6 Slider acceleration for different clearance sizes: (a) 0.05 mm, (b) 0.1 mm, (c) 0.2 mm, and (d) 0.5 mm

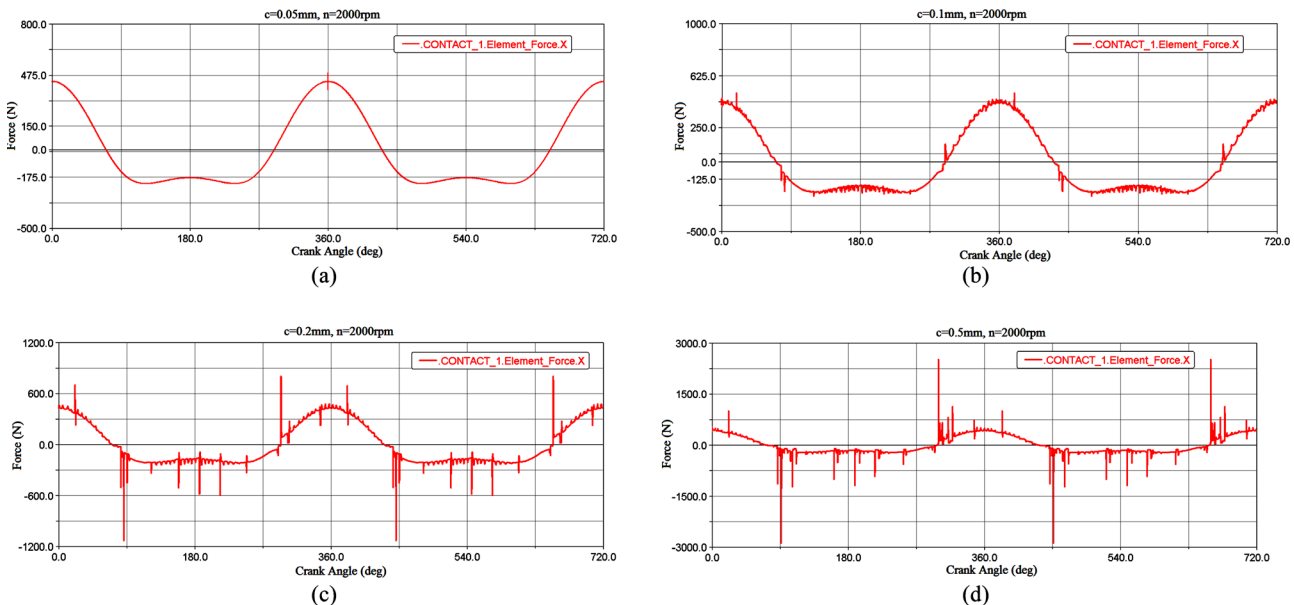


Fig. 7 Contact force for different clearance sizes: (a) 0.05 mm, (b) 0.1 mm, (c) 0.2 mm, and (d) 0.5 mm

hypercube is introduced for acquiring the initial design points. After locating several initial design points, their performance data can be obtained by the computer simulation experiment (MSC.ADAMS). Each computer simulation for a given set of design parameters requires up to 50,000 numerical integration steps for one complete crank rotation, which is quite inefficient and computationally intensive; therefore, the Kriging model is developed and utilized instead in this research to optimize the process. The objective here is to develop a prediction model to estimate the value of the objective function for any given design point in the design space using the Kriging model instead of the computer simulation experiment. For this purpose, the Kriging model can be constructed based on the initial design points and their performances. The implementation of the method is shown in Fig. 12. The Kriging model is constructed by using the results from sample points coming from individual computer simulations. A genetic algorithm is used to obtain optimal results on the design parameter.

The neural network and Kriging model are two potential techniques, among others, and both can capture the unknown nonlinearity in the system performance. Based on a study by Yuan and Bai [1], in which they compared the neural network and Kriging model, the Kriging model can usually produce meta-model optima that are superior in precision. Additionally, for a given sample size, the Kriging model tends to provide a better overall fit than the neural networks.

In this research, the objective is to utilize a nonparameter Kriging model to predict the dynamic response for any given design point within the design space. In order to construct the surrogate Kriging model, several points inside the design space must first be utilized and their corresponding responses must be obtained at these points first, using the computer simulations (here, ADAMS). The constructed Kriging model can then be used as a surrogate model instead of the computer simulation model, in order to predict the response at any other design point within the design space. In addition to the use of the Kriging model for the prediction of

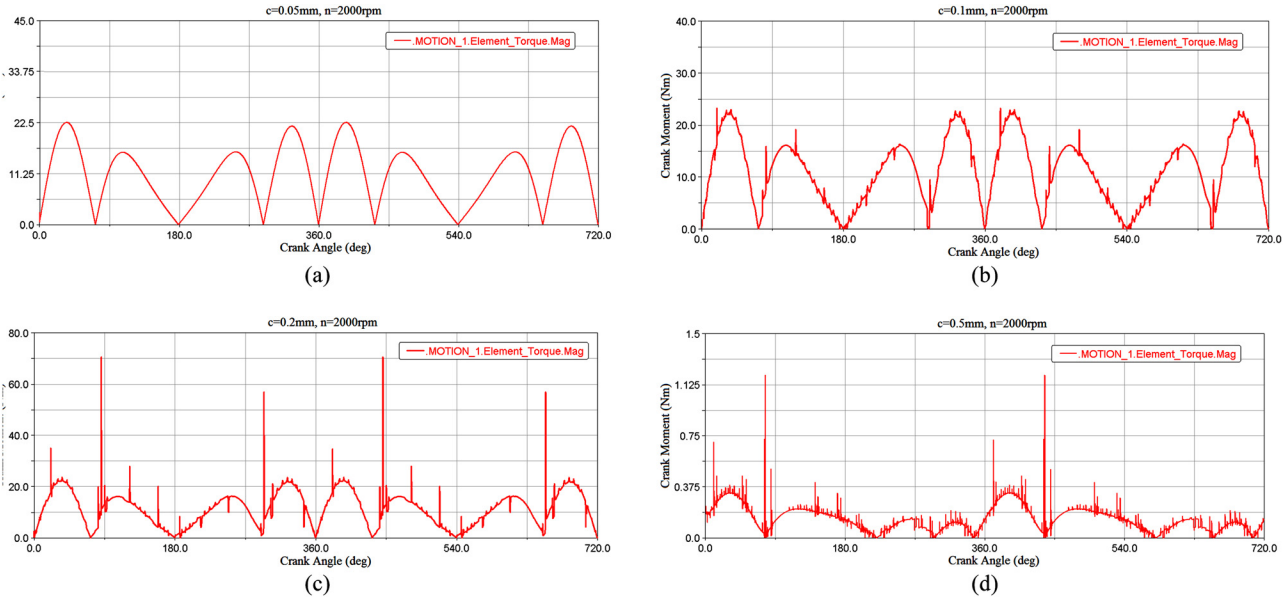


Fig. 8 Crank moment for different clearance sizes: (a) 0.05 mm, (b) 0.1 mm, (c) 0.2 mm, and (d) 0.5 mm

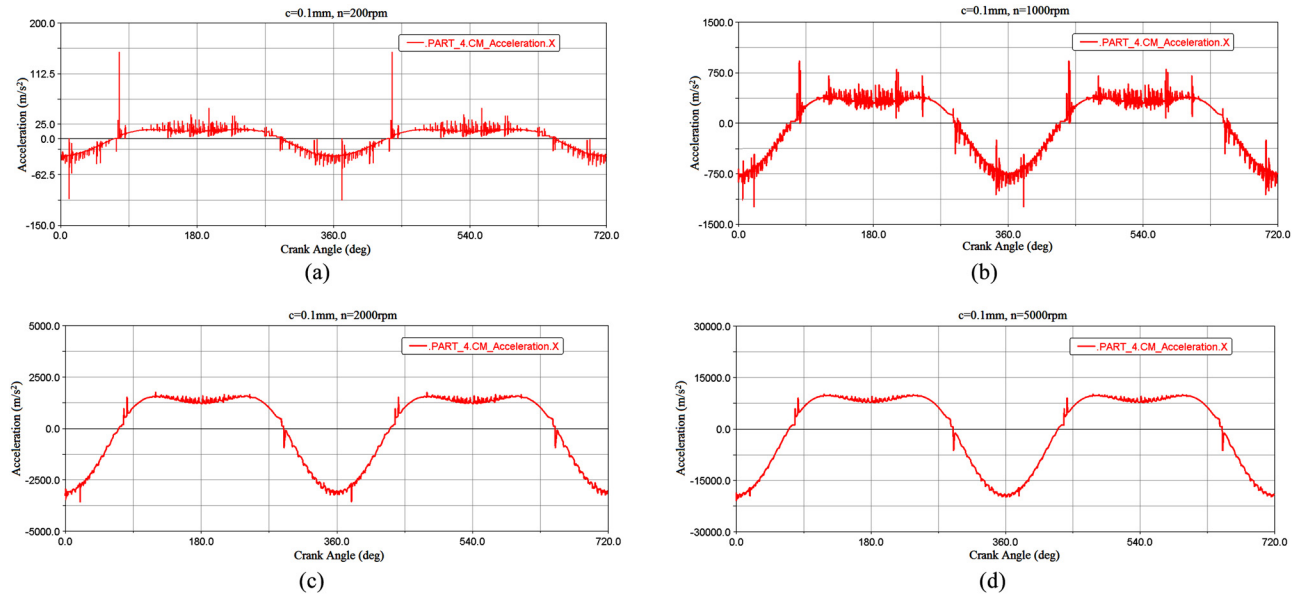


Fig. 9 Slider acceleration for different crank speeds: (a) 200 rpm, (b) 1000 rpm, (c) 2000 rpm, and (d) 5000 rpm

the response at different design points, the scheme allows the visualization of the trends of the response surfaces when the design variables are changed.

4.1 Latin Hypercube Sampling. In order to acquire a set of initial samples from the ranges of the parameter variables to confine the number of simulations, the LHS is used to ensure that each value of a variable is equally important in the sample. This method not only reduces the number of simulations but also retains the proper orthogonality and proportionality of the sample. The Latin hypercube is a statistical method for placing M sample points, which are divided into equally probable intervals in every variable, when a function has N variables. In addition, the M sample points must be satisfied by the Latin hypercube requirement that each sample is the only one in each axis-aligned hyper-plane containing it [23].

4.2 Kriging Model. The Kriging model is a nonparametric interpolation model for integrating the given sample points to

approximate the model parameters and forecasting the unknown response of a new design point [24–26]. Considering a performance function with k random inputs, a Kriging model can be constructed with n samples, which is (x_i, y_i) , where $x_i = (x_i^1 \dots x_i^n)$, $i = 1, \dots, n$ are simple inputs and y_i is the system performance when the system is given the inputs x_i . The term x_i^n represents the n th design point for input x_i .

In the Kriging model, system performances are generated from the following:

$$Y(x) = f(x) + G(x) \quad (8)$$

where $Y(x)$ is the unknown function, $f(x)$ is a polynomial function of x , and $G(x)$ is the realization of a Gaussian stochastic process with zero mean and variance σ^2 . The polynomial term $f(x)$ is simplified by a constant value μ . Hence, the Kriging model can be rewritten as

$$Y(x) = \mu + G(x) \quad (9)$$

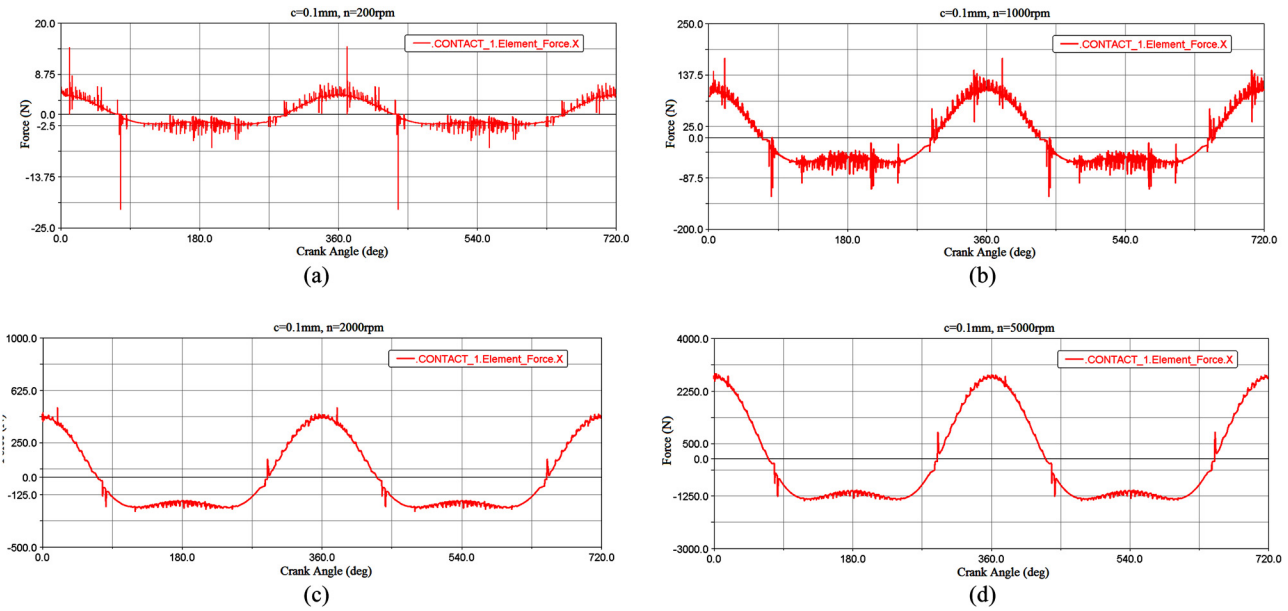


Fig. 10 Contact force for different crank speeds: (a) 200 rpm, (b) 1000 rpm, (c) 2000 rpm, and (d) 5000 rpm

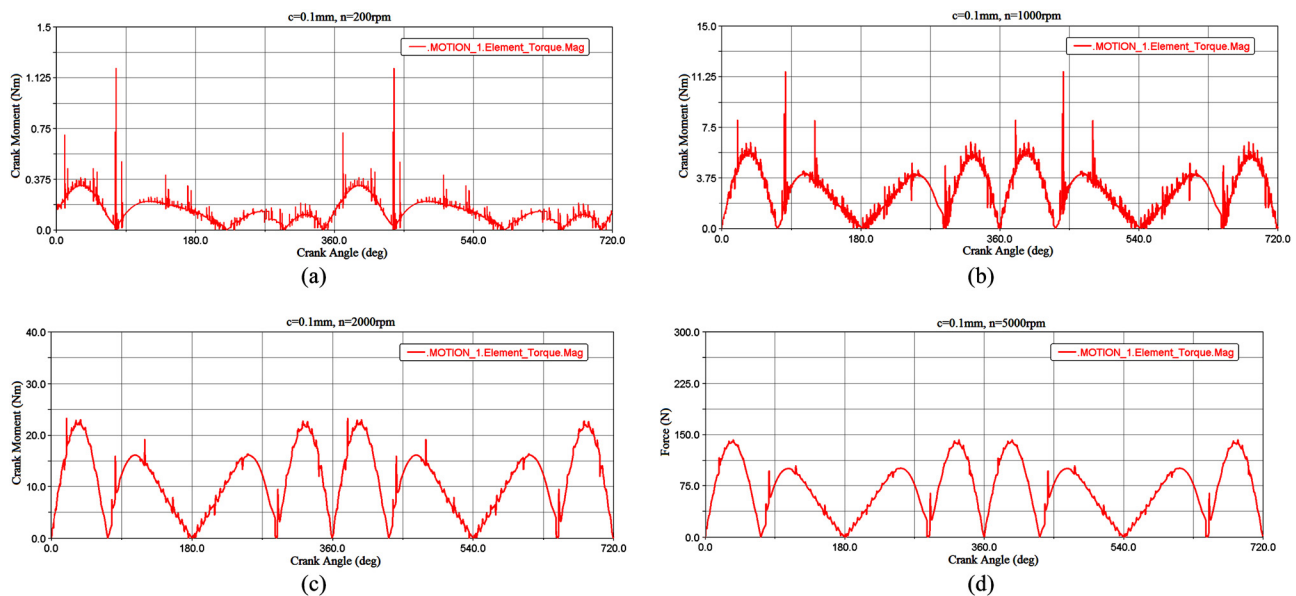


Fig. 11 Crank moment for different crank speeds: (a) 200 rpm, (b) 1000 rpm, (c) 2000 rpm, and (d) 5000 rpm

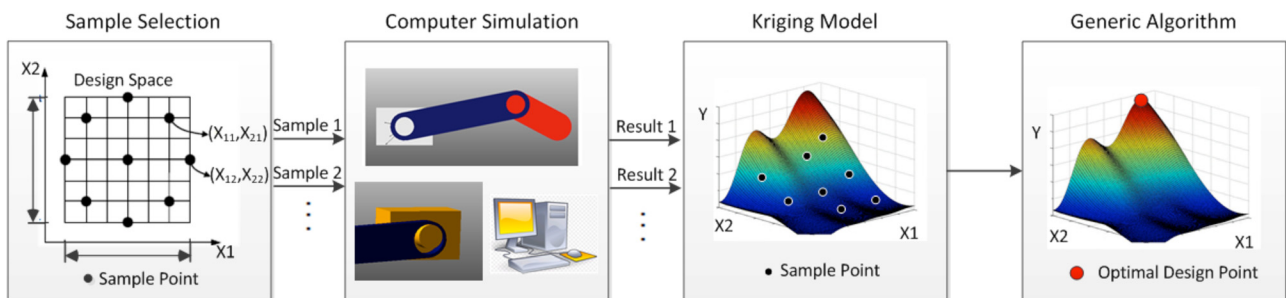


Fig. 12 Flow chart for implementation of the DOE and Kriging-based optimization model

The entry correlation matrix for $G(x)$ is given by [16]

$$\text{Corr}[G(x_i, x_j)] = \sigma^2 R(x_i, x_j) \quad (10)$$

where $R(x_i, x_j)$ represents the (i, j) entry of an $n \times n$ matrix and this correlation matrix is defined by the distance between two sample points x_i, x_j with ones along the diagonal, which can be expressed as

$$R(x_i, x_j) = \exp \left[-\sum_{p=1}^k \theta_p |x_i^p - x_j^p|^{\alpha_p} \right] \quad (11)$$

The term inside the exponential is the distance between the two designed sample points (x_i, x_j) , and θ_p and α_p are two parameters that must be determined in order to make a proper prediction using the Kriging model. With n sample points (x_i, x_j) , the likelihood function of the model parameters can be given as

Likelihood

$$= -\frac{1}{2} \left[n \ln(2\pi) + n \ln \sigma^2 + \ln|R| + \frac{1}{2\sigma^2} (y - A\mu)^T R^{-1} (y - A\mu) \right] \quad (12)$$

where y is the column vector of the response and A is a $n \times 1$ vector filled with ones. The term μ can be estimated as

$$\mu = [A^T R^{-1} A]^{-1} A^T R^{-1} y \quad (13)$$

The σ^2 also can be estimated as [21]

$$\sigma^2 = \frac{(y - A\mu)^T R^{-1} (y - A\mu)}{n} \quad (14)$$

With the preceding two equations, the likelihood function is transformed into a function, which depends only upon the parameters θ_p and α_p . In addition, these two parameters can be determined by maximizing the likelihood function and, therefore, the correlation matrix R can be calculated. With this prediction model, the system performance can be estimated for any given design point x^* as

$$Y(x^*) = \mu + r^T(x^*) R^{-1} (y - A\mu) \quad (15)$$

where $r(x^*)$ is the correlation vector between the prediction point x^* and the design points $x_1 - x_n$, which is given by

$$r^T(x^*) = [\text{Corr}[G(x^*, x_1)], \dots, \text{Corr}[G(x^*, x_n)]] \quad (16)$$

4.3 Example Use of Kriging Model. In order to explain the sampling method and the Kriging model, a mathematical model, which is shown as the Branin function, is considered in term of two variables x_1 and x_2 as [27]

$$Y(x) = \left(x_2 - \frac{5.1}{4\pi^2} x_1^2 + \frac{5}{\pi} x_1 - 6 \right)^2 + 10 \left[\left(1 - \frac{1}{8\pi} \right) \cos x_1 + 1 \right] \\ x_1 \in [-5, 10] \\ x_2 \in [0, 15] \quad (17)$$

In the first step of this example, 20 design points are selected by LHS, as shown in Fig. 13.

Figure 14(a) shows what the entire model looks like as a meta-model and the 20 design points are shown in the image as small

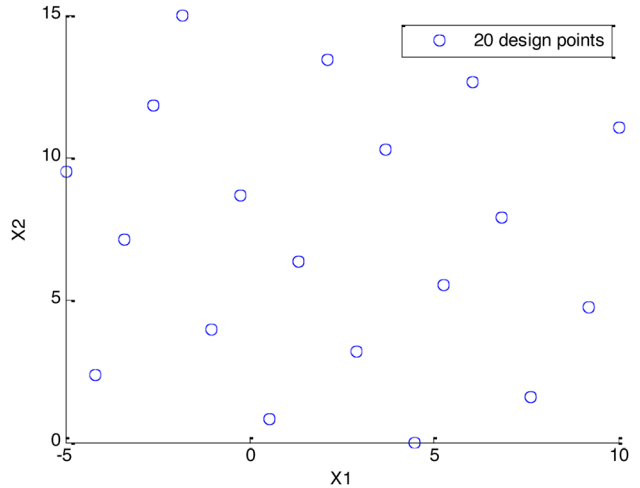


Fig. 13 Design points selected by the LHS

dots. In Fig. 14(b), a surrogate model is built using the Kriging model. The Kriging model with these 20 design points has been used to assume the response surface. Comparing this to the exact results, the Kriging model uses only 20 design points to obtain acceptable and reasonably accurate results.

Among the interpolation methods, the neural network and Kriging model are two potential techniques, among others, and both can capture the unknown nonlinearity in the system performance. Based on a study by Yuan and Bai [1], in which they compared the neural network and the Kriging model, the Kriging model can usually produce meta-model optima that are superior in precision. Additionally, for a given sample size, the Kriging model tends to provide a better overall fit than the neural networks.

4.4 Genetic Algorithm. Genetic algorithms are nongradient-based methods [28] that can generate a global promising result for a complex optimization problem. In most cases, the GA is divided into three steps: evaluation, crossover, and mutation. An initial population of the design variable is selected by some cost functions. Then the initial population is changed depending on the fitness function and, using a crossover strategy and mutation, a new generation of population is created. This process continues until the fitness function converges to the global optimal point. The input variables for this point will be the strongest population selected by the evolution. Compared to the gradient method, a GA can successfully avoid local minima since it tests the design points over a large domain in global space. However, this method is computationally expensive, especially when it is applied to computer simulation models. In order to overcome this weak point and to compensate for the expensive optimization process, this research replaces the ordinary computer simulation model with the cost-effective Kriging model. The objective functions considered in this study are as follows:

$$\min \{\ddot{x}_{\text{slider}}\}_{\max} \quad (18)$$

$$\min \{F_N\}_{\max} \quad (19)$$

$$\min \{P\}_{\max} \quad (20)$$

where \ddot{x}_{slider} , F_N , and P are, respectively, the acceleration of the slider block, the contact force at the pin, and the power input requirement for the operation of the mechanism. The power is calculated as the product of the input torque T and crank angular velocity ω , i.e.

$$P = T\omega \quad (21)$$

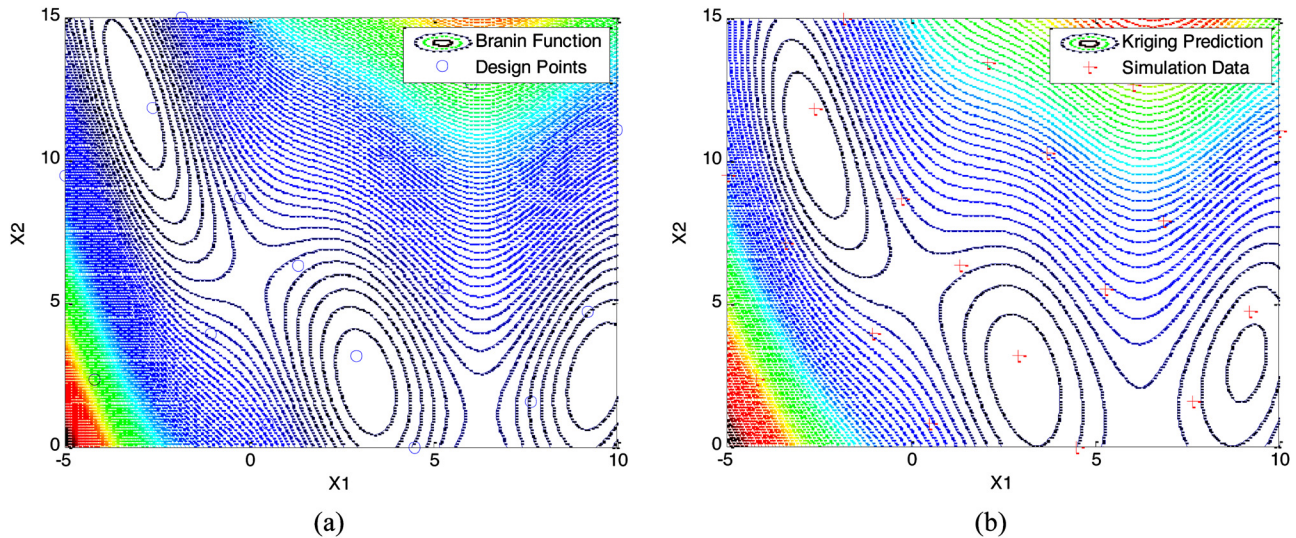


Fig. 14 (a) Exact model of the Branin function, and (b) surrogate model predicted by the Kriging model

5 DOE- and Kriging-Based Study of Slider-Crank Mechanism

In this section, the dynamic behavior of the slider-crank mechanical system with a revolute clearance joint will be studied further, using two simple examples that use the DOE method introduced in the previous sections. The Kriging meta-model is constructed in order to optimize and analyze the computer simulation experiment process and the genetic algorithm is used to find the minimal contact force in the joint by controlling appropriate values of the design parameters. The implementation of this method was previously shown in Fig. 12. Sample points are selected from design variables by the LHS and the slider-crank mechanism model developed in the previous section is used to evaluate performances acquired from the sample points. Then the absolute maximum value for dynamic behavior such as the contact forces, slider accelerations, crank moment, and power consumption, all from the simulation model, can be treated as the system performance and a surrogate model is built using the Kriging meta-model to replace the expensive computer simulation model. The remaining quantitative values from the objective functions can be predicted by the Kriging model. The GA is then used to optimize the results. In the process, the dynamic behavior of the mechanical system with a revolute clearance joint case is obtained for a range of design parameters.

5.1 Demonstrative Example 1. An illustrative example is presented here to investigate the influence of the radial clearance size and the material/contact stiffness coefficient on the dynamic behavior of the slider-crank mechanism with a revolute clearance joint. The computer simulation model built in MSC.ADAMS is used in this experiment. A constant input speed of 5000 rpm is set up on the crank. At a high constant input speed, contact forces at the joint can also become quite large and the impact of the change of the clearance size and stiffness coefficient can be more visible on

the dynamic response of the system. Since the system is dynamically quite stiff due to the existence of large contact forces, which act and disappear for a very short period of time, the numerical integrator used in the study is the enhanced GSTIFF integrator, developed Gear [29]. A variable integration time step selection scheme was chosen for the simulations with a reporting time step of 10^{-6} s [30].

Table 3 shows the radial clearance size and material/contact coefficient, which are selected as the design variables, and that the slider acceleration, contact force in the revolution joint, and the power consumption are investigated as the objective functions. The diametric clearance size of the nonideal revolute joint drops in the interval between 0.05 mm and 0.5 mm, which corresponds to the clearance size in a typical journal-bearing. For the stiffness coefficient, common steel and iron alloys are chosen as experimental materials. Young's modulus of metal is taken to be between 113 GPa and 210 GPa and Poisson's ratio falls into the region between 0.23 and 0.3. The stiffness coefficient is taken to be between $3.4 \times 10^{+9}$ N/m^{1.5} and $1.7 \times 10^{+9}$ N/m^{1.5}.

Ten design points were generated by the Latin hypercube method (see Table 4) and inserted in the simulation model to evaluate the objective functions. In Fig. 15, the surface plots are acquired by utilizing the Kriging model.

After the Kriging model is built by following the methodology, in order to detect its accuracy, another point (the 11th point) is used as the clearance size of 0.18 mm and the contact stiffness of $1.0 \times 10^{+10}$ N/m^{1.5}. Both the computer simulation model and Kriging meta-model are used to examine the highest absolute value of the slider acceleration of the slider-crank mechanism. The result for the highest absolute value of slider acceleration

Table 4 Sample points and the computer simulation results

Sample number	Clearance size (mm)	Stiffness (N/m ^{1.5})	Slider acceleration (m/s ²)	Contact force (N)	Power (W)
1	0.5	$9.4 \times 10^{+9}$	$1.1 \times 10^{+5}$	$1.5 \times 10^{+4}$	$1.2 \times 10^{+5}$
2	0.45	$3.4 \times 10^{+9}$	$1.0 \times 10^{+5}$	$1.4 \times 10^{+4}$	$0.9 \times 10^{+5}$
3	0.05	$1.5 \times 10^{+10}$	$2.0 \times 10^{+4}$	$2.7 \times 10^{+3}$	$1.9 \times 10^{+4}$
4	0.3	$1.1 \times 10^{+10}$	$8.5 \times 10^{+4}$	$1.2 \times 10^{+4}$	$8.2 \times 10^{+4}$
5	0.15	$1.2 \times 10^{+10}$	$2.7 \times 10^{+4}$	$3.7 \times 10^{+3}$	$2.5 \times 10^{+4}$
6	0.35	$6.4 \times 10^{+9}$	$9.3 \times 10^{+4}$	$1.3 \times 10^{+4}$	$9.1 \times 10^{+4}$
7	0.25	$1.7 \times 10^{+10}$	$6.8 \times 10^{+4}$	$9.6 \times 10^{+3}$	$6.2 \times 10^{+4}$
8	0.1	$7.9 \times 10^{+9}$	$2.0 \times 10^{+4}$	$2.8 \times 10^{+3}$	$1.8 \times 10^{+4}$
9	0.2	$4.9 \times 10^{+9}$	$4.5 \times 10^{+4}$	$6.3 \times 10^{+3}$	$4.3 \times 10^{+4}$
10	0.4	$1.4 \times 10^{+10}$	$9.1 \times 10^{+4}$	$1.3 \times 10^{+4}$	$9.3 \times 10^{+4}$

Table 3 General experiment objects in example 1

Design variables	1. Radial clearance size (mm) 2. Material/contact stiffness coefficient (N/m ^{1.5})	0.05–0.5 $3.4 \times 10^{+9}$ – $1.7 \times 10^{+9}$
Objective functions	1. Slider acceleration 2. Contact force at joint clearance 3. Power consumption	

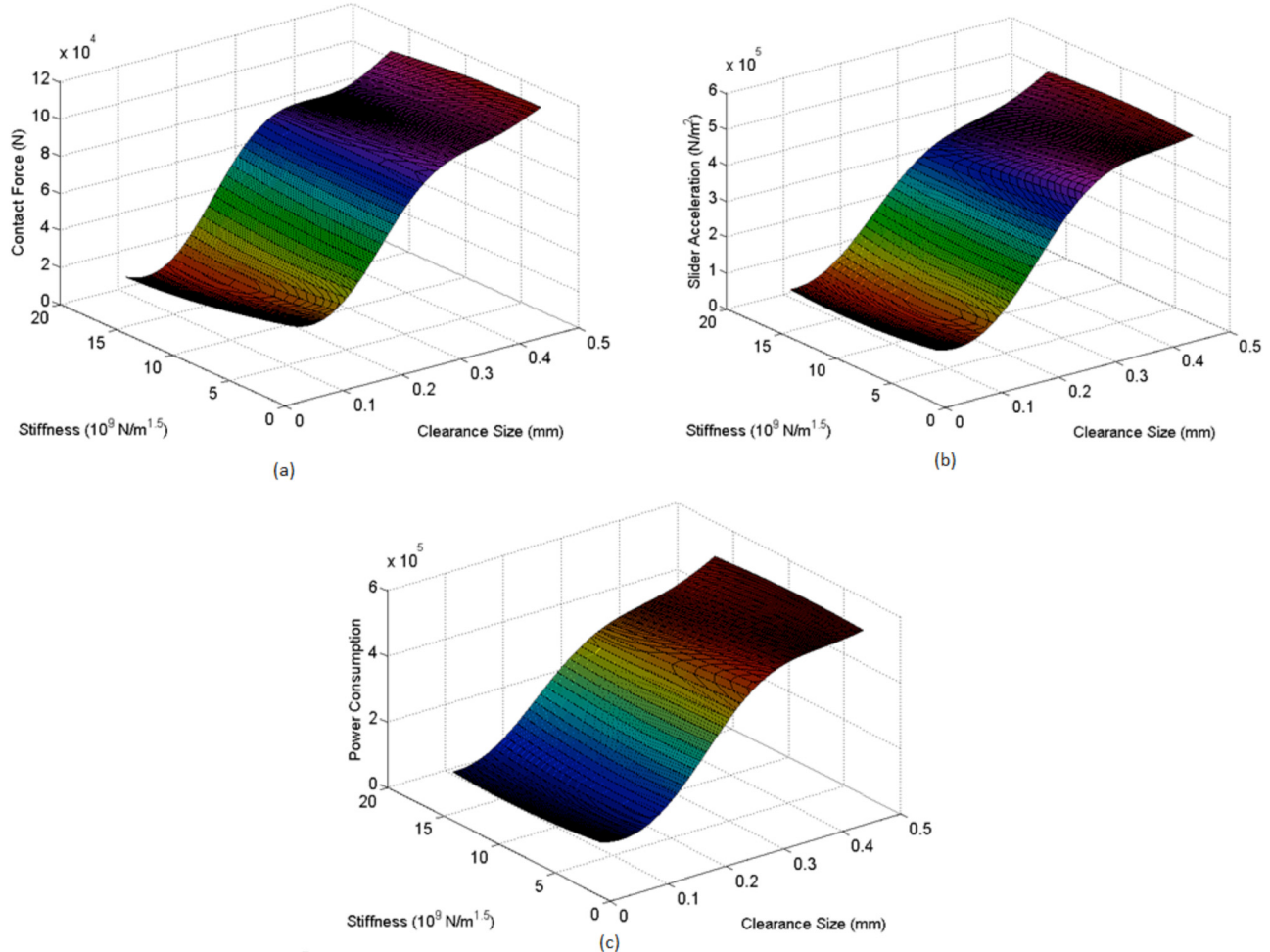


Fig. 15 (a) Surface plot for joint contact force, (b) surface plot for slider acceleration, and (c) surface plot for crank power consumption

from the computer simulation model is $3.2 \times 10^{+4} \text{ m/s}^2$. The highest absolute value of slider acceleration from the Kriging model is $3.0 \times 10^{+4} \text{ m/s}^2$. The results indicate that the respective error for the highest absolute value of acceleration for the Kriging model is within 6% of the actual value. Hence, the Kriging model can reasonably predict the response of this system for the studied range of parameters.

Figure 15(a) presents the contact force between the bearing and journal for the dynamic response histories as the functions of the clearance size and the stiffness coefficient. Figures 15(b) and 15(c) show the surface plots for the slider acceleration and power consumption. From Fig. 15, it is clear that the contact force grows monotonically as the clearance size increases at the center of the image and the change gradually becomes smooth when the curve tends to the edge of the image. In addition, the clearance size is more sensitive than the stiffness in the studied range. The results for the slider acceleration show similar phenomena on the contact force. After applying the genetic algorithm, the optimal point is found to have a material stiffness coefficient of $3.4 \times 10^{+4} \text{ N/m}^{1.5}$ and a radial clearance size of 0.05 mm. The results from this DOE-based study show that the lowest values in the range of design variables are optimal. In the next demonstrative example, a larger range of design variables will be selected to investigate the dynamic response of the same system.

5.2 Demonstrative Example 2. In this section, another example of the use of the DOE and Kriging model is presented in order to illustrate the dynamic response of the revolute clearance

joint. The same slider-crank mechanical system is also used in this experiment, but three input design variables are utilized instead. For this analysis, the three design variables are the input crank speed, material stiffness, and size of the radial joint clearance and the objective functions are the contact force between the bearing and the journal and the power consumption (see Table 5). The larger ranges of the parameter variables are given in the example, because the diametric clearance size is chosen in the interval between 0.02 mm and 1 mm, the range of the stiffness coefficient is taken between $3.3 \times 10^{+8} \text{ N/m}^{1.5}$ and $3.3 \times 10^{+11} \text{ N/m}^{1.5}$, and the value of the crank speed is chosen between 50 rpm and 5000 rpm.

The LHS is used to choose the 30 sample points. Importing the samples in the simulation model, the absolute maximum values for the objective functions are shown in Table 6.

The data from Table 6 are used to build the Kriging meta-model. The Kriging model is established as a prediction model to estimate the objective function for any given design point and it is

Table 5 General experiment objects in example 2

Design variables	1. Input crank speed (rpm) 2. Material/contact stiffness coefficient ($\text{N/m}^{1.5}$) 3. Radial clearance size (mm)	50–5000 $3.3 \times 10^{+8}$ – $3.3 \times 10^{+11}$ 0.02–1.00
Objective functions	1. Contact force at joint clearance 2. Power consumption	

Table 6 Sample points and the computer simulation results

Sample number	Crank speed (rpm)	Stiffness ($\text{N}/\text{m}^{1.5}$)	Clearance size (mm)	Contact force (N)	Acceleration (m/s^2)	Power (W)
1	$7.33 \times 10^{+2}$	$2.16 \times 10^{+11}$	0.76	$9.03 \times 10^{+2}$	$6.45 \times 10^{+3}$	$4.30 \times 10^{+3}$
2	$5.00 \times 10^{+1}$	$2.31 \times 10^{+10}$	0.39	$1.32 \times 10^{+1}$	$9.40 \times 10^{+1}$	$1.40 \times 10^{+4}$
3	$3.80 \times 10^{+3}$	$2.62 \times 10^{+11}$	0.63	$9.24 \times 10^{+3}$	$6.60 \times 10^{+4}$	$2.18 \times 10^{+5}$
4	$3.12 \times 10^{+3}$	$9.13 \times 10^{+10}$	0.8	$8.45 \times 10^{+3}$	$6.35 \times 10^{+4}$	$1.61 \times 10^{+5}$
5	$3.30 \times 10^{+3}$	$1.59 \times 10^{+11}$	0.05	$1.19 \times 10^{+3}$	$8.48 \times 10^{+3}$	$2.09 \times 10^{+4}$
6	$1.07 \times 10^{+3}$	$1.94 \times 10^{+11}$	0.19	$5.00 \times 10^{+2}$	$3.57 \times 10^{+3}$	$5.30 \times 10^{+3}$
7	$2.62 \times 10^{+3}$	$3.30 \times 10^{+8}$	0.49	$5.03 \times 10^{+3}$	$3.59 \times 10^{+4}$	$8.58 \times 10^{+4}$
8	$9.03 \times 10^{+2}$	$1.17 \times 10^{+10}$	0.7	$1.11 \times 10^{+3}$	$7.92 \times 10^{+3}$	$5.06 \times 10^{+3}$
9	$2.78 \times 10^{+3}$	$2.96 \times 10^{+11}$	0.09	$9.26 \times 10^{+2}$	$6.61 \times 10^{+3}$	$1.34 \times 10^{+4}$
10	$5.62 \times 10^{+2}$	$3.07 \times 10^{+11}$	0.56	$6.79 \times 10^{+2}$	$4.80 \times 10^{+3}$	$1.80 \times 10^{+3}$
11	$2.43 \times 10^{+3}$	$2.39 \times 10^{+11}$	0.53	$4.80 \times 10^{+3}$	$3.43 \times 10^{+4}$	$6.30 \times 10^{+4}$
12	$1.25 \times 10^{+3}$	$1.37 \times 10^{+11}$	0.97	$1.83 \times 10^{+3}$	$1.30 \times 10^{+3}$	$1.50 \times 10^{+4}$
13	$4.15 \times 10^{+3}$	$1.48 \times 10^{+11}$	0.59	$9.05 \times 10^{+3}$	$6.46 \times 10^{+4}$	$2.52 \times 10^{+5}$
14	$4.83 \times 10^{+3}$	$3.44 \times 10^{+10}$	0.12	$2.89 \times 10^{+3}$	$2.06 \times 10^{+4}$	$7.28 \times 10^{+4}$
15	$2.95 \times 10^{+3}$	$3.19 \times 10^{+11}$	0.9	$8.83 \times 10^{+3}$	$6.30 \times 10^{+4}$	$1.82 \times 10^{+5}$
16	$3.98 \times 10^{+3}$	$1.03 \times 10^{+11}$	0.22	$5.02 \times 10^{+3}$	$3.58 \times 10^{+4}$	$1.28 \times 10^{+5}$
17	$3.47 \times 10^{+3}$	$1.71 \times 10^{+11}$	0.93	$1.14 \times 10^{+4}$	$8.11 \times 10^{+4}$	$2.76 \times 10^{+5}$
18	$1.75 \times 10^{+3}$	$1.25 \times 10^{+11}$	0.46	$2.40 \times 10^{+3}$	$1.71 \times 10^{+4}$	$2.38 \times 10^{+4}$
19	$4.67 \times 10^{+3}$	$3.30 \times 10^{+11}$	0.29	$1.11 \times 10^{+4}$	$7.94 \times 10^{+4}$	$3.14 \times 10^{+5}$
20	$4.48 \times 10^{+3}$	$2.85 \times 10^{+11}$	0.86	$1.73 \times 10^{+4}$	$1.23 \times 10^{+5}$	$4.90 \times 10^{+5}$
21	$1.42 \times 10^{+3}$	$1.14 \times 10^{+11}$	0.02	$2.22 \times 10^{+2}$	$1.58 \times 10^{+3}$	$2.10 \times 10^{+3}$
22	$3.63 \times 10^{+3}$	$2.50 \times 10^{+11}$	0.26	$5.85 \times 10^{+3}$	$4.17 \times 10^{+4}$	$1.32 \times 10^{+5}$
23	$2.10 \times 10^{+3}$	$5.72 \times 10^{+10}$	1	$5.29 \times 10^{+3}$	$3.77 \times 10^{+4}$	$7.70 \times 10^{+4}$
24	$2.27 \times 10^{+3}$	$6.85 \times 10^{+10}$	0.16	$9.47 \times 10^{+2}$	$6.76 \times 10^{+3}$	$1.45 \times 10^{+4}$
25	$2.20 \times 10^{+2}$	$2.28 \times 10^{+11}$	0.43	$3.50 \times 10^{+2}$	$2.50 \times 10^{+3}$	$4.58 \times 10^{+2}$
26	$3.92 \times 10^{+2}$	$7.99 \times 10^{+10}$	0.83	$4.16 \times 10^{+2}$	$2.97 \times 10^{+3}$	$1.13 \times 10^{+2}$
27	$1.59 \times 10^{+3}$	$2.73 \times 10^{+11}$	0.32	$2.24 \times 10^{+3}$	$1.59 \times 10^{+4}$	$3.37 \times 10^{+4}$
28	$5.00 \times 10^{+3}$	$2.05 \times 10^{+11}$	0.36	$1.39 \times 10^{+4}$	$9.90 \times 10^{+4}$	$4.05 \times 10^{+5}$
29	$1.93 \times 10^{+3}$	$1.82 \times 10^{+11}$	0.66	$4.09 \times 10^{+3}$	$2.92 \times 10^{+4}$	$3.85 \times 10^{+4}$
30	$4.32 \times 10^{+3}$	$4.58 \times 10^{+10}$	0.73	$1.36 \times 10^{+4}$	$9.68 \times 10^{+4}$	$3.64 \times 10^{+5}$

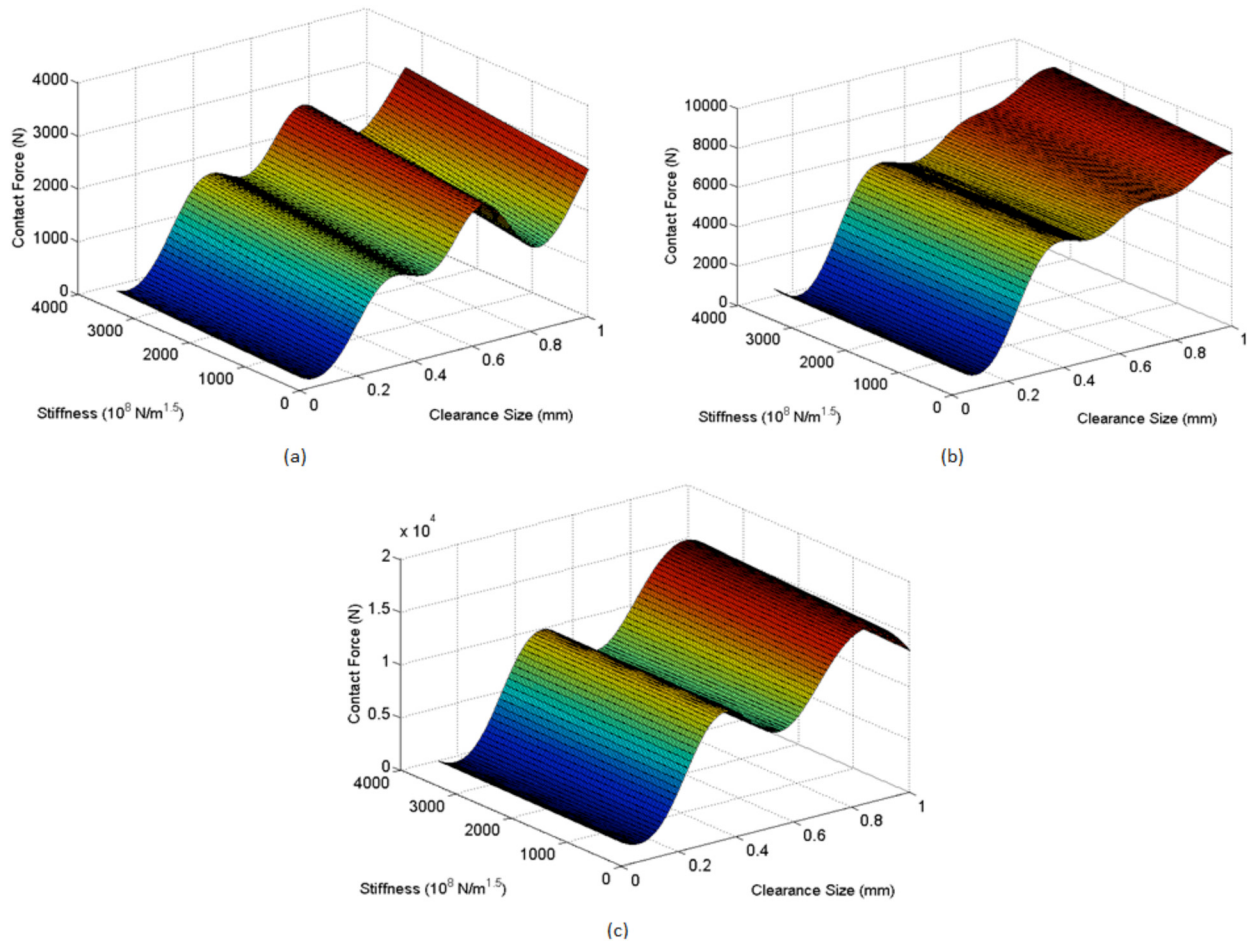


Fig. 16 Surface plots for contact forces: (a) low-speed input, (b) medium-speed input, and (c) high-speed input

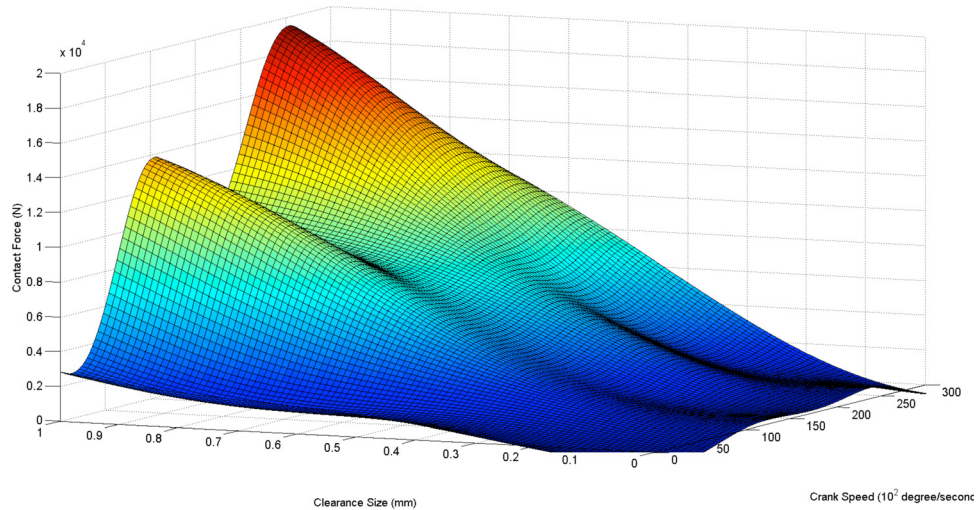


Fig. 17 Dynamic response in terms of contact force with constant stiffness coefficient

used to replace the computer simulation experiment. A similar accuracy test, as in the demonstrative example 1, is presented again for this example. After obtaining 30 design points by Latin hypercube sampling, another point (the 31st point) is obtained to evaluate the accuracy of the Kriging model. This 31st point is set with the clearance size of 0.5 mm, contact stiffness of $2.2 \text{ N/m}^{1.5}$, and input crank speed of 3000 rpm. The highest absolute value of the slider acceleration from the computer simulation model is $4.5 \times 10^{+4} \text{ m/s}^2$. The highest absolute value of the slider acceleration from the Kriging model is $4.4 \times 10^{+4} \text{ m/s}^2$. The results indicate that the respective error for the highest absolute value of acceleration for the Kriging model is within 2% of the actual value. Hence, the Kriging model can reasonably predict the response of this system for the range of studied parameters.

Figure 16 shows the dynamic response histories of the contact forces between the bearing and the journal, as functions of the clearance size and the stiffness coefficient, with the input crank speed set to three different levels: the low-speed input of 1480 rpm, the medium-speed input of 3000 rpm, and the high-speed input of 4450 rpm. In each radial clearance situation, the contact force remains constant with respect to the stiffness coefficient, as shown in Fig. 16(b). However, the contact force between the bearing and the journal shows a clear increase for an increase in the clearance size. In this case, the effects of the dynamic response are more sensitive to the clearance size than the stiffness coefficient in this mechanical system with one revolute clearance joint. Figure 16 also indicates that when the mechanical system operates at the lower- and higher-speed levels, the nonperiodic behavior can clearly be observed. The curve for the contact force is more linear when the system operates at the medium-speed level. The contact force and the crank speed are positively correlated in this case. Similar conclusions can be drawn from Fig. 17, since it illustrates the influence of the radial clearance and crank speed on the contact force for a given stiffness coefficient of $1.63 \times 10^{+11} \text{ N/m}^{1.5}$. A rising trend of the contact force between the bearing and the journal is obtained with an increase in the radial clearance size and crank speed.

6 Conclusion

The influence of the dynamic behavior of a multibody mechanical system with a revolute clearance joint was investigated in this study. A computer-aided analysis of the mechanical system and the framework of the DOE modeling were presented to study the effect of the joint clearance size, input crank speed, and material/contact stiffness coefficient on the dynamic response of a multibody system with one clearance joint. The classical slider-crank

mechanism with revolute joint clearance at the piston pin was considered in this study. The Kriging meta-model was used to replace the computer simulation experiment as a cost-effective mathematical tool for optimizing the system performance.

This research was focused on using the design-of-experiment method to develop a surrogate Kriging meta-model instead of the computer simulation model. The use of the Kriging model allowed the prediction of the system's response at other design points with a significantly lower computational time and cost. For the studied mechanism, the predictions were shown to be within 5% of the actual values from dynamic simulations, for which close to an hour of computational time is to be spent for each simulation. In addition to the use of the Kriging model for the prediction of the response at different design points, the scheme allows for the visualization of the trends of the response surfaces when the design variables are changed. The global results obtained from this study indicate that the dynamic behavior of the mechanical system with clearance is quite sensitive to the crank speed and clearance size. The contact force is increased when the crank speed increases and the decrease in crank speed tends to make the results more noisy. The contact force significantly increases with the increase in the clearance size and, as the clearance size decreases, the dynamic behavior tends to be close to the ideal situation. The dynamic response of the mechanism does not significantly change with a change in the contact stiffness coefficient. In general, the reduction in the input crank speed and clearance size minimizes the contact force between the bearing and the journal.

The method presented in this paper can be utilized for optimizing the performance of mechanical systems with joint clearances. By utilizing the Kriging meta-model, the computer simulation time can be significantly reduced, while the response of the system can be studied and optimized for a range of input design variables.

References

- [1] Yuan, R. and Bai, G., 2009, "Comparison of Neural Network and Kriging Method for Creating Simulation-Optimization Metamodels," Proceedings of the Eighth IEEE International Conference, Dependable Autonomic and Secure Computing, DASC'09.
- [2] Laribi, M. A., Mlika, A., Romdhane, L., and Zeghloul, S., 2004, "A Combined Genetic Algorithm-Fuzzy Logic Method (GA-FL) in Mechanisms Synthesis," *Mech. Mach. Theory*, **39**(7), pp. 717–735.
- [3] Erkaya, S. and Uzmay, I., 2008, "A Neural-Genetic (NN-GA) Approach for Optimizing Mechanisms Having Joints With Clearance," *Multibody Syst. Dyn.*, **20**(1), pp. 69–83.
- [4] Flores, P. and Lankarani, H. M., 2012, "Dynamic Response of Multibody Systems With Multiple Clearance Joints," *ASME J. Comput. Nonlinear Dyn.*, **7**(3), p. 031003.
- [5] Flores, P., Ambrósio, J., Claro, J. C. P., and Lankarani, H. M., 2008, "Kinematics and Dynamics of Multibody Systems With Imperfect Joints:

- Models and Case Studies," *Lecture Notes in Applied and Computational Mechanics*, Vol. 34, Springer-Verlag, New York.
- [6] Haug, E. J. and Huston, R. L., 1985, "Computer Aided Analysis and Optimization of Mechanical System Dynamics," *ASME J. Appl. Mech.*, **52**(1), pp. 243.
- [7] Dubowsky, S., Norris, M., Aloni, E., and Tamir, A., 1984, "An Analytical and Experimental Study of the Prediction of Impacts in Planar Mechanical Systems With Clearances," *ASME J. Mech., Transm., Autom. Des.*, **106**(4), pp. 444–451.
- [8] Dubowsky, S. and Moening, M., 1978, "An Experimental and Analytical Study of Impact Forces in Elastic Mechanical Systems With Clearances," *Mech. Mach. Theory*, **13**(4), pp. 451–465.
- [9] Furuhashi, T., Morita, N., and Matsuura, M., 1977, "Dynamic Researches of Four-Bar Linkage With Clearance at Turning Pairs: 4th Report, Forces Acting at Joints of Crank-Lever Mechanism," *Trans. Jpn. Soc. Mech. Eng.*, **43**(376), pp. 4644–4651.
- [10] Lankarani, H. M. and Nikravesh, P. E., 1990, "A Contact Force Model With Hysteresis Damping for Impact Analysis of Multibody Systems," *ASME J. Mech. Des.*, **112**(3), pp. 369–376.
- [11] Flores, P., Ambrosio, J., Claro, J. C. P., Lankarani, H. M., and Koshy, C., 2006, "A Study on Dynamics of Mechanical Systems Including Joints With Clearance and Lubrication," *Mech. Mach. Theory*, **41**(3), pp. 247–261.
- [12] Flores, P., Lankarani, H. M., Ambrósio, J., and Claro, J. C. P., 2004, "Modelling Lubricated Revolute Joints in Multibody Mechanical Systems," *Proc. Inst. Mech. Eng., Part K*, **218**(4), pp. 183–190.
- [13] Flores, P. and Lankarani, H. M., 2010, "Spatial Rigid-Multi-Body Systems With Lubricated Spherical Clearance Joints: Modeling and Simulation," *Nonlinear Dyn.*, **60**(1–2), pp. 99–114.
- [14] Mahrus, D., 1974, "Experimental Investigation Into Journal Bearing Performance," *Rev. Bras. Tecol.*, **5**(3–4), pp. 139–152.
- [15] Wilson, R. and Fawcett, J. N., 1974, "Dynamics of Slider-Crank Mechanism With Clearance in the Sliding Bearing," *Mech. Mach. Theory*, **9**(1), p. 61–80.
- [16] Haines, R. S., 1980, "A Theory of Contact Loss at Resolute Joints With Clearance," *Proc. Inst. Mech. Eng., Part C: J. Mech. Eng. Sci.*, **22**(3), pp. 129–136.
- [17] Flores, P., Ambrósio, J., Claro, J. C. P., and Lankarani, H. M., 2007, "Dynamic Behaviour of Planar Rigid Multi-Body Systems including Revolute Joints With Clearance," *Proc. Inst. Mech. Eng., Part K*, **221**(2), pp. 161–174.
- [18] Bengisu, M. T., Midayetoglu, T., and Akay, A., 1986, "A Theoretical and Experimental Investigation of Contact Loss in the Clearances of a Four-Bar Mechanism," *ASME J. Mech., Transm., Autom. Des.*, **108**, pp. 237–244.
- [19] Feng, B., Morita, N., and Torii, T., 2002, "A New Optimization Method for Dynamic Design of Planar Linkage With Clearances at Joints—Optimizing the Mass Distribution of Links to Reduce the Change of Joint Forces," *ASME J. Mech. Des.*, **124**(1), pp. 68–73.
- [20] Tsai, M. and Lai, T., 2004, "Kinematic Sensitivity Analysis of Linkage With Joint Clearance Based on Transmission Quality," *Mech. Mach. Theory*, **39**(11), pp. 1189–1206.
- [21] Yıldırım, S., Erkaya, S., Su, S., and Uzmay, I., 2005, "Design of Neural Networks Model for Transmission Angle of a Modified Mechanism," *J. Mech. Sci. Technol.*, **19**(10), pp. 1875–1884.
- [22] Flores, P., Koshy, C. S., Lankarani, H. M., Ambrósio, J., and Claro, J. C. P., 2011, "Numerical and Experimental Investigation on Multibody Systems With Revolute Clearance Joints," *Nonlinear Dyn.*, **65**(4), pp. 383–398.
- [23] Hirsa, A., 2011, *Computational Methods in Finance*, CRC, Boca Raton, FL, pp. 224–228.
- [24] Simpson, T. W., Mauery, T. M., Korte, J. J., and Mistree, F., 1998, "Comparison of Response Surface and Kriging Models for Multidisciplinary Design Optimization," Proceedings of the 7th AIAA/USA/NASA/ISSMO Symposium on Multidisciplinary Analysis and Optimization, AIAA Paper No. 98-4758.
- [25] Kibobi, D. G., 1951, "A Statistical Approach to Some Basic Mine Valuation Problems on the Witwatersrand," *J. Chem. Metall. Min. Soc. S. Afr.*, **52**, pp. 119–139.
- [26] Cressie, N., 1990, "The Origins of Kriging," *Math. Geol.*, **22**(3), pp. 239–252.
- [27] Forrester, A., Sobester, A., and Keane, A., 2008, *Engineering Design Via Surrogate Modeling: A Practical Guide*, Wiley, New York.
- [28] Goldberg, D. E., 1985, *Genetic Algorithms in Search, Optimization, and Machine Learning*, Addison-Wesley, Reading, MA.
- [29] Gear, C. W., Leimkuhler, B., and Gupta, G. K., 1985, "Automatic Integration of Euler-Lagrange Equations With Constraints," *J. Comput. Appl. Math.*, **12**, pp. 77–90.
- [30] Flores, P., Machado, M., Seabra, E., and Silva, M. T., 2011, "A Parametric Study on the Baumgarte Stabilization Method for Forward Dynamics of Constrained Multibody Systems," *ASME J. Comput. Nonlinear Dyn.*, Vol. 6(1), p. 011019.



Dynamic behaviour analysis of planar mechanical systems with clearance in revolute joints using a new hybrid contact force model

Zheng Feng Bai*, Yang Zhao

Department of Astronautic Engineering, Harbin Institute of Technology, Harbin 150001, Heilongjiang, PR China

ARTICLE INFO

Article history:

Received 20 August 2011

Received in revised form

23 October 2011

Accepted 25 October 2011

Available online 4 November 2011

Keywords:

Clearance joint

Contact model

Friction force

Mechanism

Dynamic behaviour

ABSTRACT

In this study, the dynamic behaviour of planar mechanical systems including revolute joints with clearance is investigated using a computational methodology. The contact model in revolute joint clearance is established using a new nonlinear continuous contact force model, which is a hybrid contact force model, and the friction effect is considered using modified Coulomb friction model. And then, the dynamic characteristics of planar mechanical system with revolute joint clearance are analysed based on the new contact model. Numerical results for two simple planar mechanisms with revolute clearance joints are presented and discussed. The correctness and validity of the new contact force model of revolute joint clearance is verified through the demonstrative application examples. Clearance size and friction effect are analysed separately. The numerical simulation results show that the proposed contact force model is a new method to predict the dynamic behaviour of planar mechanical system with clearance in revolute joints.

© 2011 Elsevier Ltd. All rights reserved.

1. Introduction

Clearances in mechanism are unavoidable due to assemblage, manufacturing errors and wear. Moreover, clearance occurs in each active joint with the movement of mechanism. The movement of the real mechanisms is deflected from the ideal mechanism and the motion accuracy is decreased due to joint clearances. The existence of clearance in joints also causes impact dynamic load, affects the transfer of the system load and may lead to destruction and failure of mechanism. These clearances modify the dynamic response of the system, justify the deviations between the numerical predictions and experimental measurements and eventually lead to important deviations between the projected behaviour of mechanisms and their real outcome [1–11].

Over the last few decades, effects of clearance on dynamic behaviour of planar and spatial mechanisms using theoretical and experimental approaches have been studied by many researchers. Stoenescu and Marghitu [12] investigated the dynamic response of a planar, rigid-link mechanism with a sliding joint clearance and the response of the system with clearance was chaotic at relatively high crank speeds and low values of the coefficient of restitution. Khemili and Romdhane [13] investigated the dynamic behaviour of a planar flexible slider-crank mechanism having joint with clearance. And simulation and experimental tests were

carried out for this goal. Zhao and Bai [14] studied the dynamics of a space robot manipulator with one joint clearance. The nonlinear equivalent spring-damper model is established for the contact model in joint clearance. Also, the friction effect is considered using the Coulomb friction model. Flores et al. [15] presented dynamic analysis of planar multi-body systems with revolute joint clearances, including dry contact and lubricant effect. Liu et al. [16] developed a class of non-conformal contact model caused by joint clearance, which is based on the improved Winkler elastic foundation model and Hertz quadratic pressure distribution assumption. Rhee and Akay [17] investigated dynamic response of a revolute joint with clearance. A four-bar mechanism was implemented as an example used to model the motion of a rocker arm pin at the ground connection. Flores et al. [18] also presented a methodology to assess the influence of the spherical joint clearances in spatial multibody systems. Bauchau and Ju [19] focus on the development of methodologies for the analysis of unilateral contact conditions in joints with clearance and of the resulting normal and friction forces. Two joint configurations were developed, the planar and spatial clearance joints that can deal with typical configurations where contact and clearance are likely to occur. Shi and Jin [20] presented a general methodology for dynamic characterisation of the reheat-stop-valve mechanism with revolute clearance joints, in which the leading ingredients of the model proposed were the contact force model in consideration of the manufacturing tolerance and the thermal effects of the high temperature steam in working condition. In conclusion, a great deal of researches on dynamic

* Corresponding author. Tel./fax: +86 451 8640 2079.
E-mail address: baizhengfeng@126.com (Z.F. Bai).

characteristics of mechanism with clearance are progressing and lots of productions are obtained, which have played a positive role in dynamic design, optimisation analysis and performance improvement of mechanism with joint clearance.

Contact and impact are the typical phenomena of mechanism with joint clearance. Contact force model of revolute joints with clearance is one of the important contents in dynamics analysis of mechanism with clearance. Moreover, reasonable contact force model is crucial to design and analysis of mechanism with clearance. The contact–impact models of mechanism with clearance are mainly focus on the discrete analysis method and continuous contact analysis method [15,20,21]. The former assumes that the contact–impact is very short and does not change the overall configuration of the object. Then, the contact–impact process is divided into two stages, before and after impact, as well as relative sliding, viscous stagnation and reverse movement will occur between two objects after the impact. The latter assumes that interaction forces between the impact objects are continuous in the entire contact–impact process. This approach in line tallies with real contact–impact behaviour of objects. The continuous contact force model is widely used for contact–impact analysis of mechanism with clearance. The elastic contact force is widely represented by Hertz contact law. The representative contact force model is Lankarani–Nikravesh model [18,20,22,23] established by Lankarani and Nikravesh [22]. A common Hertz contact force expression is used in this model and the damping effect is considered, which can describe the energy loss during the impact process.

Hertz theory is available only in solving the contact problem that the geometric shape of contact bodies is non-conformal. The properties of conformal contact at the contact surfaces of revolute joints consequentially result in the limitation of Hertz model in solving the contact problem of revolute joints with clearances. And Hertz model is available only in the case that there is a large clearance with a small normal load. However, clearance in actual revolute joint is very small and the contact process of journal and bearing does not always satisfy the non-conformal contact condition. Usually, the achieved results are not precise, especially in small clearance for bearing and journal contact. Besides, in most of the past literatures, contact stiffness and damping coefficient were calculated simply according to the impact situation of two sphere bodies or taken as a constant according to experience, which does not meet the actual situation [16,24–27].

Liu et al. [16] developed a class of non-conformal contact model caused by joint clearance, which was based on the improved Winkler elastic foundation model and Hertz quadratic pressure distribution assumption. The model was applied to static contact analysis of cylindrical joints with clearance and verified by finite element method. The application of the above model was not only in the contact problem of revolute joint with big clearance but also the contact analysis of revolute joint with small clearance, which developed the clearance contact analysis. Based on the research mentioned above, nonlinear stiffness coefficient is proposed for contact and a new nonlinear continuous contact model in the joint clearance is proposed in this paper, which is a hybrid model of Lankarani–Nikravesh model and improved elastic foundation model.

The objective of this paper is to study the dynamic behaviour of planar mechanical systems with revolute joint clearance base on the new nonlinear continuous contact force model using a computational methodology. The slider-crank mechanism with revolute joint clearances is used as numerical example to demonstrate and validate the hybrid contact force model presented in this work. The dynamic response obtained with numerical models is compared with that of experimental slider-crank setup [28]. Furthermore, numerical results for planar four-bar mechanism

with revolute clearance joints are presented and discussed. The clearance size and friction effects are analysed separately.

This paper is organised as follows. Section 2 defines the clearance and presents the mathematic model of revolute joint with clearance. Section 3 establishes the new hybrid contact model of revolute joint with clearance. Section 4 establishes the modified friction force model of revolute joint with clearance. In Section 5 the slider-crank mechanism [28] with revolute joint clearance is used as numerical example to demonstrate and validate the new hybrid contact force model. In Section 6 the planar four-bar mechanism with revolute joint clearance is used as numerical example to investigate the dynamic behaviour of mechanical system with revolute clearance joints. Finally, Section 7 ends the paper with the concluding remarks.

2. Model of revolute joint with clearance

2.1. Vector model in joint clearance

The existence of clearance in joints of mechanical system is inevitable. Joint clearance of mechanical system is necessary to allow the relative motion of connected bodies, as well as to permit the assemblage of the mechanical system. Clearance exists also due to manufacturing tolerances, imperfections, wear and material deformation [3,28–31]. It is known that the performance of mechanisms is degraded by the presence of clearance due to the contact–impact force. These clearances modify the dynamic response of the system and eventually lead to important deviations between the projected behaviour of mechanisms and their real outcome as well as energy dissipation and unwanted shake responses.

In general, a clearance joint can be included in mechanism much like a revolute joint. The classical approach, known as zero-clearance approach, considers that the connecting points of two bodies linked by a revolute joint are coincident. The introduction of clearance in a joint separates these two points.

The study performs of dynamics analysis of planar mechanical system with clearance joint based on the clearance vector model [20], which is developed by introducing a clearance vector, e_{ij} , in a revolute joint, as shown in Fig. 1. Clearance vector represents the potential real movement and the relative position between journal and bearing.

Clearance vector is defined in a local floating Cartesian coordinate frame. The origin of clearance vector fixes at the centre of bearing and ends at the centre of journal, as shown in Fig. 1. It shows that clearance vector must be within the clearance circle, whose radius is determined by the tolerances of the journal

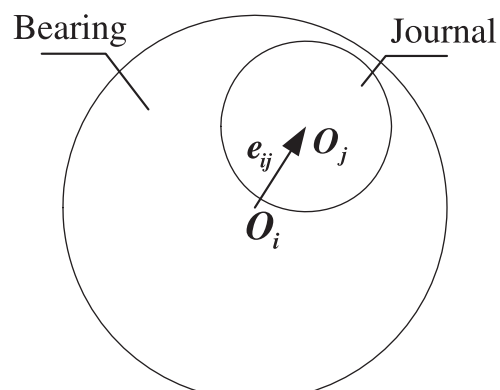


Fig. 1. Sketch map of clearance vector model in clearance joint.

and bearing diameters. And clearance vector can identify whether the journal and bearing of joint contact or not. Furthermore, it should be noted that the proposed clearance vector does not depend on the local configuration of revolute joint because clearance is unavoidable existent in revolute joint.

2.2. Definition of clearance

Fig. 2 depicts a revolute joint with clearance. The difference in radii between the bearing and journal defines the size of radial clearance [1,11,20]. Although, a revolute joint with clearance does not constrain any degree of freedom from the mechanical system like the ideal joint, it imposes some kinematic restrictions, limiting the journal to move within the bearing. Thus, when clearance is present in a revolute joint, two kinematic constraints are removed and two degrees of freedom are introduced instead. The dynamics of the joint are then controlled by forces working on the journal and bearing. Thus, whilst a perfect revolute joint in a mechanical system imposes kinematic constraints, a revolute clearance joint leads to force constraints. When contact exists between the journal and bearing, a contact force is applied perpendicular to the plane of collision.

Therefore, the motion of mechanical system with clearance always includes contact-impact process. The key point of dynamics model for mechanical system with clearance is to incorporate the clearance model and dynamics model, which needs accurate definition of the contact-impact process in the joint clearance.

The clearance is defined as follows:

$$c = R_B - R_J \quad (1)$$

where R_B and R_J are the radii of bearing and journal, respectively.

2.3. Mathematic model of revolute joint with clearance

As shown in **Fig. 3**, O_i and O_j define the centres of bearing and journal, respectively. \mathbf{r}_i^o and \mathbf{r}_j^o are the vectors denoting the positions of bearing and journal in the global inertia coordinate, respectively. Thus, in **Fig. 3**, clearance vector is represented as Eq. (2):

$$\mathbf{e}_{ij} = \mathbf{r}_j^o - \mathbf{r}_i^o \quad (2)$$

where e_{ij} represents the eccentric vector of journal relative to bearing. So the eccentricity of clearance vector can be represented as following:

$$e_{ij} = \sqrt{e_x^2 + e_y^2} \quad (3)$$

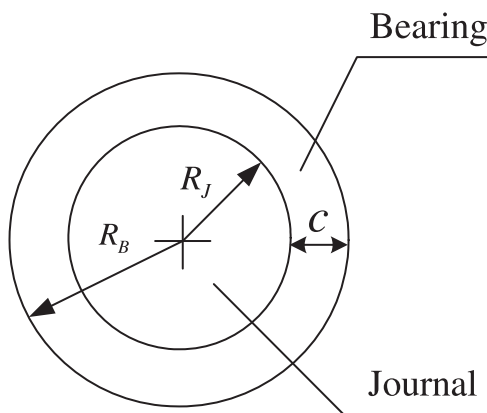


Fig. 2. Schematic of revolute joints with clearance.

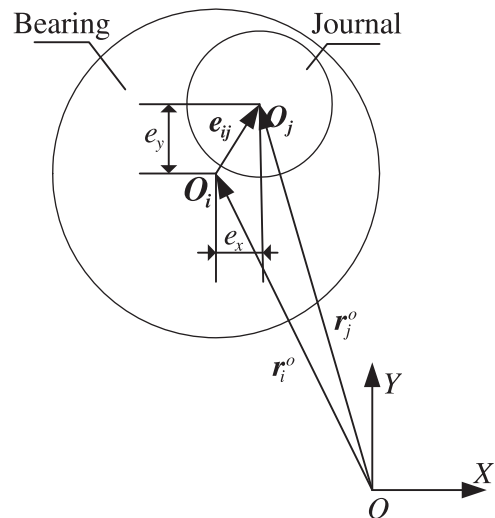


Fig. 3. Clearance model in revolute joint of mechanism system.

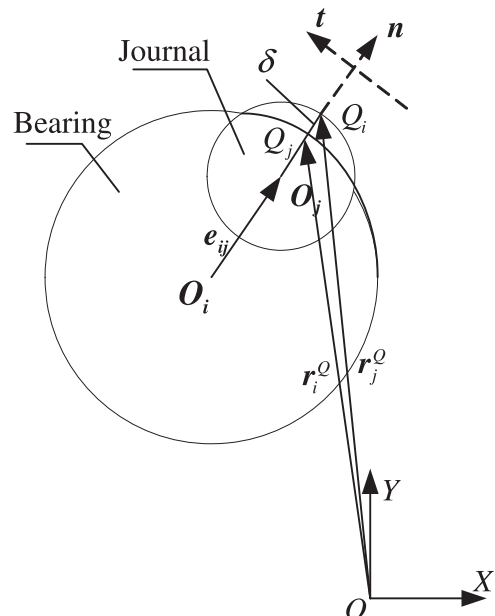


Fig. 4. Revolute joint clearance with contact.

The unit normal vector of bearing and journal at the point of their contact is represented as Eq. (4):

$$n = \mathbf{e}_{ij} / e_{ij} \quad (4)$$

That is

$$n = \frac{\mathbf{e}_{ij}}{\sqrt{e_x^2 + e_y^2}}$$

Fig. 4 describes the collision between bearing and journal. \mathbf{r}_i^o and \mathbf{r}_j^o are the positional vectors of bearing and journal, respectively, which are described in global coordinate frame. The contact deformation caused by collision between bearing and journal can be represented as Eq. (5):

$$\delta = e_{ij} - c \quad (5)$$

where c represents the clearance and it is a constant.

Thus, δ can be used to decide whether the bearing and journal have contacted. The kinematic contact condition between the

bearing and journal can be given by Eq. (6):

$$\delta = \sqrt{e_x^2 + e_y^2} - c \geq 0 \quad (6)$$

It is important to estimate the energy loss in the course of contact between bearing and journal, so it is necessary to calculate the relative speed between the surfaces of them. When projecting $\dot{\delta}$ to the facet of contact, we can get the normal speed and tangential speed of the potential points of contact between the bearing and journal, as shown in Eq. (7):

$$\begin{aligned} \mathbf{v}_n &= (\dot{\delta})^T \mathbf{n} \\ \mathbf{v}_t &= (\dot{\delta})^T \mathbf{t} \end{aligned} \quad (7)$$

where the unit tangential vector t can be achieved by reversing the unit normal vector n for 90° .

3. Hybrid contact force model of revolute joint with clearance

Contact force model of revolute joint with clearance is one of the important contents of mechanical system with joint clearance. This paper proposes a new contact force model in joint clearance, which is a hybrid model of Lankarani–Nikravesh model and the improved Winkler elastic foundation model.

A common expression of Hertz contact force is adopted in Lankarani–Nikravesh model, which considers the effect of damping and describes the energy loss in contact process. The expression of Lankarani–Nikravesh model is shown in Eq. (8) [22]:

$$F_n = K\delta^n + D\dot{\delta} \quad (8)$$

where elastic deformation force is represented by the first item of the right side of Eq. (8) and the energy loss is represented by the second item. δ is the deformation and $\dot{\delta}$ is the relative deformation velocity. K is the contact stiffness coefficient of contact bodies, which is obtained from impact experiment of two spheres and calculated from the following expressions:

$$K = \frac{4}{3\pi(\sigma_i + \sigma_j)} \left[\frac{R_i R_j}{R_i - R_j} \right]^{1/2} \quad (9)$$

$$\begin{aligned} \sigma_i &= \frac{1 - v_i^2}{\pi E_i} \\ \sigma_j &= \frac{1 - v_j^2}{\pi E_j} \end{aligned} \quad (10)$$

where v and E are Poisson ratio and Young modulus, respectively. R_i and R_j are radii of the two spheres.

Coefficient, D , in Eq. (8) is damping coefficient and $\dot{\delta}$ is relative impact velocity in impact process. The expression of D is shown in Eq. (11) [22]:

$$D = \frac{3K(1 - c_e^2)\delta^n}{4\dot{\delta}^{(-)}} \quad (11)$$

where c_e is coefficient of restitution and $\dot{\delta}^{(-)}$ is initial relative velocity of the impact point.

Due to the coefficient of restitution, c_e , is closed to unity in Eq. (11) [22], the expression of D is used only for high coefficients of restitution [9], which is improved by Qin and Lu [32]. The improved relationship between coefficient of restitution and damping coefficient is represented as follows [32]:

$$D_l = \frac{3K(1 - c_e^2)e^{2(1 - c_e)}\delta^n}{4\dot{\delta}^{(-)}} \quad (12)$$

where D_l is not restricted by coefficient of restitution and it is applicable for both large and small coefficient of restitution.

Hertz theory is available only in solving the contact problem that the geometric shape of contact bodies is non-conformal

[16,24]. Moreover, Hertz model is available only in the case that there is a large clearance with a small normal load. However, clearance in actual revolute joint is very small and the contact process of journal and bearing does not always satisfy the non-conformal contact condition. The achieved results are not precise for bearing and journal contact in small clearance. In addition, in most of the published literatures, contact stiffness and damping coefficient are calculated simply according to the impact situation of two sphere bodies or taken as a constant according to experience, which does not tally with the actual situation. Liu et al. [16] presented a new relationship between load and displacement for cylindrical joint with clearance based on the improved Winkler elastic foundation model and Hertz quadratic pressure distribution assumption. Bases on the improved elastic foundation model, the relationship between load, F_N , and deformation, δ , of cylindrical joint clearance is obtained as shown in Eq. (13):

$$F_N = \frac{1}{2} \pi \delta E^* \sqrt{\frac{\delta}{2(R_i - R_j + \delta)}} \quad (13)$$

where E^* is compound elastic modulus in Eq. (13) and the expression is represented as

$$\frac{1}{E^*} = \frac{1 - v_i^2}{E_i} + \frac{1 - v_j^2}{E_j} \quad (14)$$

The above model is applied in contact analysis of revolute joint with both big clearance and small clearance. Compared to the results of finite element numerical calculation, this contact model has a better precision and a greater applicable scope than Hertz model [16].

Based on the improved elastic foundation model mentioned above, nonlinear stiffness coefficient is proposed in this paper. The nonlinear stiffness coefficient is found as the slope of the load–displacement relationship curve by improved elastic foundation model around the point of instantaneous deformation. Further, based on contact theory, nonlinear stiffness coefficient, K_n , is achieved from Eq. (13) as shown in Eq. (15):

$$K_n = \frac{1}{8} \pi E^* \sqrt{\frac{2\delta(3(R_i - R_j) + 2\delta)^2}{(R_i - R_j + \delta)^3}} \quad (15)$$

The nonlinear stiffness coefficient, K_n , is related to material property, geometry property, clearance size and deformation of contact bodies. It varies with δ and is not constant during the contact process.

Contact force model in clearance is improved by adding some form of damping force based on elastic contact force [23,28]. Further, the stiffness coefficient of Lankarani–Nikravesh model, K , as shown the Eq. (12) is modified by the nonlinear stiffness coefficient, K_n , so the modified damping coefficient is achieved as following:

$$D_{mod} = \frac{3K_n(1 - c_e^2)e^{2(1 - c_e)}\delta^n}{4\dot{\delta}^{(-)}} \quad (16)$$

where D_{mod} is the modified damping coefficient and it is related with the nonlinear stiffness coefficient, K_n .

Thus, it can be found that the modified damping coefficient, Eq. (16), introduced the ratio of nonlinear stiffness coefficient and stiffness coefficient of Lankarani–Nikravesh model, can be simply expressed as Eq. (17):

$$D_{mod} = \frac{K_n}{K} D_l \quad (17)$$

Based on the research above, a hybrid contact force model of Lankarani–Nikravesh model and the improved elastic foundation model is established with the framework of Lankarani–Nikravesh

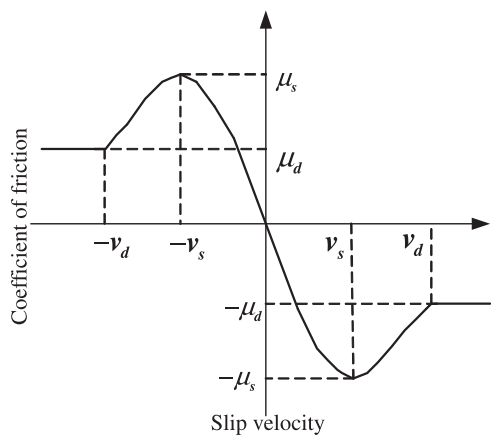


Fig. 5. Coefficient of friction vs. slip velocity.

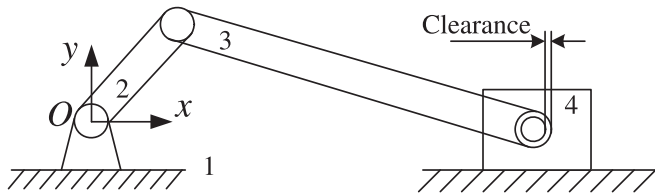


Fig. 6. Slider-crank mechanism with a clearance joint [28].

Table 1
Geometric and inertia properties of the slider-crank mechanism.

Body	Length (m)	Mass (kg)	Moment of inertia (kg m^2)
Crank	0.05	17.900	0.460327
Connection rod	0.3	1.130	0.015300
Sliding block	–	1.013	0.000772

Table 2
Simulation parameters for the slider-crank mechanism.

Restitution coefficient	0.46
Dynamic friction coefficient	0.01
Young's modulus	207 GPa
Poisson's ratio	0.3

model. Stiffness coefficient of the hybrid model is the nonlinear stiffness coefficient from the improved elastic foundation model. And the damping force applies in introducing the ratio of nonlinear stiffness coefficient from the improved elastic foundation model and contact stiffness coefficient of Lankarani–Nikravesh model, with the modified damping coefficient D_{mod} in the hybrid model.

Hence, the expression of hybrid contact force model of revolute joint with clearance is represented in Eq. (18):

$$F_{nmod} = K_n \delta^n + D_{mod} \dot{\delta} \quad (18)$$

where the elastic deformation force is represented by the first item of the right side of Eq. (18) and the energy losing is represented by the second item. δ is the deformation and $\dot{\delta}$ is the relative deformation velocity. K_n is the nonlinear stiffness coefficient and D_{mod} is the modified damping coefficient.

In most of the past literatures, contact stiffness and damping coefficient were calculated simply according to the impact situation of two sphere bodies or taken as a constant according to experience, which does not meet the actual situation. However, in the new contact force model, nonlinear stiffness coefficient is proposed based on contact theory and it is useful for calculating and determining stiffness coefficient. Besides, the nonlinear stiffness coefficient is related to material property, geometry property, clearance size and deformation of contact bodies. It varies with δ and is not constant during the contact process. Therefore, it is varies with condition process and it is more realistic. Besides, the hybrid contact force model of revolute joint is applicable for both big clearance and small clearance.

In addition, due to the coefficient of restitution, c_e , is closed to unity in Eq. (11) [22], the expression obtained is only with higher coefficient of restitution, and the calculation error is higher for the lower coefficient of restitution according to Schwab [9]. The new model contains modified damping coefficient, D_{mod} , which is not restricted by coefficient of restitution and it is applicable for both large and small coefficient of restitution. Therefore the new nonlinear contact force model describes the energy loss during contact process accurately for different coefficients of restitution and extends the application scope of coefficient of restitution. So the contact model is applicable to a wider range, and not only can be applied to higher coefficient of restitution, but also small coefficient of restitution.

Hereby, the hybrid contact force model is a new nonlinear continuous contact force model, which combines Lankarani–Nikravesh model and the improved elastic foundation model. It extends contact modelling of clearance in revolute joints and has a greater applicable scope.

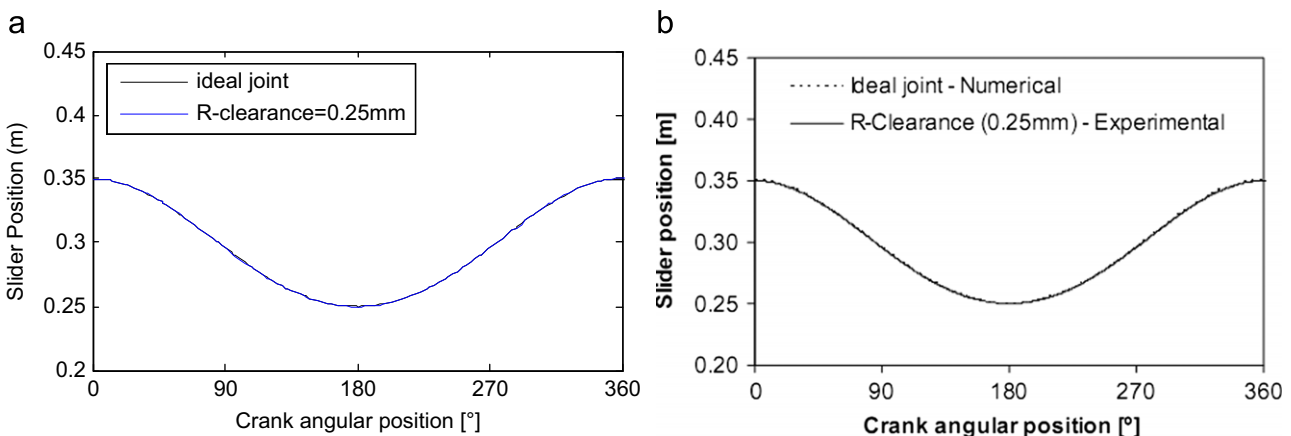


Fig. 7. Numerical and experimental slider position for clearance size equal to 0.25 mm: (a) simulation results based on the hybrid contact model in present work; (b) experimental results from Flores [28].

4. Friction force model of revolute joint with clearance

The tangential contact characteristic of clearance is represented using tangential friction force model. The most famous one is Coulomb friction model, which is used to represent the

friction response in impact and contact process. In this paper, a modified Coulomb friction model is used to represent the friction response between the journal and bearing. Friction coefficient, which is not a constant, is introduced in the modified Coulomb friction model. Friction coefficient is a function of tangential

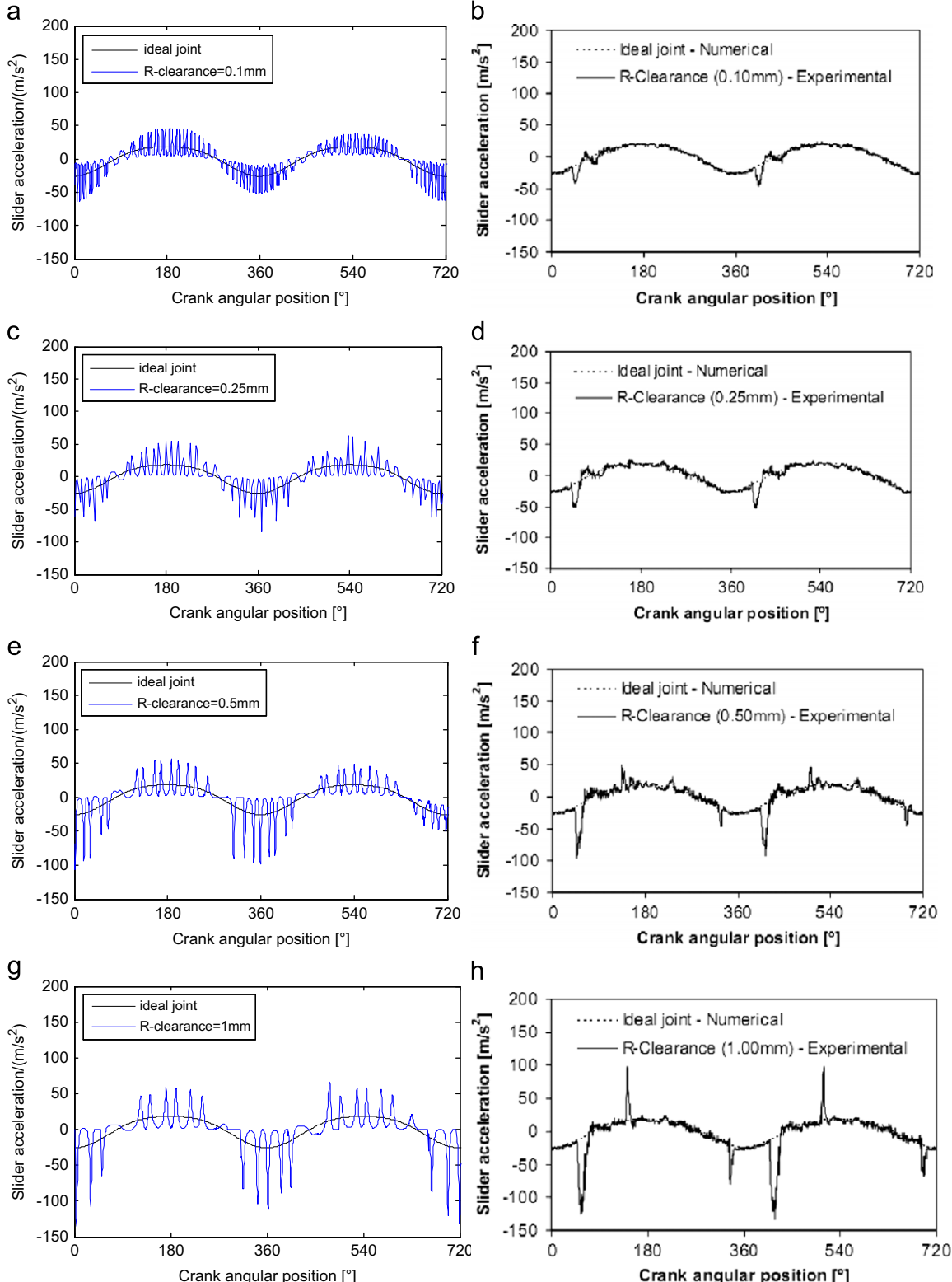


Fig. 8. Numerical and experimental slider acceleration for crank speed of 200 rpm and different clearance sizes: (a) and (b) $c=0.1$ mm; (c) and (d) $c=0.25$ mm; (e) and (f) $c=0.5$ mm; (g) and (h) $c=1.0$ mm. (a), (c), (e), and (g) are the numerical simulation results based on the hybrid contact model in present work; (b), (d), (f), and (h) are the experimental results from Flores [28].

sliding velocity, which can represent the friction response in impact and contact process as well as the viscous and micro-slip phenomenon in relative low-velocity case more accurately. And also, the modified Coulomb friction model can avoid the case of abrupt change of friction in numerical calculation as the change of velocity direction.

The expression of tangential friction force is shown as Eq. (19):

$$F_t = -\mu(v_t)F_n \frac{v_t}{|v_t|} \quad (19)$$

where, friction coefficient $\mu(v_t)$ is a function of tangential sliding velocity and which can be expressed as

$$\mu(v_t) = \begin{cases} -\mu_d \text{sign}(v_t) & \text{for } |v_t| > v_d \\ -\left\{ \mu_d + (\mu_s - \mu_d) \left(\frac{|v_t| - v_s}{v_d - v_s} \right)^2 [3 - 2 \left(\frac{|v_t| - v_s}{v_d - v_s} \right)] \right\} \text{sign}(v_t) & \text{for } v_s \leq |v_t| \leq v_d \\ \mu_s - 2\mu_s \left(\frac{v_t + v_s}{2v_s} \right)^2 \left(3 - \frac{v_t + v_s}{v_s} \right) & \text{for } |v_t| < v_s \end{cases} \quad (20)$$

where v_t is relative sliding velocity in the collision point of journal and bearings, which is the velocity component in tangential direction. μ_d is dynamic friction coefficient. μ_s is static friction coefficient. v_s is critical velocity of static friction. v_d is critical velocity of the maximum dynamic friction. The function curve of dynamic friction coefficient is shown as Fig. 5.

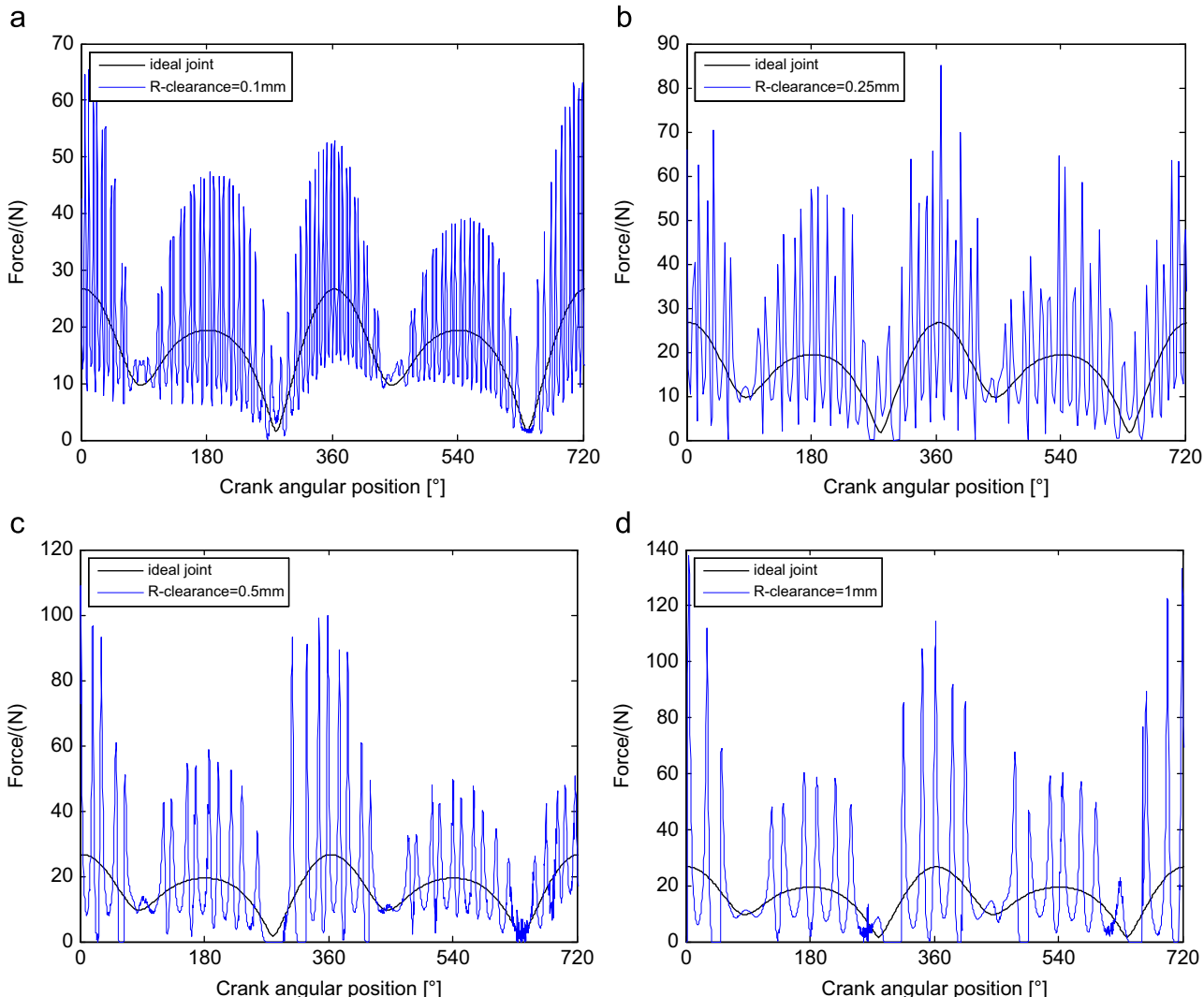


Fig. 9. Contact force in joint based on the hybrid contact model in present work ((a) $c=0.1$ mm; (b) $c=0.25$ mm; (c) $c=0.5$ mm; (d) $c=1.0$ mm.).

5. Demonstrative application example 1: slider-crank mechanism

In this section, the slider-crank mechanism [28] is used to demonstrate and validate the hybrid contact model presented in this paper. The dynamic responses obtained with experimental slider-crank setup are compared with that of the numerical models. Fig. 6 depicts the kinematic configuration of the slider-crank mechanism, which consists of four bodies, including ground, two ideal revolute joints, and one ideal translational joint. A revolute clearance joint exists between the connecting rod and slider. In order to keep the analysis simple and to illustrate the dynamic behaviour, all the bodies are considered to be rigid. The length and inertia properties of the slider-crank mechanism components are listed in Table 1 and the parameters used in dynamic simulations are given in Table 2.

5.1. Simulation and validate with different clearance size

In the dynamic simulation, crank is the driving body and rotates with a constant angular velocity equal to 200 rpm. The initial configuration corresponds to crank and connecting rod collinear and the position and velocity of journal centres are taken to be zero. Initially, the journal and bearing centres are coincident. Note that the results are plotted against those

obtained for ideal joint, being reported for the two full crank rotations after steady-state has been reached.

The simulation results are compared with the experimental results from Flores [28]. The simulation and experimental results are as following.

Figs. 7 and 8 show that the numerical simulations results based on the hybrid contact model in present work agrees quite well with experimental tests with different clearance sizes, suggesting that the proposed hybrid contact model is a reasonable and precise approach to model mechanical systems with revolute clearance joint.

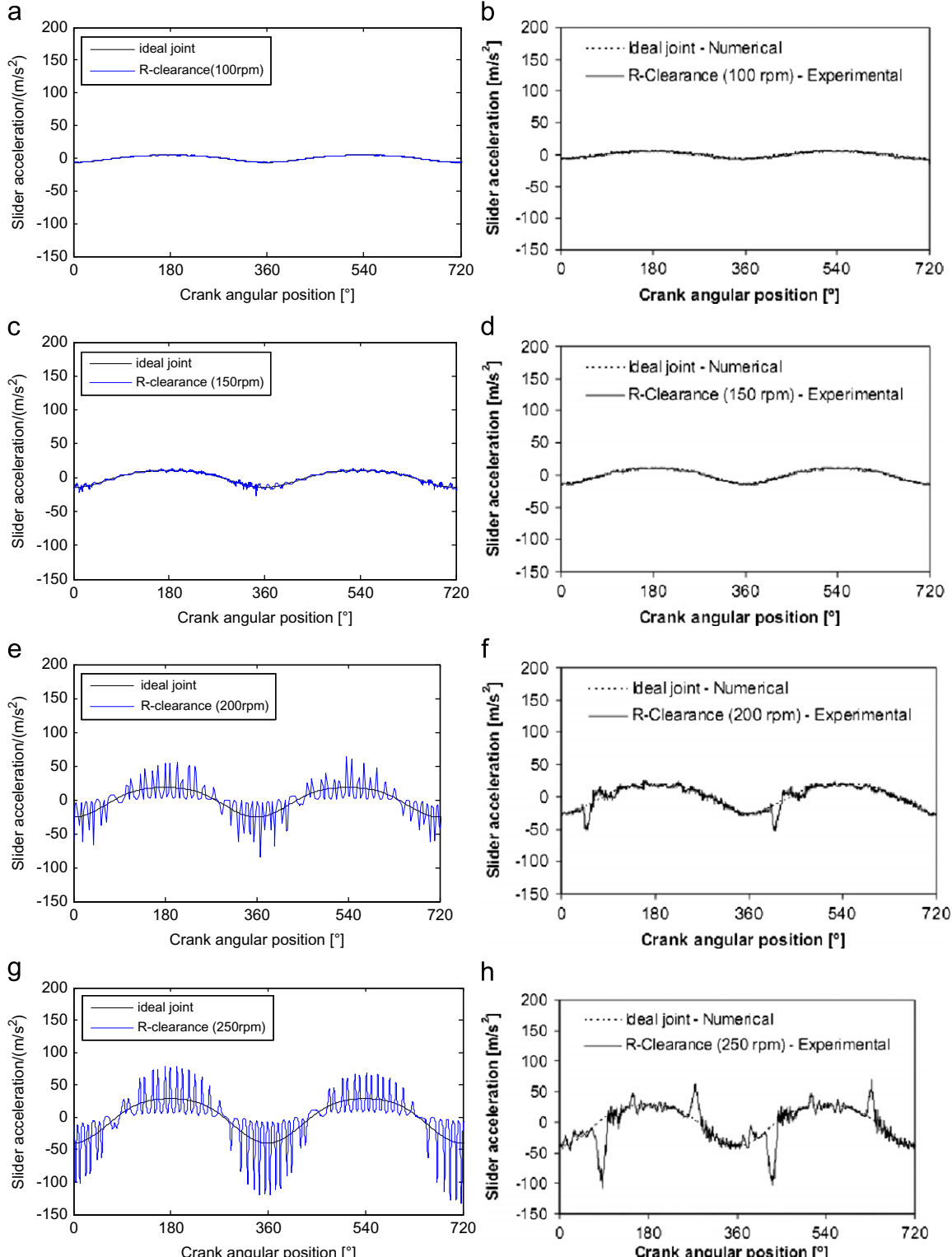


Fig. 10. Numerical and experimental slider acceleration for clearance size of 0.25 mm and different driving velocities: (a) and (b) 100 rpm; (c) and (d) 150 rpm; (e) and (f) 200 rpm; (g) and (h) 250 rpm. (a), (c), (e), and (g) are the numerical simulation results based on the hybrid contact model in present work; (b), (d), (f), and (h) are the experimental results from Flores [28].

Fig. 7 shows that the position of the slider is not greatly affected by the clearance. **Fig. 8** shows that the effects of clearance on the acceleration of slider-crank mechanism are extraordinarily obvious. The acceleration of slider-crank mechanism with clearance is obviously shaking and the amplitude is increased from the slider-crank mechanism without clearance, which indicates that the existence of clearance will lead to oscillation of the slider-crank mechanism.

The differences between the experimental and numerical system response, plotted in **Figs. 7 and 8** are resulted from the assumptions made in the formulation for the mathematical model of clearance joints, namely in what concerns to the joints flexibility, which was ignored. Furthermore, misalignment between journal and bearing elements, always present in actual mechanical systems, were not considered in the numerical simulations [28]. Another important feature in the numerical simulations is the choice of the restitution and friction coefficients. However, in present work, the choice of the restitution and friction coefficients were based on the best published data.

Fig. 9 shows that the contact force curve in revolute joint based on the hybrid contact model. As shown in **Fig. 9**, the existence of clearance leads to the impact force in joint increase, and the impact force is high-frequency oscillation. And it indicates the higher size of clearance, the higher contact force and

lower contact frequency. The same phenomena can be observed in the curve of slider acceleration represented in **Fig. 8**.

It can be found that, the hybrid contact model of revolute joint with clearance in present work agrees quite well with experimental tests, and describes the contact process of revolute joint with clearance reasonably. And it describes the contact features in clearance and the dynamic characteristic of mechanism precisely. The effects of clearance on the dynamic characteristic of mechanism cannot be ignored, and the existence of clearance causes oscillation of the acceleration and decrease of the motion stability. In addition, it causes the impact force increase and the impact force is high frequency oscillation. When increase the clearance size, the impact force is larger but the impact frequency is lower.

Further, the simulation results based on the hybrid contact force model are compared to other studies from previous literatures [4,6,7,9,13,28], in which the research results also showed that clearance had important effects on the dynamics characteristics of mechanical systems and bigger size of clearance caused higher peaks of impact force and worse characteristics of the systems. So the simulation results based on the new contact force model are validated by other data published on the field on dynamics of multibody systems with clearance joints. The fact that the existence of the clearance joint has an important effect on the slider acceleration supports the idea that the model of

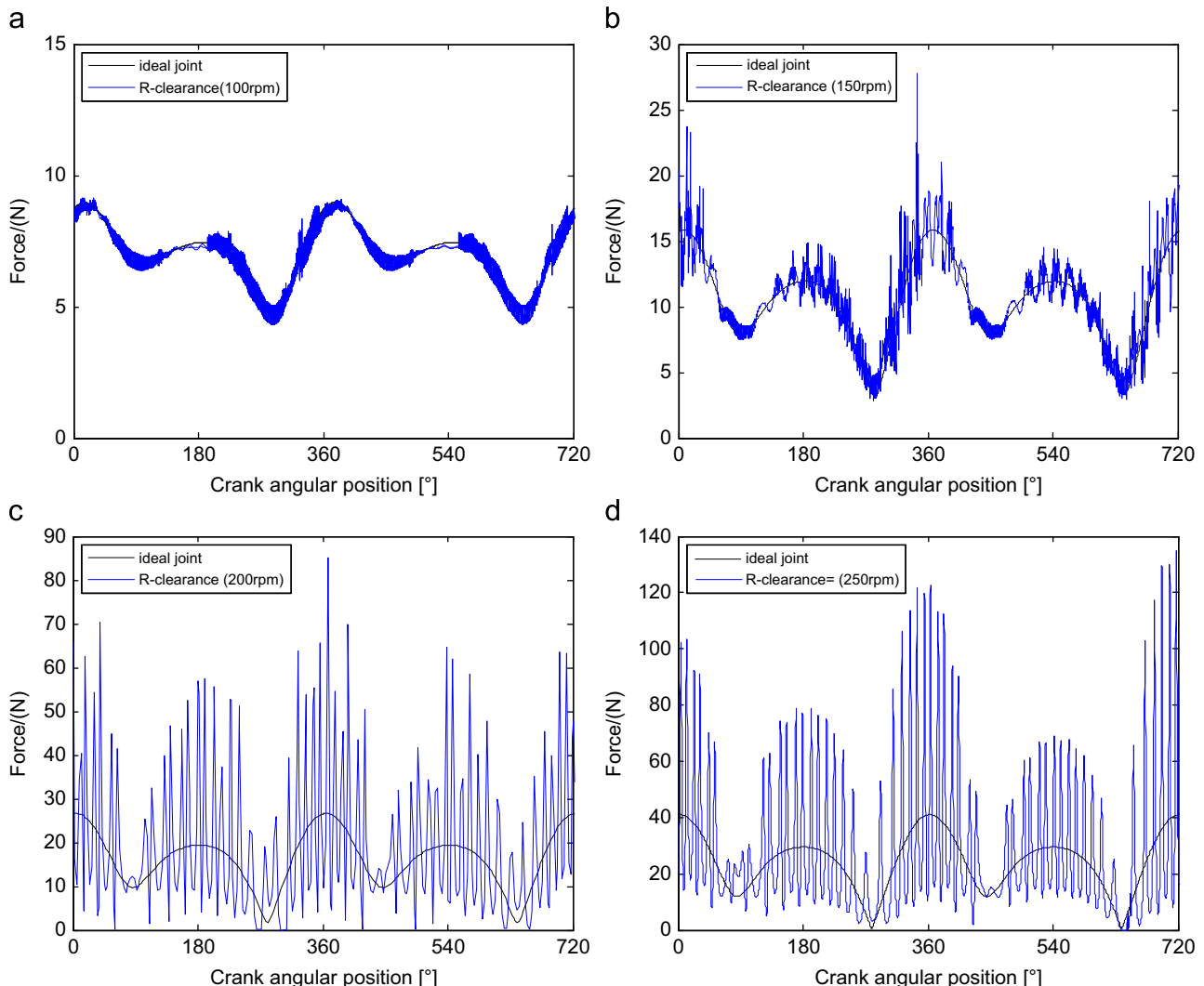


Fig. 11. Contact force in clearance joint ((a) 100 rpm; (b) 150 rpm; (c) 200 rpm; (d) 250 rpm.).

clearance joints must be considered in the analysis and design of the real mechanical system.

5.2. Simulation and validate with different crank driving velocities

In the dynamic simulation, the driving body is crank, which rotates with a constant angular velocity. The initial angular velocities are 100 rpm, 150 rpm, 200 rpm and 250 rpm, respectively. The initial clearance size is 0.25 mm.

The initial configuration corresponds to crank and connecting rod collinear and the position and velocity of journal centres are taken to be zero. Initially, the journal and bearing centres are coincident. Note that the results are plotted against those obtained for ideal joint, being reported for the two full crank rotations after steady-state has been reached.

The simulation results are compared with the experimental results from Flores [28]. The simulation and experimental results are as following.

Fig. 10 shows that the numerical simulation results based on the hybrid contact model in present work agrees quite well with experimental tests with different driving velocities, suggesting that the proposed hybrid contact model is a reasonable approach to model mechanical systems with revolute clearance joint.

Fig. 10 shows that the effects of clearance on the acceleration of slider-crank mechanism are slight when the driving velocity is low. However, as the driving velocity increase, the effects of clearance on the acceleration of slider-crank mechanism are more severe. The higher driving velocity, the more obvious shake and higher amplitude of acceleration, which is agrees quite well with experimental tests.

Further, the simulation results are compared to other studies from previous literatures [4,13,23,28,33], in which the research results also showed that clearance had important effects on the dynamics characteristics of mechanical systems and higher speed of crank caused higher peaks of impact force and the characteristics of the systems were worse. So the simulation results based on the new contact force model are validated by other data published on the field on dynamics of mechanical systems with clearance joints. The fact that the existence of the clearance joint has an important effect on the slider acceleration supports the idea that the model of clearance joints must be considered in the analysis and design of the real mechanical system.

The differences between the experimental and numerical system response, plotted in **Fig. 10** are resulted from the assumptions made in the formulation for the mathematical model of clearance joints, namely in what concerns to the joints flexibility, which was ignored. Furthermore, misalignment between journal and bearing elements, always exist in actual mechanical systems, were not considered in the numerical simulations [28]. Another important feature in the numerical simulations is the choice of the restitution and friction coefficients. However, in present work, the choice of the restitution and friction coefficients were based on the best published data.

Fig. 11 shows that the contact force curve in revolute joint based on the hybrid contact model. As shown in **Fig. 11**, the existence of clearance leads to the impact force in the joint increase, and the impact force is high-frequency oscillation. And it indicates the higher driving angular velocity of crank, the higher contact force. The same phenomena can be observed in the curve of slider acceleration represented in **Fig. 10**.

It can be found that, the hybrid contact model of revolute joint with clearance in present work agrees quite well with experimental tests, and describes the contact process of revolute joint with clearance reasonably. And it describes the contact features in clearance and the dynamic characteristic of mechanism precisely. The effects of clearance on the dynamic characteristic of mechanism

cannot be ignored, and the existence of clearance causes oscillation of the acceleration and decrease of the motion stability. In addition, it causes the impact force increase and the impact force is high frequency oscillation. When the driving angular velocity of crank increasing, the impact force in clearance increases.

The simulation results based on the hybrid contact model for mechanism with joint clearance agree quite well with experimental tests and indicate that:

- (1) The proposed hybrid contact force model is a reasonable approach to model mechanical systems with revolute clearance joint, and it reflects the contact characterizers of joint clearance and dynamic response of mechanism accurately.
- (2) The effects of clearance on dynamic behaviour of mechanism cannot be ignored. The acceleration of mechanism with clearance is obviously shaking and the amplitude increases from the mechanism without clearance, which indicates that the existence of clearance will lead to oscillation of the mechanism. Besides, the existence of clearance leads to impact force in joint increase, and the impact force is high-frequency oscillation. And it indicates the higher size of clearance and higher velocity, the higher contact force in the clearance joint.

Numerical example of slider-crank mechanism is presented and compared to experimental tests and other data published on

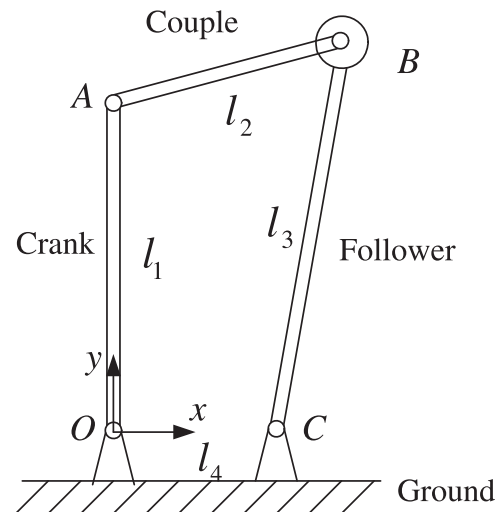


Fig. 12. Four-bar mechanism with a clearance joint between couple and follower (joint B).

Table 3
Geometric and inertia properties of the four-bar mechanism.

Body	Length (m)	Mass (kg)	Moment of inertia (kg m^2)
Crank	0.55	3.6235	0.10214
Couple	0.36	2.4394	0.031428
Follower	0.64	4.1894	0.15796
Ground	0.21	-	-

Table 4
Simulation parameters for the four-bar mechanism.

Restitution coefficient	0.9
Dynamic friction coefficient	0.1
Young's modulus	207 GPa
Poisson's ratio	0.3

the field on dynamics of mechanical systems with clearance joints for two cases: different clearance sizes and different crank driving velocities. The main advantages of the new hybrid contact force model are its accuracy and reality of contact analysis in joint clearance as well as dynamics behaviour analysis of mechanical systems. It combines Lankarani–Nikravesh model and the improved elastic foundation model by introducing the nonlinear stiffness coefficient and the modified damping coefficient. And it is not restricted by clearance size and coefficient of restitution. The hybrid contact model can effectively describe the dynamic behaviour of mechanism with clearance and extend the contact modelling of clearance in revolute joints.

6. Demonstrative application example 2: four-bar mechanism

In this section, the academic planar four-bar mechanism is used to illustrate the dynamic behaviour of revolute clearance joints in mechanical system. The four-bar mechanism consists of four rigid bodies that represent the crank, coupler, follower and ground. Fig. 12 depicts the kinematic configuration of the four-bar mechanism. The joints of this mechanism include three ideal

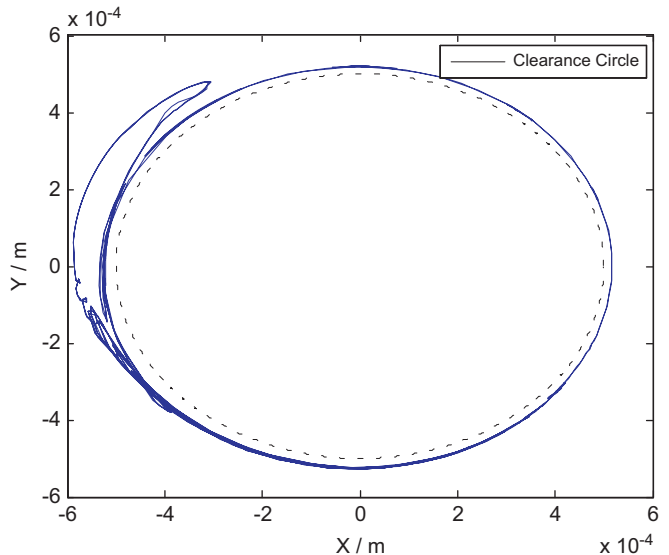


Fig. 14. Journal centre orbit relative to the bearing centre.

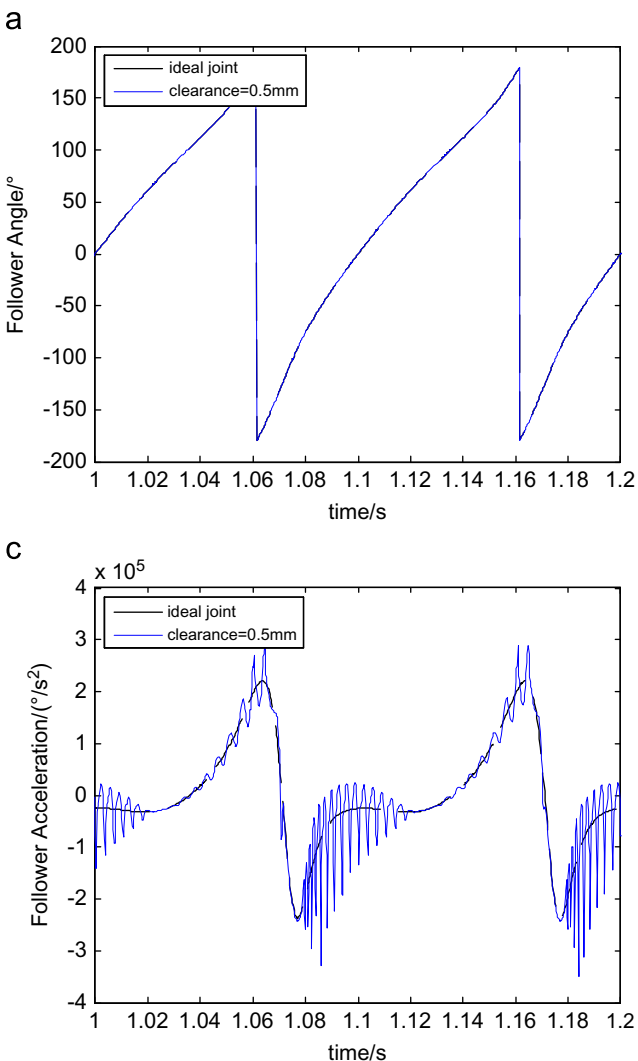


Fig. 13. Dynamic behaviour of mechanism with joint clearance ((a) follower angle displacement; (b) follower angular velocity; (c) follower angular acceleration; (d) crank moment required to maintain the crank angular velocity constant).

revolute joints connecting the ground to the crank, the crank to the coupler and the ground to the follower. A revolute joint with clearance exists between the couple and follower, in which the clearance is zoomed-in. The length and inertia properties of the four-bar mechanism components are listed in Table 3 and the parameters used in the dynamic simulations are given in Table 4.

In the dynamic simulation, the crank is the driving link and rotates at a constant angular velocity of 600 rpm. The initial configuration corresponds to crank and ground is vertical and initial angular velocity is zero. Initially, the journal and bearing centres are coincident. In order to analyse the dynamic behaviour of the system, long time simulations are performed and the results presented below are plotted against to full crank rotations after steady-state has been reached.

The dynamic behaviour of the four-bar mechanism is obtained and represented in Fig. 13. Two different kinds of results are presented. One is all the joints of four-bar mechanism are considered as ideal, in which no clearances exist. The other is the mechanism is simulated with a revolute joint clearance, which between couple and follower (as shown in Fig. 12). Figs. 13(a)–(c) by the time plots are the angle displacement, velocity and acceleration of the follower, respectively. The moment acting on the crank, which is required to maintain the crank angular velocity constant, is represented in Fig. 13(d). The relative motion between the journal

and bearing centres is plotted in Fig. 14. Note that results are plotted against those obtained for ideal joints, being reported for two full crank rotations after steady-state has been reached.

Fig. 13(a) shows that the angle displacement curves of follower are almost completely a coincidence between the ideal mechanism without clearance and real mechanism with clearance. Fig. 13(b) shows that the angular velocity of follower is not greatly affected by the existence of the joint clearance. It indicates that clearance has less effect on angular velocity of follower. However, in contrast to the follower angle displacement and angular velocity, the angular acceleration of the follower shows significant differences between the dynamic behaviour of the mechanism when modelled with and without joint clearance, as shown in Fig. 13(c). The existence of clearance affects the angular acceleration of follower by leading to vibration. The sudden changes in angular acceleration of follower are due to the impact between the journal and bearing for the clearance joint. The angular acceleration of follower with clearance is obviously shaky and presents high peaks of its values, which indicates that, when considering the clearance, the existence of clearances will cause oscillation of the four-bar mechanism and influence the dynamic behaviour of the system. The same phenomena can be observed in the curve of crank moment, which is required to maintain the crank angular velocity constant, presented in Fig. 13(d). Furthermore, the system's

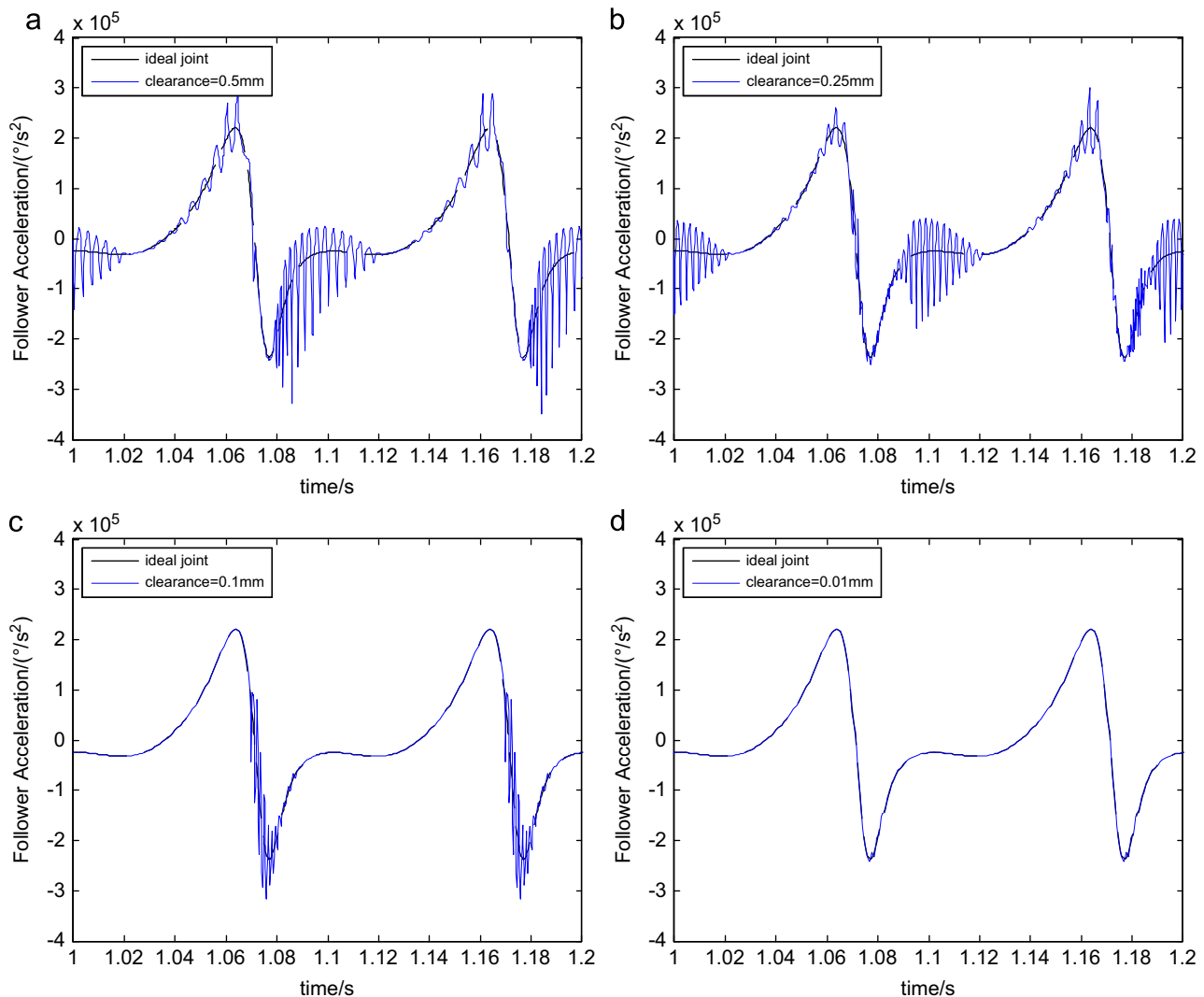


Fig. 15. Acceleration of follower with different clearance sizes ((a) $c=0.5$ mm; (b) $c=0.2$ mm; (c) $c=0.1$ mm; (d) $c=0.01$ mm).

response repeats itself from cycle to cycle clearly. Fig. 14 shows that the journal is always in contact with the bearing wall. This observation is logical since the two bodies are moving in the same direction [34].

Further, the effects of the clearance size and friction effect are studied separately. Clearance size is one of the most important parameters that affect the dynamic behaviour of mechanical system. In the first case, the dynamics simulation of four-bar mechanism with different clearance sizes is carried out to analyse the effects of clearance size on dynamics behaviour of four-bar mechanism. The values of the clearance size are considered as 0.5, 0.25, 0.1 and 0.01 mm. Fig. 15 presents the effects of clearance size on angular acceleration of follower. The angular accelerations tend to be close to those obtained for ideal joint when clearance size is reduced. However, when the clearance size is increased the dynamic characteristics of mechanism are changed obviously, which is represented by shaky with higher peaks. It also shows that the higher size of clearance, the more obvious shake and higher peaks of angular acceleration of follower. The same conclusion can be drawn from Fig. 16, where the crank moment, which is required to maintain the crank angular velocity constant, is presented.

In the second case, the dynamics simulation of four-bar mechanism is carried out, in which the friction phenomenon is included in the dynamics of the revolute clearance joint. The clearance size is considered as 0.5 mm and four different values

for dynamic friction coefficient are used, which are 0.05, 0.1, 0.15 and 0.2. The angular accelerations of follower are presented in Fig. 17. It is shown that when the dynamic friction coefficient increases, the dynamics response of mechanism is less shaky. And for low value of friction coefficient, the system response is changed obviously, which is represented by shaky with higher peaks. It also shows that the lower value of the dynamic friction coefficient, the more obvious shake and higher peaks of angular acceleration of follower. However, when the value of the dynamic friction coefficient is higher, the dynamics response of mechanism is less shaky. The same conclusion can be drawn from Fig. 18, where the crank moment, which is required to maintain the crank angular velocity constant, is presented. It can be concluded that the increase of dynamic friction coefficient leads to a better response of the mechanical system. The reason is that friction can dissipate energy during the work process of mechanism, when the dynamic friction coefficient is higher, the energy dissipation of the system is more rapid, thus the mechanism is less shaky.

In addition, the simulation results based on the new hybrid contact force model are compared to other studies from previous literatures [3,17,34–36], in which the research results also showed that clearance had important effects on the dynamics characteristics of mechanical systems, and clearance size as well as friction effect played important roles that affect the dynamic behaviour of mechanical system. So the simulation results based

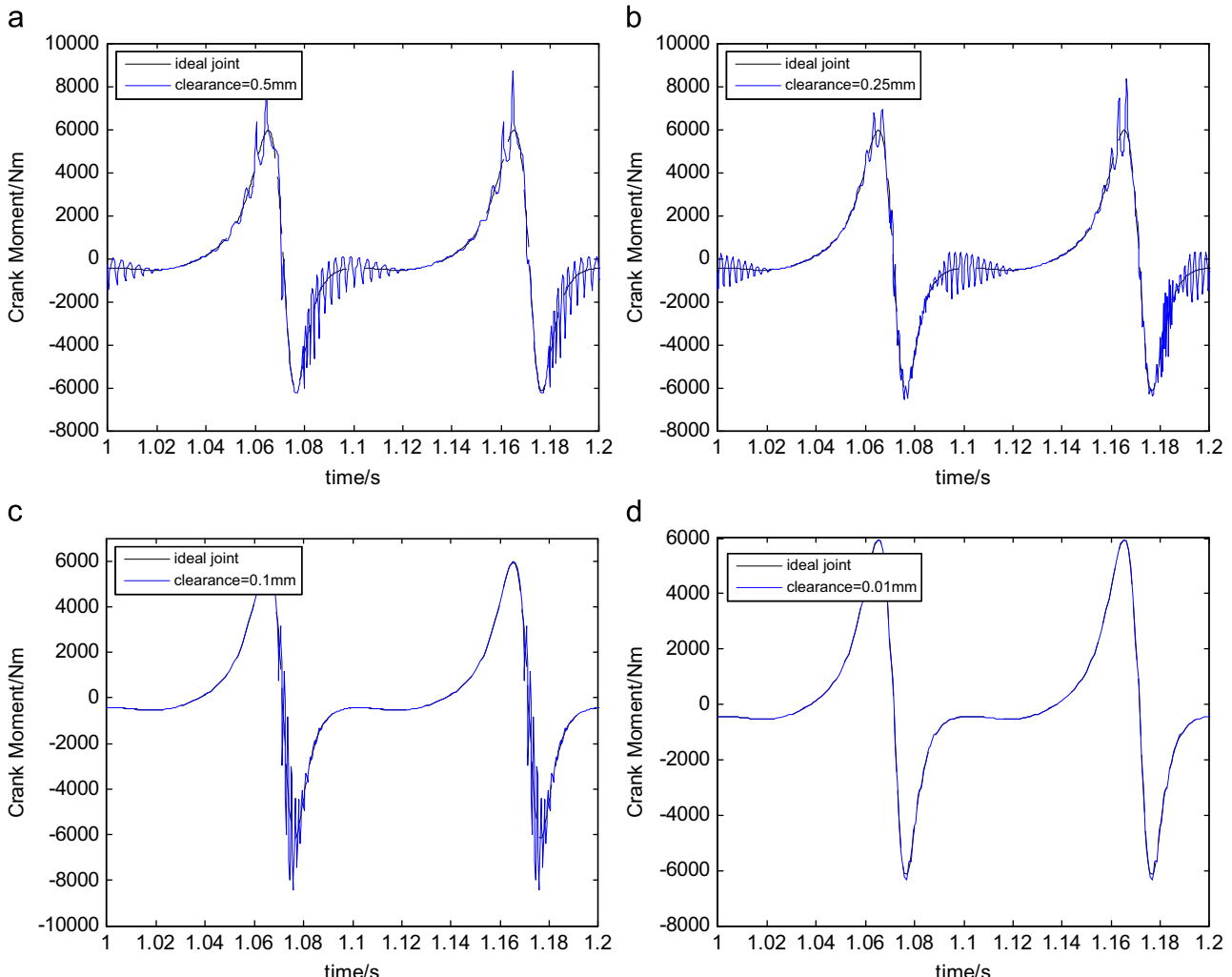


Fig. 16. Crank moment with different clearance sizes ((a) $c=0.5$ mm; (b) $c=0.2$ mm; (c) $c=0.1$ mm; (d) $c=0.01$ mm).

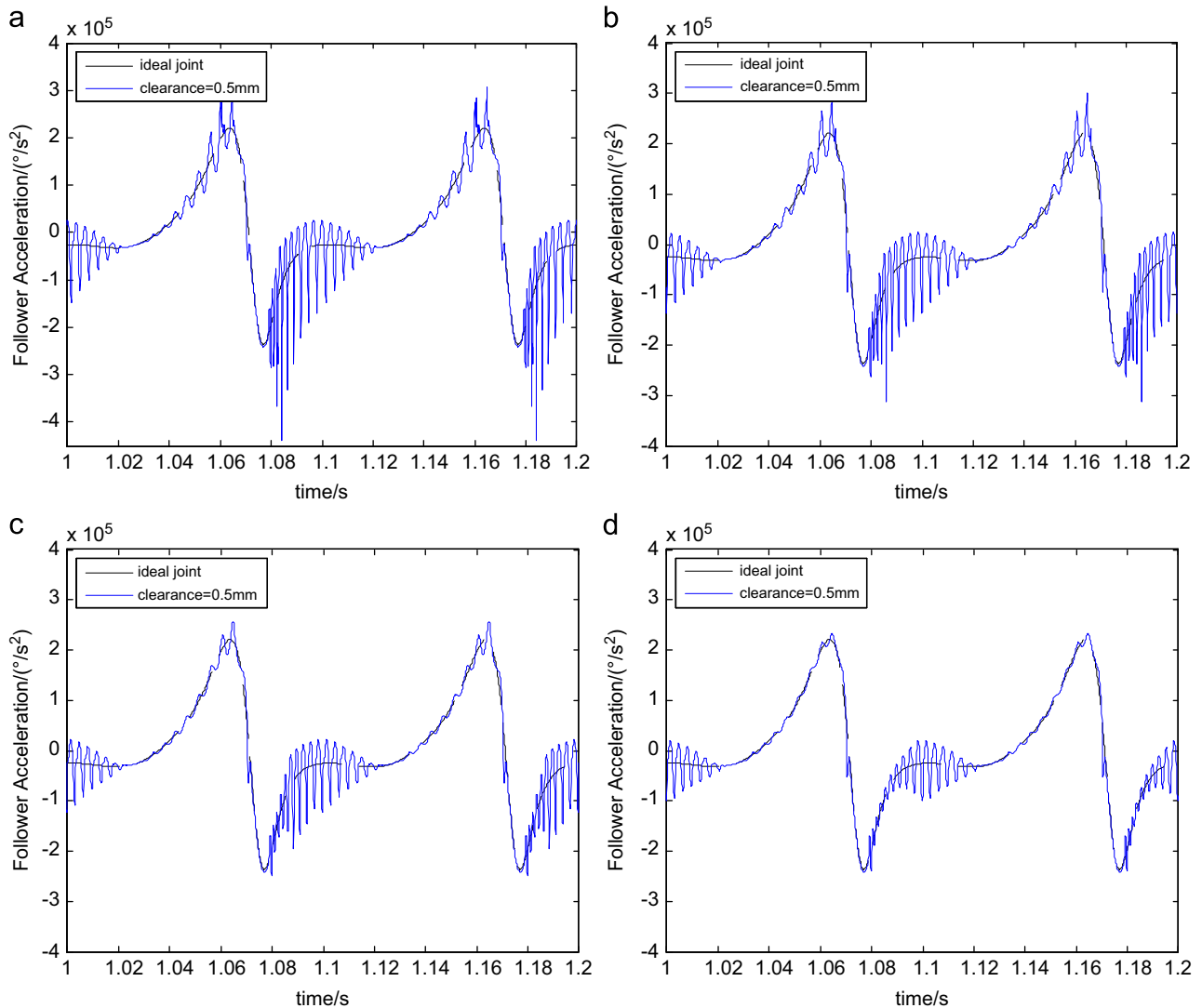


Fig. 17. Acceleration of follower with different dynamic friction coefficients ((a) 0.05; (b) 0.1; (c) 0.15; (d) 0.2).

on the new contact force model are validated by other data published on the field on dynamics of multibody systems with clearance joints. The fact that the existence of the clearance joint has an important effect on the dynamics response of the mechanical systems supports the idea that the model of clearance joints must be considered in the analysis and design of the real mechanical system. The new hybrid contact force model and modified Coulomb friction model can effectively describe the dynamic behaviour of mechanism with different clearance sizes as well as different friction effects.

7. Conclusions

This work studies the dynamic behaviour of mechanical systems with revolute clearance joint based on a new nonlinear continuous contact force model. The study performs of the dynamic behaviour analysis of mechanical systems including revolute joints with clearance using a computational methodology. The contact model in revolute joint clearance is established using a new nonlinear continuous contact force model, which is a hybrid model of Lankarani–Nikravesh model and the improved elastic foundation model. And the tangential contact is represented using a modified Coulomb friction model.

Numerical results for two simple planar mechanisms with revolute clearance joints are presented and discussed. The correctness and validity of the new contact force model of revolute joint clearance is verified through the demonstrative application examples. The numerical simulation results based on the hybrid contact force model agrees quite well with experimental tests, suggesting that the proposed hybrid contact model is a reasonable approach to model mechanical systems with revolute clearance joint. And it is shown that the presented hybrid contact force model is a new and effective method to predict the dynamic characteristics of mechanism with clearance in revolute joints. The hybrid contact model can effectively describe the dynamic behaviour of mechanism with clearance and extend the contact modelling of clearance in revolute joints.

The effects of clearance on dynamic behaviour of mechanism cannot be ignored. The existence of clearance leads to impact force in joint increase and the impact force is high-frequency oscillation. The acceleration of mechanism with clearance is obviously shaking and the amplitude increases from the mechanism without clearance, which indicates that the existence of clearance will lead to shaky of the mechanism with high peaks.

In addition, the clearance size and friction effects are analysed separately. The results show that when the clearance size is increased the dynamic characteristics of mechanism are changed

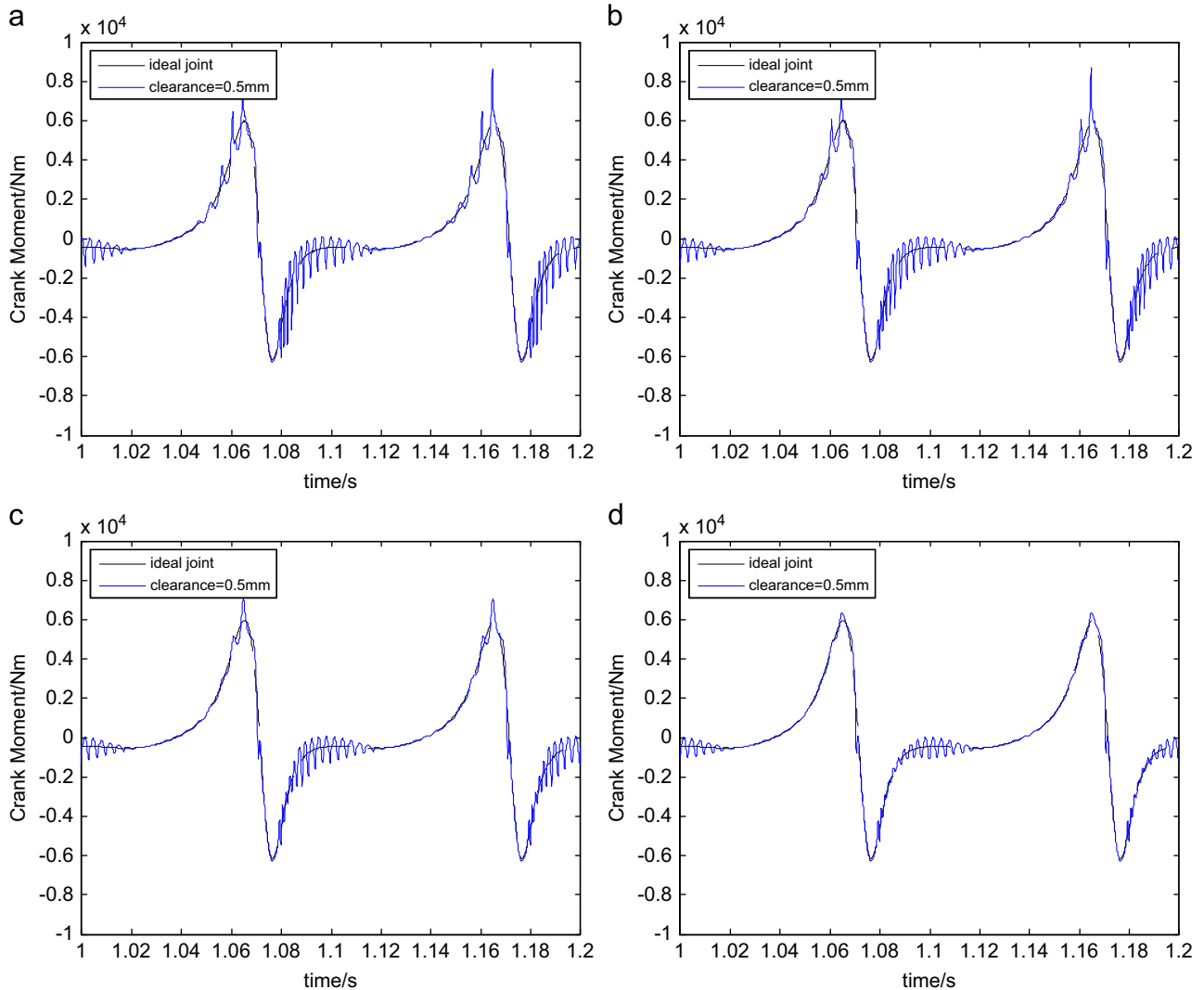


Fig. 18. Crank moment with different dynamic friction coefficients ((a) 0.05; (b) 0.1; (c) 0.15; (d) 0.2).

obviously and higher size of clearance, more obvious shake and higher peaks of angular acceleration of mechanism. And it indicates the higher size of clearance, the higher contact force and lower contact frequency. The results also show that when the dynamic friction coefficient increases, the dynamics response of mechanism is less shaky. It indicates that the lower value of the dynamic friction coefficient, the more obvious shake and higher peaks of acceleration of mechanism. It can be concluded that the increase of dynamic friction coefficient leads to a better response of the mechanical system.

In this study, only one joint is considered as imperfect and exists clearance. But, it is realized that the increased number of revolute joint with clearance makes the dynamic behaviour of mechanical systems worse. More applications and tests of the hybrid contact force model need further study, particularly for the three-dimensional case. The dynamic behaviour analysis of mechanical systems considering clearance joints is the basis of precision analysis, design of mechanical systems.

Acknowledgements

This work was supported by the National Natural Science Foundation of China (Grant nos.: 50975056 and 11072066).

References

- [1] Flores P, Ambrosio J, Claro JCP, Lankarani HM, Koshy CS. A study on dynamics of mechanical systems including joints with clearance and lubrication. *Mech Mach Theory* 2006;41:247–61.
- [2] Erkaya S, Uzmay I. A neural-genetic (NN-GA) approach for optimizing mechanisms having joints with clearance. *Multibody Syst Dyn* 2008;20(1):69–83.
- [3] Flores P. Modeling and simulation of wear in revolute clearance joints in multibody systems. *Mech Mach Theory* 2009;44(6):1211–22.
- [4] Flores P. A parametric study on the dynamic response of planar multibody systems with multiple clearance joints. *Nonlinear Dyn* 2010;61:633–53.
- [5] Garcia OJC. Analysis of clearance in multibody system. *Multibody Syst Dyn* 2005;13:401–20.
- [6] Erkaya S, Uzmay I. Experimental investigation of joint clearance effects on the dynamics of a slider-crank mechanism. *Multibody Syst Dyn* 2010;24:81–102.
- [7] Bauchau OA, Rodriguez J. Modeling of joints with clearance in flexible multibody system. *Int J Solids Struct* 2002;34:41–63.
- [8] Flores P, Ambrósio J. On the contact detection for contact-impact analysis in multibody systems. *Multibody Syst Dyn* 2010;24(1):103–22.
- [9] Schwab AL, Meijaard JP, Meijers PA. Comparison of revolute joint clearance model in the dynamic analysis of rigid and elastic mechanical systems. *Mech Mach Theory* 2002;37(9):895–913.
- [10] Ting KL, Zhu JD, Watkins D. The effects of joint clearance on position and orientation deviation of linkages and manipulators. *Mech Mach Theory* 2000;35:391–401.
- [11] Tian Q, Zhang YQ, Chen LP, Flores P. Dynamics of spatial flexible multibody systems with clearance and lubricated spherical joints. *Comput Struct* 2009;87:913–29.
- [12] Stoenescu ED, Marghitu DB. Dynamic analysis of a planar rigid-link mechanism with rotating slider joint and clearance. *J Sound Vib* 2003;266:394–404.

- [13] Khemili I, Romdhane L. Dynamic analysis of a flexible slider-crank mechanism with clearance. *Eur J Mech A/Solids* 2008;27:882–98.
- [14] Zhao Y, Bai ZF. Dynamics analysis of space robot manipulator with joint clearance. *Acta Astronaut* 2011;68:1147–55.
- [15] Flores P, Ambrósio J, Claro JP. Dynamic analysis for planar multibody mechanical systems with lubricated joints. *Multibody Syst Dyn* 2004;12:47–74.
- [16] Liu CS, Zhang K, Yang R. The FEM analysis and approximate model for cylindrical joints with clearances. *Mech Mach Theory* 2007;42:183–97.
- [17] Rhee J, Akay A. Dynamic response of a revolute joint with clearance. *Mech Mach Theory* 1996;31(1):121–34.
- [18] Flores P, Ambrósio J, Claro JCP, Lankarani HM. Dynamics of multibody systems with spherical clearance joints. *J Comput Nonlinear Dyn* 2006;1(3):240–7.
- [19] Bauchau OA, Ju CK. Modeling friction phenomena in flexible multibody dynamics. *Comput Methods Appl Mech Eng* 2006;195:6909–24.
- [20] Shi B, Jin Y. Dynamic analysis of the reheat-stop-valve mechanism with revolute clearance joint in consideration of thermal effect. *Mech Mach Theory* 2008;43(12):1625–38.
- [21] Ravn PA. Continuous analysis method for planar multibody systems with joint clearance. *Multibody Syst Dyn* 1998;2:1–24.
- [22] Lankarani HM, Nikravesh PEA. Contact force model with hysteresis damping for Impact analysis of multibody systems. *ASME J Mech Des* 1990;112:369–76.
- [23] S.K. Cherian, Characterization of mechanical systems with real joints and flexible links. Ph.D. thesis. Wichita State University; 2006.
- [24] Johnson KL. Contact Mechanics. London: Cambridge University Press; 1992.
- [25] Liu CS, Zhang K, Yang L. Normal force-displacement relationship of spherical joints with clearances. *Trans. ASME, J Comput Nonlinear Dyn* 2006;1:160–7.
- [26] Ciavarella M, Decuzzi P. The state of stress induced by the plane frictionless cylindrical contact 1: the case of elastic similarity. *Int J Solids Struct* 2001;38:4507–23.
- [27] Ciavarella M, Decuzzi P. The state of stress induced by the plane frictionless cylindrical contact 2: the general case (elastic dissimilarity). *Int J Solids Struct* 2001;38:4523–33.
- [28] Flores P. Dynamic analysis of mechanical systems with imperfect kinematic joints. Ph.D. thesis. Universidade Do Minho; 2004.
- [29] Mukras S, Kim NH, Mauntler NA, Schmitz TL, Sawyer WG. Analysis of planar multibody systems with revolute joint wear. *Wear* 2010;268:643–52.
- [30] Flores P, Ambrosio J, Claro JCP, Lankarani HM. Influence of the contact-impact force model on the dynamic response of multibody systems. *Proc Inst Mech Eng, Part-K: J Multi-body Dyn* 2006;220(1):21–34.
- [31] Tian Q, Zhang YQ, Chen LP, Yang JZ. Simulation of planar flexible multibody systems with clearance and lubricated revolute joints. *Nonlinear Dyn* 2010;60(4):489–511.
- [32] Qin ZY, Lu QS. Analysis of impact process model based on restitution coefficient. *J Dyn Control* 2006;4(4):294–8.
- [33] Flores P, Koshy CS, Lankarani HM, Ambrósio J, Claro JCP. Numerical and experimental investigation on multibody systems with revolute clearance joints. *Nonlinear Dyn* 2010;65:383–98.
- [34] Flores P, Ambrósio J, Claro HCP, Lankarani HM. Dynamic behaviour of planar rigid multibody systems including revolute joints with clearance. *Proc Inst Mech Eng, Part-K: J Multi-body Dyn* 2007;221:161–74.
- [35] Jin CM, Fan L, Qiu Y. The vibration control of a flexible linkage mechanism with impact. *Commun Nonlinear Sci Numer Simul* 2004;9:459–69.
- [36] Erkaya S, Uzmay I. Investigation on effect of joint clearance on dynamics of four-bar mechanism. *Nonlinear Dyn* 2009;58:179–98.

A method for modeling three-dimensional flexible mechanisms based on an equivalent rigid-link system

Renato Vidoni¹, Alessandro Gasparetto² and Marco Giovagnoni²

Abstract

Accurate modeling of flexible mechanisms is an open research topic, and different models have been presented since the 1970s. In this work, a novel approach for modeling of three-dimensional flexible mechanisms is presented, based on an equivalent rigid-link system, with respect to which elastic deformations are defined and computed. Concepts of three-dimensional kinematics are used in order to define an effective relationship between the rigid body and the elastic motion. The model is based on a compact kinematic formulation and, for a specific mechanism, there is no need for customizing the formulation. By using the principle of virtual work, a coupled dynamic formulation is found. A crucial advantage of this method is that it is not necessary to explicitly formulate the compatibility equations expressing the link connections, since they are included in the matrices of the system dynamics. The model was applied to a specific three-dimensional flexible mechanism. The results, compared with the Adams-Flex™ software, show a good agreement, thus proving the effectiveness of the methodology.

Keywords

Flexible spatial mechanism, multibody system, vibration

Received: 12 March 2012; accepted: 7 September 2012

I. Introduction

Dynamic models and formulations for multibody rigid–flexible-link systems have been proposed and refined since the 1970s, and are still an open field of investigation. This is mainly due to the fact that the development of new lightweight materials and the demand for higher operating speeds require the development of accurate methodologies. In this manner, the effect of deformation of the mechanism components can be accurately taken into account. In Shabana (1997), Wasfy and Noor (2003), Dwivedy and Eberhard (2006), Tokhi and Azad (2008) and Bauchau (2011), comprehensive reviews of the work carried out in this area have been presented. Moreover, due to the dynamic effects of structural flexibility, the control of these lightweight systems is more difficult, the motion should be smooth to avoid excitation of mechanical resonances (Zanotto et al., 2011; Gasparetto et al., 2012), and accurate dynamic models can be exploited to set-up

effective controllers (Benosman and Vey, 2004; Caracciolo et al., 2006, 2008; Boscaroli et al., 2011; Boschetti et al., 2011, 2012).

The classical approach used in multibody dynamics for dealing with mechanisms featuring large displacements and small deformations is based upon the dynamical model of a rigid-body mechanism, then flexibility is taken into account by introducing elastic deformations.

¹FaST, Faculty of Science and Technology, Free University of Bozen-Bolzano, Italy

²Department of Electrical, Management and Mechanical Engineering, University of Udine, Italy

Corresponding author:

Renato Vidoni, FaST, Faculty of Science and Technology, Free University of Bozen-Bolzano, Piazza Universit, 5 - Bolzano, Italy.

Email: renato.vidoni@unibz.it

The developed complete dynamic formulation of flexible multibody systems leads to a set of coupled partial differential equations that cannot be analytically solved, since these equations are space and time dependent.

In order to overcome this problem, finite-dimensional models must be used. Some approaches have thus been formulated in the scientific literature. The most popular are: (a) the finite-element method (FEM), (b) the assumed mode method and (c) the lumped parameter method (Nagarajan and Turcic, 1990; Theodore and Ghosal, 1995; Wang et al., 1996; Ge et al., 1997; Martins et al., 2003; Dwivedy and Eberhard, 2006). In all these approaches, the original infinite-dimensional model is reduced to a finite-dimensional one, and a set of ordinary differential equations is obtained, starting from the original system of partial differential equations.

In order to obtain the dynamic equations of motion, taking into account both the rigid-body motion and the elastic deformations, an ad hoc model must be developed. In the literature, the most important approaches for defining a dynamic model are: (1) the floating frame of reference (FFR), (2) the linear theory of elastodynamics (LTE) and (3) the finite-segment method (FSM) (Shabana, 1997, 2005).

1. The FFR formulation is currently the most used method, and is adopted and implemented in several multibody computer software. In this formulation, two sets of coordinates are used: the first set describes the location and orientation of a local reference attached to each link and the second set describes the deformation of the body with respect to its coordinate system. With this description, there is no separation between the rigid-body motion and the elastic deformations of the flexible body. In other words, a system of coupled differential equations is obtained. The main drawback of this approach is that the constraint conditions, which express the connection through mechanical joints between different deformable bodies in the system, are defined in the global coordinate system and introduced into the dynamic equations by means of a set of nonlinear algebraic constraint equations, which depend both on the elastic deformations and on the reference rigid motion of the deformable bodies (e.g. through a vector of Lagrange multipliers). Hence, the resulting constraint equations are coupled, and do not have an immediate formulation.
2. The second approach, namely the LTE, was used in the past to model multibody systems by analyzing the system as a collection of rigid bodies independently from the deformation, then superimposing vibration effects on the rigid-body motion. In such

a formulation, the main assumption is that the coupling between the elastic deformation and the rigid-body displacements is negligible, thus, the inertia terms in the reference formulation are considered to be independent of the elastic deformations. The main drawback of this method is that it neglects the effect of the elastic deformations on the rigid-body reference motion; hence, in many cases, the method cannot provide accurate results.

3. The third method, namely the FSM, models the deformable bodies as a set of rigid bodies that are connected by springs and dampers; hence, the elasticity can be computed, for instance, by using the FEM. The main drawback of this method is that its accuracy depends upon the number of elements in the model, thus an increase in accuracy requires a considerable increase in the computational load. Furthermore, the way of dividing each deformable body into finite rigid bodies, connected by spring and dampers, is not unique.

It should be remarked that the above-mentioned methods are appropriate for modeling large rigid displacement and elastic deformations that are small with respect to the link length. If large elastic deformations have to be modeled, alternative approaches must be considered, such as the absolute nodal coordinate formulation proposed by Schwab and Meijaard (2005), Shabana (2005), Sugiyama et al. (2006) and Garca-Vallejo et al. (2008). In this formulation, the position of a point within the element is expressed by interpolations based on the Cartesian absolute coordinates of the nodal points and on gradients of these positions with respect to a reference configuration. This leads to constant mass matrices for the elements, at the cost of a more complicated description for the stiffness. This approach is very effective for modeling large displacements and large elastic deformations, but is, in general, less accurate than the FFR, LTE and FSM when dealing with small elastic deformations.

In this paper, a novel multibody dynamics approach for three-dimensional (3-D) flexible-link systems is presented. The method is intended for accurate dynamic modeling of systems with large displacements and small elastic deformation, and tries to overcome the main drawbacks of the FFR, LTE and FSM methods described above. The model of a 3-D multibody system is based on an equivalent rigid-link system (ERLS) that enables the kinematic equations of the ERLS to be decoupled from the compatibility equations of the displacements at the joints. Then, standard concepts of 3-D kinematics can be adopted to formulate and solve the ERLS kinematics. The results can then be used in the equations of the dynamic model of the flexible multibody system. The ERLS concept

was first introduced by Turcic and Midha (1984a,b), Turcic et al. (1984) and Chang and Hamilton (1991), and an ERLS-based approach suitable only for the particular case of planar mechanisms with revolute joints was presented by Giovagnoni (1994) and Gasparetto (2001).

Moreover, taking into account that the relative position of the ERLS system with respect to the deformable real system is not unique, it is possible to choose an ERLS that is as close as possible to the deformed system, in order to obtain the best match with the small-displacement assumption. This method presents, on the one hand, a coupled approach that takes into account the mutual influence between rigid-body motion and vibration and, on the other hand, allows some inertia coupling terms to be easily identified and neglected, taking into account their negligible effect with respect to the others. Once the ERLS kinematics has been described, the dynamic model of the system can be formulated. The mechanism links may be modeled using whatsoever finite-dimensional model; in the applications described in this paper, they are modeled by 3-D Euler–Bernoulli beam elements according to the FEM. For the ERLS, centroidal body coordinate systems are assumed, while deformable body coordinate systems that satisfy the mean axis conditions are chosen. This dynamic model enables one to obtain a set of differential equations of motion, which can be integrated to get the system motion.

With respect to the FFR, LTE and FSM methods described above, the technique described in this manuscript has the following advantages.

1. The compatibility equations work only on the elastic displacements and are never used explicitly, since they are automatically taken into account when assembling the system matrices. The result is a simple and iterative procedure and formulation that can be easily exploited to compute the dynamic motion equations.
2. The effects of the elastic deformations on the rigid-body reference motion are taken into account.
3. The method has a good degree of accuracy, even if a small number of beam elements is used to dynamically model the links of the system.

The paper is organized as follows. The kinematics of the ERLS and of the flexible-link mechanism is described in Section 2. Dynamic formulation is presented in Section 3, while Section 4 deals with the simulation of a benchmark flexible-link mechanism dynamics. The simulation results are compared with those obtained using the Adams-Flex™ multibody dynamic software.

2. Kinematics of a flexible-link spatial robotic mechanism

The formulation adopted here considers an ERLS, with respect to which the elastic displacements are defined. Each link is subdivided into finite elements; in this work, the Euler–Bernoulli model for a spatial beam has been considered for the definition of each finite element. Referring to Figure 1, the vector of the nodal elastic displacements of the k -th finite element belonging to the ℓ -th link is called \mathbf{u}_k . Since in this work, 3-D Euler–Bernoulli beam elements are adopted, hence beams with two nodes per element, \mathbf{u}_k is a $[12 \times 1]$ vector. The vector of the nodal positions and orientations for the k -th finite element of the ERLS ℓ -th link is called \mathbf{r}_k . The sum of the nodal elastic displacements and of the ERLS positions and orientations is expressed by a vector \mathbf{b}_k , which represents the absolute nodal positions and orientations of k -th finite element with respect to the global reference frame

$$\mathbf{b}_k = \mathbf{r}_k + \mathbf{u}_k \quad (1)$$

By considering a generic point inside the ℓ -th link, let \mathbf{w}_χ be the position vector of the generic point of the ERLS and \mathbf{v}_χ its elastic displacement. The absolute position \mathbf{p}_χ of a generic point is given by

$$\mathbf{p}_\chi = \mathbf{w}_\chi + \mathbf{v}_\chi \quad (2)$$

The vectors in equation (2) are defined with respect to a fixed global reference frame $\{X, Y, Z\}$ moreover, for each k -th finite element, a local coordinate system $\{x_k, y_k, z_k\}$, which follows the ERLS motion, is defined. The position and orientation of a local reference frame with respect to the global one is given by the position and orientation of the ERLS, which in turn can be expressed by means of a set of generalized coordinates \mathbf{q} . The number of the generalized coordinates of the ERLS is the number of the rigid degrees of mobility of the mechanism (m), which is given by Kutzbach's equation

$$m = 6(n - 1) + \sum_{i=1}^N (6 - f_i) \quad (3)$$

where n is the number of links, N the number of joints and f_i the degrees of freedom (DOFs) of each joint.

2.1. ERLS kinematics

Since the ERLS is a rigid mechanism, its kinematics can be described by means of a finite number of DOFs,

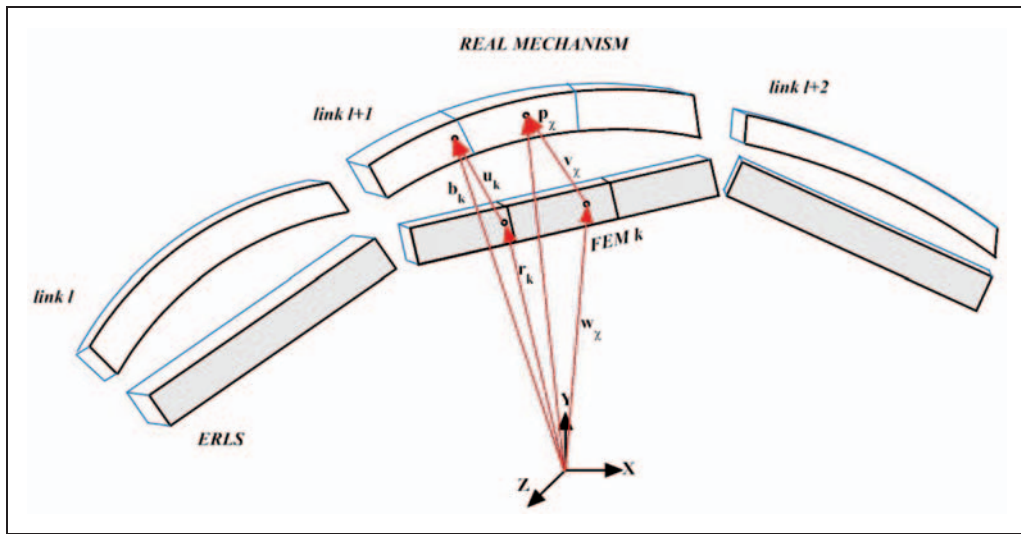


Figure 1. Model of the mechanism and kinematic definitions; as an example, the $\ell + 1$ -link has been discretized with three finite elements.

expressed by a set of generalized coordinates, given by the vector \mathbf{q} . Among the different methods used to describe the translational and rotational motion between different links of a rigid-multibody system, the Denavit–Hartenberg (DH) notation (Denavit and Hartenberg, 1955) was adopted in this work. According to this formulation, four kinematic entities are sufficient to build a transformation (also called roto-translation) matrix A_i^j between the frames of two links along the kinematic chain of the mechanism

$$A_i^j = \begin{bmatrix} \mathbf{R}_i^j & \mathbf{O}_i^j \\ 0 & 1 \end{bmatrix} \quad (4)$$

where \mathbf{R}_i^j is the rotation matrix between the j -th and i -th frames and \mathbf{O}_i^j the position of the origin of the i -th frame with respect to the j -th frame.

The nodal position and orientation vector \mathbf{r}_k for a k -th finite element can then be expressed with respect to a suitable local frame. All the \mathbf{r}_k 's can then be gathered into a unique vector \mathbf{r} , representing the position and orientation of the whole ERLS. The variation $d\mathbf{r}$ of the vector \mathbf{r} can be expressed, through the Jacobian matrix, as a function of the variation of the vector of the generalized coordinates

$$d\mathbf{r} = \mathbf{J}(\mathbf{q})d\mathbf{q} \quad (5)$$

The first-order differential kinematics of the ERLS is expressed by a similar relation that holds between the velocities

$$\dot{\mathbf{r}} = \mathbf{J}(\mathbf{q})\dot{\mathbf{q}} \quad (6)$$

where the Jacobian matrix is a function of the generalized coordinates \mathbf{q} of the ERLS. The second-order

differential kinematics (i.e. the expression for the acceleration) can be obtained by differentiation of equation (6)

$$\ddot{\mathbf{r}} = \mathbf{J}(\mathbf{q})\ddot{\mathbf{q}} + \mathbf{J}(\mathbf{q}, \dot{\mathbf{q}})\dot{\mathbf{q}} = \mathbf{J}(\mathbf{q})\ddot{\mathbf{q}} + \left(\sum_j \frac{\partial \mathbf{J}}{\partial q_j} \dot{q}_j \right) \dot{\mathbf{q}} \quad (7)$$

where $\mathbf{J}(\mathbf{q}, \dot{\mathbf{q}})$ is the time derivative of the Jacobian matrix.

2.2. Kinematics of the elastic multibody system

In order to correctly account for the displacement interpolations inside the finite elements, two matrices have to be defined.

- $\mathbf{R}_\ell(\mathbf{q})$, which is a rotation matrix from coordinates with respect to the reference frame of the ℓ -link (defined according to the DH notation) to the fixed global reference frame.
- $\mathbf{T}_i^\ell(\mathbf{q})$, which is a block-diagonal rotation matrix expressing the transformation from the frame i , in which are expressed the nodal elastic displacements of the considered k -th finite element \mathbf{u}_k^i , to the reference frame of the ℓ -th link. Since there are two nodes per beam element (six elastic DOFs per node), the T-matrix dimension is $[12 \times 12]$,

$$\mathbf{T}_i^\ell(\mathbf{q}) = \begin{bmatrix} \mathbf{R}_i^\ell & \mathbf{0} & \mathbf{0} & \mathbf{0} \\ \mathbf{0} & \mathbf{R}_i^\ell & \mathbf{0} & \mathbf{0} \\ \mathbf{0} & \mathbf{0} & \mathbf{R}_i^\ell & \mathbf{0} \\ \mathbf{0} & \mathbf{0} & \mathbf{0} & \mathbf{R}_i^\ell \end{bmatrix} \quad (8)$$

For each node of each k -th finite element, in order to make compatibility conditions trivial (see explanation in Section 3.1), nodal elastic displacements have to be rotated in an own i -th coordinate frame \mathbf{u}_k^i . Thus, the i -th frame can be different between two nodes in the same finite element and, as a consequence, the local transformations \mathbf{R}_i^ℓ in the $\mathbf{T}_i^\ell(\mathbf{q})$ matrix can be different for the first and second $[6 \times 6]$ diagonal blocks.

Now, equation (2) can be rewritten as

$$\mathbf{p}_\chi = \mathbf{w}_\chi + \mathbf{R}_\ell(\mathbf{q}) \mathbf{N}_\ell(x_\chi, y_\chi, z_\chi) \mathbf{T}_i^\ell(\mathbf{q}) \mathbf{u}_k^i \quad (9)$$

where $\mathbf{N}_\ell(x_k, y_k, z_k)$ is the shape function matrix for the interpolation of the $\{k\}$ -th finite element defined in the local frame. Note that, in the ERLS, the rotation matrix from the reference frame of each finite element of the ℓ -th link to the fixed global reference frame is equal to the rotation matrix from the reference frame of the ℓ -th link to the fixed global reference frame.

In order to apply the virtual work principle, the virtual displacements should be used

$$\delta\mathbf{p}_\chi = \delta\mathbf{w}_\chi + \delta\mathbf{v}_\chi \quad (10)$$

where $\delta\mathbf{w}_\chi$ is the virtual displacement of point \mathbf{p}_χ according to the rigid-body kinematics (see equation (5)) and $\delta\mathbf{v}_\chi$ is the virtual displacement of point \mathbf{p}_χ due to the nodal displacements of the k -th finite element relative to the rigid-body displacements of link ℓ in which \mathbf{p}_χ is contained.

Thus, taking into account that the interpolation function matrix $\mathbf{N}_\ell(x_\chi, y_\chi, z_\chi)$ can be used to interpolate infinitesimal rigid-body displacements if the proper reference frames are employed, the first term on the right-hand side is given by

$$\delta\mathbf{w}_\chi = \mathbf{R}_\ell(\mathbf{q}) \mathbf{N}_\ell(x_\chi, y_\chi, z_\chi) \mathbf{T}_i^\ell(\mathbf{q}) \delta\mathbf{r}_k^i \quad (11)$$

The second virtual term of the right-hand side in equation (10), $\delta\mathbf{v}_\chi$, is obtained by considering both virtual nodal elastic displacements $\delta\mathbf{u}_k^i$ and virtual displacements $\delta\mathbf{q}$ of the generalized coordinates. So, the expression for the virtual displacements in the fixed reference frame becomes

$$\begin{aligned} \delta\mathbf{p}_\chi = & \mathbf{R}_\ell(\mathbf{q}) \mathbf{N}_\ell(x_\chi, y_\chi, z_\chi) \mathbf{T}_i^\ell(\mathbf{q}) \delta\mathbf{r}_k^i + \mathbf{R}_\ell(\mathbf{q}) \mathbf{N}_\ell(x_\chi, y_\chi, z_\chi) \mathbf{T}_i^\ell(\mathbf{q}) \mathbf{u}_k^i \\ & + \mathbf{R}_\ell(\mathbf{q}) \mathbf{N}_\ell(x_\chi, y_\chi, z_\chi) \delta\mathbf{T}_i^\ell(\mathbf{q}) \mathbf{u}_k^i + \mathbf{R}_\ell(\mathbf{q}) \mathbf{N}_\ell(x_\chi, y_\chi, z_\chi) \mathbf{T}_i^\ell(\mathbf{q}) \delta\mathbf{u}_k^i \end{aligned} \quad (12)$$

The nodal elastic displacements \mathbf{u}_k^i are small with respect to the rigid-body displacements of the ERLS due to the small deformations and large rotation hypothesis assumed in this work.

The second and third terms of equation (12) contain the virtual rigid-body rotation $\delta\mathbf{R}_\ell$ or $\delta\mathbf{T}_i^\ell$, which can be expressed as

$$\begin{aligned} \delta\mathbf{R}_\ell(\mathbf{q}) &= \left(\sum_j \frac{\partial \mathbf{R}_\ell}{\partial q_j} \right) \delta\mathbf{q} = \mathbf{R}'_\ell \delta\mathbf{q}, \quad \delta\mathbf{T}_i^\ell(\mathbf{q}) \\ &= \left(\sum_j \frac{\partial \mathbf{T}_i^\ell}{\partial q_j} \right) \delta\mathbf{q} = \mathbf{T}'_i \delta\mathbf{q} \end{aligned} \quad (13)$$

By differentiating equation (9) twice, the expression of the acceleration of a generic point inside the k -th finite element can be computed,

$$\begin{aligned} \ddot{\mathbf{p}}_\chi = & \mathbf{R}_\ell(\mathbf{q}) \mathbf{N}_\ell(x_\chi, y_\chi, z_\chi) \mathbf{T}_i^\ell(\mathbf{q}) \ddot{\mathbf{r}}_k^i + \mathbf{R}_\ell(\mathbf{q}) \mathbf{N}_\ell(x_\chi, y_\chi, z_\chi) \mathbf{T}_i^\ell(\mathbf{q}) \ddot{\mathbf{u}}_k^i \\ & + 2(\dot{\mathbf{R}}_\ell(\mathbf{q}) \mathbf{N}_\ell(x_\chi, y_\chi, z_\chi) \mathbf{T}_i^\ell(\mathbf{q}) + \mathbf{R}_\ell(\mathbf{q}) \mathbf{N}_\ell(x_\chi, y_\chi, z_\chi) \dot{\mathbf{T}}_i^\ell(\mathbf{q})) \dot{\mathbf{u}}_k^i \\ & + (\ddot{\mathbf{R}}_\ell(\mathbf{q}) \mathbf{N}_\ell(x_\chi, y_\chi, z_\chi) \mathbf{T}_i^\ell(\mathbf{q}) + 2\dot{\mathbf{R}}_\ell(\mathbf{q}) \mathbf{N}_\ell(x_\chi, y_\chi, z_\chi) \dot{\mathbf{T}}_i^\ell(\mathbf{q})) \dot{\mathbf{u}}_k^i \\ & + \mathbf{R}_\ell(\mathbf{q}) \mathbf{N}_\ell(x_\chi, y_\chi, z_\chi) \ddot{\mathbf{T}}_i^\ell(\mathbf{q}) \mathbf{u}_k^i \end{aligned} \quad (14)$$

where the term $\ddot{\mathbf{r}}_k^i$ expresses the linear and angular acceleration of the k -th finite element of the ERLS expressed in the i -th reference frame.

If the kinematic entities of all the finite elements are grouped into a unique vector, taking into account equation (1), after differentiation,

$$d\mathbf{b} = d\mathbf{r} + d\mathbf{u} \quad (15)$$

Then, by substituting equation (5) into equation (15), and setting the expression in matrix form, one obtains

$$d\mathbf{b} = [\mathbf{I} \quad \mathbf{J}] \begin{bmatrix} d\mathbf{u} \\ d\mathbf{q} \end{bmatrix} \quad (16)$$

where, if the mechanism is discretized into N beam elements, thus $2N$ nodes, $\dim(d\mathbf{b}) = [6 \times 2N, 1]$, $\dim(d\mathbf{u}) = [6 \times 2N, 1]$, $\dim(d\mathbf{q}) = [m, 1]$ and $\dim(\mathbf{J}) = [6 \times 2N, m]$ with m the number of rigid DOFs of the ERLS mechanism (i.e. number of generalized coordinates \mathbf{q} of the ERLS). The coefficient matrix of the above equation (16) is not square; hence, a given configuration $d\mathbf{b}$ of infinitesimal nodal displacements corresponds to more sets of increments of $[d\mathbf{u}^T \ d\mathbf{q}^T]$ of the generalized coordinates of the system. The easiest way to eliminate this redundancy is to force to zero a number of elements of $d\mathbf{u}$ equal to the number of generalized coordinates of the ERLS. The choice is free and it is usually made by zeroing some DOFs that

will be less deformed, i.e. where the link is stiffer. If $d\mathbf{u}$ is partitioned into its independent part ($d\mathbf{u}_{in}$) and into its zeroed part ($d\mathbf{u}_0$), and if \mathbf{J} is correspondingly partitioned, the elements forced to zero can be eliminated from equation (16). Thus,

$$d\mathbf{b} = \begin{bmatrix} \mathbf{I} & \mathbf{J}_{in} \\ 0 & \mathbf{J}_0 \end{bmatrix} \begin{bmatrix} d\mathbf{u}_{in} \\ d\mathbf{q} \end{bmatrix} \quad (17)$$

where $\dim(d\mathbf{b}) = [6 \times 2N, 1]$, $\dim(d\mathbf{u}_{in}) = [6 \times 2N - m, 1]$, $\dim(\mathbf{J}_0) = [m, m]$ and $\dim(\mathbf{J}_{in}) = [6 \times 2N - m, m]$. The square matrix of the coefficient of equation (17) must be nonsingular, which implies that the determinant of \mathbf{J}_0 must be different from zero; a correct ERLS definition requires the generalized coordinates of the ERLS to be chosen in such a way that no singular configuration is encountered during the motion. As a conclusive remark, the use of the ERLS allows a solution for direct kinematics to be extensively exploited based on the DH notation, widely adopted in robotics.

As stated before, the first-order differential kinematics, based on the Jacobian matrix, depends on the configuration of the ERLS, which in turn is a function of the generalized coordinates \mathbf{q} . Virtual displacements, velocities and accelerations of \mathbf{r} can be computed if the matrices $\mathbf{R}_\ell, \dot{\mathbf{R}}_\ell, \mathbf{T}_\ell, \dot{\mathbf{T}}_\ell, \mathbf{J}, \dot{\mathbf{J}}$, which are functions of \mathbf{q} and $\dot{\mathbf{q}}$, are known.

The use of the DH notation enables one to unambiguously define the local frames as well as to compute all the aforementioned matrices in a symbolic form, if the DH parameters are known. This leads to a major advantage, namely, that it is no more necessary to include a specific kinematic solution into the dynamic formulation, in order to obtain the law of motion. Moreover, since a specific kinematic solution is not required in the dynamic formulation and the ERLS kinematics is completely uncoupled with respect to the elastic terms, these allow us to work both with closed-chain spatial mechanisms or parallel kinematic machines. Indeed, if the kinematic solution is known in a closed form, it can be directly applied in the model; if not, numerical solutions can be exploited.

3. Dynamics

Once the kinematics has been solved, the dynamic equations of motion for the flexible-link mechanism can be obtained by applying the principle of virtual work,

$$\delta\mathbf{W}^{inertia} + \delta\mathbf{W}^{elastic} + \delta\mathbf{W}^{external} = 0 \quad (18)$$

where gravity effects are included among external force effect. A more explicit definition of equation (18) is given by

$$\begin{aligned} & \sum_k \int_{v_k} \delta\mathbf{p}_k^T \ddot{\mathbf{p}}_k \rho_k dv + \sum_k \int_{v_k} \delta\epsilon_k^T \mathbf{D}_k \epsilon_k dv \\ &= \sum_k \int_{v_k} \delta\mathbf{p}_k^T \mathbf{g} \rho_k dv + (\delta\mathbf{u}^T + \delta\mathbf{r}^T) \mathbf{f} \\ & \delta\mathbf{W}^{inertia} + \delta\mathbf{W}^{elastic} = -\delta\mathbf{W}^{external} \end{aligned} \quad (19)$$

where \mathbf{D}_k , ϵ_k and ρ_k are, respectively, the stress-strain matrix, the strain vector and the mass density for the k -th volume (finite) element, \mathbf{g} is the gravity acceleration vector and \mathbf{f} is the vector of the concentrated external forces and torques.

The total virtual work is split into the integrals over element volumes v_k and in the virtual work due to \mathbf{f} ; $\delta\mathbf{u}$ and $\delta\mathbf{r}$ refer to all the nodes of the model.

3.1. Formulation of compatibility equations

An important point in the modeling of multibody systems concerns the kinematic constraints that have to be imposed to the elastic displacements at the joints. These lead to a set of compatibility equations that express the relations between two consecutive links according to their connecting joint.

In order to have a trivial formulation of such compatibility equations, the frame (i), in which the nodal elastic displacements of a k -th finite element \mathbf{u}_k^i are expressed, has to be suitably chosen.

As shown in Figure 2, where a revolute pair is depicted, two consecutive links have different link frames, ℓ and $\ell + 1$, which are fixed according to the previously explained notation.

If the nodal displacements \mathbf{u}_k^i are expressed with respect to the frame of the link to which they belong, the compatibility equations cannot be written without considering both rigid and elastic terms. Indeed, each joint imposes relations between the elastic displacements of the second node of the last finite element of the ℓ -th link and the first node of the first finite element of the $(\ell + 1)$ -th link.

If the elastic deformations of the second node of the last finite element of the ℓ -th link and those of the first node of the first finite element of the $(\ell + 1)$ -th link are expressed in the frame of the latter, the compatibility equations can be written in a trivial manner, avoiding the necessity to have mixed rigid and elastic terms, and allowing us to write only identity equalities for the case of elementary joints.

For instance, see Figure 2, for a revolute joint that allows relative rotation between the ℓ -th and $(\ell + 1)$ -th links with respect to the z -axis of the $(\ell + 1)$ -th link

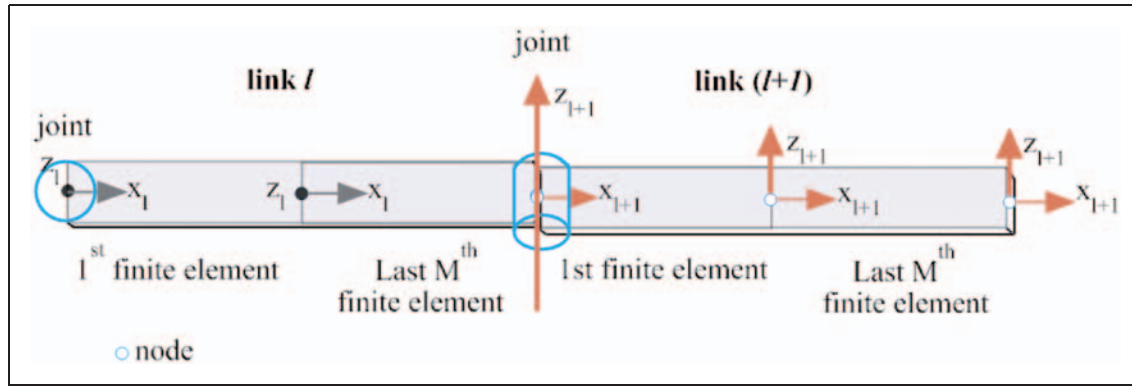


Figure 2. Frames and elastic displacements between two consecutive links.

frame, i.e. the joint axis, the rotation about such a z -axis is free while the other five elastic DOFs are constrained.

The compatibility equations between the overlying nodes, i.e. the second node of the last M -th finite element of the ℓ -th link and the first node of the first finite element of the $(\ell + 1)$ -link, result,

$$\begin{aligned} \mathbf{u}_{M_\ell}^{\ell+1}(7) &= \mathbf{u}_{1_{\ell+1}}^{\ell+1}(1) \\ \mathbf{u}_{M_\ell}^{\ell+1}(8) &= \mathbf{u}_{1_{\ell+1}}^{\ell+1}(2) \\ \mathbf{u}_{M_\ell}^{\ell+1}(9) &= \mathbf{u}_{1_{\ell+1}}^{\ell+1}(3) \\ \mathbf{u}_{M_\ell}^{\ell+1}(10) &= \mathbf{u}_{1_{\ell+1}}^{\ell+1}(4) \\ \mathbf{u}_{M_\ell}^{\ell+1}(11) &= \mathbf{u}_{1_{\ell+1}}^{\ell+1}(5) \end{aligned} \quad (20)$$

where for each beam element 1, 2, 3 and 4, 5, 6, and 7, 8, 9 and 10, 11, 12 are the translational and rotational elastic DOFs of the first and second node, respectively; hence, the positional and the x - and y -rotational elastic DOFs have to be set equal.

According to this idea, the block-diagonal rotation matrix \mathbf{T}_i^ℓ becomes the following.

- In the case of all the finite elements, except the last of a ℓ -th link, a block-diagonal identity matrix

$$\mathbf{T}_i^\ell = \mathbf{T}_\ell^\ell = \begin{bmatrix} \mathbf{R}_\ell^\ell & \mathbf{0} & \mathbf{0} & \mathbf{0} \\ \mathbf{0} & \mathbf{R}_\ell^\ell & \mathbf{0} & \mathbf{0} \\ \mathbf{0} & \mathbf{0} & \mathbf{R}_\ell^\ell & \mathbf{0} \\ \mathbf{0} & \mathbf{0} & \mathbf{0} & \mathbf{R}_\ell^\ell \end{bmatrix} = \begin{bmatrix} I & \mathbf{0} & \mathbf{0} & \mathbf{0} \\ \mathbf{0} & I & \mathbf{0} & \mathbf{0} \\ \mathbf{0} & \mathbf{0} & I & \mathbf{0} \\ \mathbf{0} & \mathbf{0} & \mathbf{0} & I \end{bmatrix} \quad (21)$$

- In the case of the last beam element of a ℓ -th link

$$\begin{aligned} \mathbf{T}_i^\ell = \mathbf{T}_{\ell,\ell+1}^\ell &= \begin{bmatrix} \mathbf{R}_\ell^\ell & \mathbf{0} & \mathbf{0} & \mathbf{0} \\ \mathbf{0} & \mathbf{R}_\ell^\ell & \mathbf{0} & \mathbf{0} \\ \mathbf{0} & \mathbf{0} & \mathbf{R}_{\ell+1}^\ell & \mathbf{0} \\ \mathbf{0} & \mathbf{0} & \mathbf{0} & \mathbf{R}_{\ell+1}^\ell \end{bmatrix} \\ &= \begin{bmatrix} I & \mathbf{0} & \mathbf{0} & \mathbf{0} \\ \mathbf{0} & I & \mathbf{0} & \mathbf{0} \\ \mathbf{0} & \mathbf{0} & \mathbf{R}_{\ell+1}^\ell & \mathbf{0} \\ \mathbf{0} & \mathbf{0} & \mathbf{0} & \mathbf{R}_{\ell+1}^\ell \end{bmatrix} \end{aligned} \quad (22)$$

If an open-chain mechanism is considered, the block-diagonal rotation matrix \mathbf{T}_i^ℓ of the last beam element of the final link is an identity matrix, as in equation (21), since there are no following joints and compatibility constraints to be written.

In comparison with other flexible-link multibody models (e.g. FFR), where the constraint equations depend on the elastic deformations as well as the reference motion of the deformable bodies, it has to be underlined how this novel approach allows us to write and include compatibility equations at the joints considering only the elastic displacements. In many other approaches, the kinematic equations of compatibility that describe the joints in the multibody system consisting of interconnected links are usually formulated by means of a set of nonlinear algebraic compatibility equations containing both flexible and rigid terms. On the contrary, in the novel formulation proposed here, the compatibility equations work only on the elastic displacements and are never used explicitly, since they

are automatically taken into account when assembling the system matrices, thus avoiding the need to write a set of nonlinear algebraic compatibility equations.

The result is a simpler formulation leading to a recursive procedure that can be exploited to compute the dynamic motion equations.

Now, taking into account that nodal elastic virtual displacements $\delta\mathbf{u}_k^i$ and virtual displacements of the ERLS $\delta\mathbf{u}_k^i$ are completely independent, the dynamic equations for the local nodal and global equilibrium can be found.

3.2. Local nodal equilibrium

A first set of equilibrium equations, i.e. the local nodal equilibrium equations, can be obtained from equation (19) by considering

$$\begin{aligned} \delta\mathbf{r} = 0 &\Rightarrow \delta\mathbf{R} = 0; \delta\mathbf{T} = 0; \\ \delta\mathbf{u} &\neq 0 \end{aligned} \quad (23)$$

So, equation (12) becomes

$$\delta\mathbf{p}_x = \mathbf{R}_\ell(\mathbf{q})\mathbf{N}_\ell(x_\chi, y_\chi, z_\chi)\mathbf{T}_i^\ell(\mathbf{q})\delta\mathbf{u}_k^i \quad (24)$$

Now, by considering equations (14), (19) and (24), the following expression can be obtained

$$\begin{aligned} &\sum_k \int_{v_k(\ell)} [\delta\mathbf{u}_k^{iT}\mathbf{T}_i^T\mathbf{N}_\ell^T\mathbf{R}_\ell^T][\mathbf{R}_\ell\mathbf{N}_\ell\mathbf{T}_i^\ell\ddot{\mathbf{r}}_k + \mathbf{R}_\ell\mathbf{N}_\ell\mathbf{T}_i^\ell\ddot{\mathbf{u}}_k^i + 2(\dot{\mathbf{R}}_\ell\mathbf{N}_\ell\mathbf{T}_i^\ell + \mathbf{R}_\ell\mathbf{N}_\ell\dot{\mathbf{T}}_i^\ell)\dot{\mathbf{u}}_k^i + (\ddot{\mathbf{R}}_\ell\mathbf{N}_\ell\mathbf{T}_i^\ell + 2\dot{\mathbf{R}}_\ell\mathbf{N}_\ell\dot{\mathbf{T}}_i^\ell + \mathbf{R}_\ell\mathbf{N}_\ell\ddot{\mathbf{T}}_i^\ell)\mathbf{u}_k^i] \rho_k dv + \sum_k \int_{v_k(\ell)} (\delta\mathbf{u}_k^{iT}\mathbf{T}_i^T\mathbf{B}_k^T)\mathbf{D}_k\mathbf{B}_k\mathbf{T}_i^\ell\mathbf{u}_k^i dv \\ &= \sum_k \int_{v_k(\ell)} (\delta\mathbf{u}_k^{iT}\mathbf{T}_i^T\mathbf{N}_\ell^T\mathbf{R}_\ell^T)\mathbf{g}\rho_k dv + (\delta\mathbf{u}^T + \delta\mathbf{r}^T)\mathbf{f} \end{aligned} \quad (25)$$

where $v_k(\ell)$ represents the volume of the k -th finite element of the system, each one belonging to its own ℓ -th link, \mathbf{T}_i^ℓ is the block-diagonal matrix of the k -th element belonging to the ℓ -th link that expresses the rotation between the appropriate ℓ -th frame and the local i -th frame, and \mathbf{B}_k is the strain-displacement matrix. The elements of the mass, Coriolis, gyroscopic damping, centrifugal stiffness and stiffness contributions can be obtained from the integrals appearing in equation (25)

$$\begin{aligned} &\int_{v_k(\ell)} \mathbf{T}_i^T\mathbf{N}_\ell^T\mathbf{R}_\ell^T\mathbf{R}_\ell\mathbf{N}_\ell\mathbf{T}_i^\ell\rho_k dv \\ &= \int_{v_k(\ell)} \mathbf{T}_i^T\mathbf{N}_\ell^T\mathbf{N}_\ell\mathbf{T}_i^\ell\rho_k dv = \mathbf{M}_k \end{aligned} \quad (26)$$

is the mass matrix of the k -th element;

$$\int_{v_k(\ell)} \mathbf{T}_i^T\mathbf{B}_k^T\mathbf{D}_k\mathbf{B}_k\mathbf{T}_i^\ell dv = \mathbf{K}_k \quad (27)$$

is the stiffness matrix of the k -th element;

$$\int_{v_k(\ell)} \mathbf{T}_i^T\mathbf{N}_\ell^T\mathbf{R}_\ell^T\mathbf{g}\rho_k dv = \mathbf{f}_{gk} \quad (28)$$

is the vector of the equivalent nodal loads due to gravity;

$$\int_{v_k(\ell)} \mathbf{T}_i^T\mathbf{N}_\ell^T\dot{\mathbf{R}}_\ell^T\mathbf{R}_\ell\mathbf{N}_\ell\mathbf{T}_i^\ell\rho_k dv = \mathbf{M}_{G1k} \quad (29)$$

$$\begin{aligned} &\int_{v_k(\ell)} \mathbf{T}_i^T\mathbf{N}_\ell^T\mathbf{R}_\ell^T\mathbf{R}_\ell\mathbf{N}_\ell\dot{\mathbf{T}}_i^\ell\rho_k dv \\ &= \int_{v_k(\ell)} \mathbf{T}_i^T\mathbf{N}_\ell^T\mathbf{N}_\ell\dot{\mathbf{T}}_i^\ell\rho_k dv = \mathbf{M}_{G2k} \end{aligned} \quad (30)$$

represent the Coriolis terms; and

$$\int_{v_k(\ell)} \mathbf{T}_i^T\mathbf{N}_\ell^T\mathbf{R}_\ell^T\ddot{\mathbf{R}}_\ell\mathbf{N}_\ell\mathbf{T}_i^\ell\rho_k dv = \mathbf{M}_{C1k} \quad (31)$$

$$\int_{v_k(\ell)} \mathbf{T}_i^T\mathbf{N}_\ell^T\mathbf{R}_\ell^T2\dot{\mathbf{R}}_\ell\mathbf{N}_\ell\dot{\mathbf{T}}_i^\ell\rho_k dv = 2\mathbf{M}_{C2k} \quad (32)$$

$$\begin{aligned} &\int_{v_k(\ell)} \mathbf{T}_i^T\mathbf{N}_\ell^T\mathbf{R}_\ell^T\mathbf{R}_\ell\mathbf{N}_\ell\ddot{\mathbf{T}}_i^\ell\rho_k dv \\ &= \int_{v_k(\ell)} \mathbf{T}_i^T\mathbf{N}_\ell^T\mathbf{N}_\ell\ddot{\mathbf{T}}_i^\ell\rho_k dv = \mathbf{M}_{C3k} \end{aligned} \quad (33)$$

represent the centrifugal stiffness terms;

The last five equations contain the first- and second-order derivatives of the rotation matrices \mathbf{R}_ℓ and of the \mathbf{T}_i^ℓ , which is a block-diagonal rotation matrix that needs to be computed. The $\dot{\mathbf{R}}_\ell$ term can be easily expressed as

$$\dot{\mathbf{R}}_\ell = \mathbf{S}(\boldsymbol{\omega}_\ell)\mathbf{R}_\ell \quad (34)$$

where $\mathbf{S}(\boldsymbol{\omega}_\ell)$ is the skew matrix as a function of the angular velocity of the link $\boldsymbol{\omega}_\ell = [\omega_{\ell,x}, \omega_{\ell,y}, \omega_{\ell,z}]$

$$\mathbf{S}(\boldsymbol{\omega}_\ell) = \begin{bmatrix} 0 & -\omega_{\ell,z} & \omega_{\ell,y} \\ \omega_{\ell,z} & 0 & -\omega_{\ell,x} \\ -\omega_{\ell,y} & \omega_{\ell,x} & 0 \end{bmatrix} \quad (35)$$

The inner term of \mathbf{M}_{G1k} related to the ℓ -th link, namely $\dot{\mathbf{R}}_\ell^T \mathbf{R}_\ell$, can be expressed as

$$\dot{\mathbf{R}}_\ell^T \mathbf{R}_\ell = -\mathbf{R}_\ell^T \mathbf{S}(\boldsymbol{\omega}_\ell) \mathbf{R}_\ell = -\mathbf{S}(\mathbf{R}_\ell^T \boldsymbol{\omega}_\ell) = -\mathbf{S}(\boldsymbol{\omega}_\ell^\ell) \quad (36)$$

Hence, the Coriolis terms can also be computed as functions of \mathbf{q} and $\dot{\mathbf{q}}$, because the angular velocity $\boldsymbol{\omega}_\ell$ depends on \mathbf{q} and $\dot{\mathbf{q}}$.

In a similar manner, the second-order derivatives and, thus, the centrifugal stiffness terms, can be expressed in an efficient and simple formulation

$$\ddot{\mathbf{R}}_\ell = \dot{\mathbf{S}}(\boldsymbol{\omega}_\ell) \mathbf{R}_\ell + \mathbf{S}(\boldsymbol{\omega}_\ell) \dot{\mathbf{R}}_\ell = \mathbf{S}(\dot{\boldsymbol{\omega}}_\ell) \mathbf{R}_\ell + \mathbf{S}^2(\boldsymbol{\omega}_\ell) \mathbf{R}_\ell \quad (37)$$

Since the \mathbf{T}_i^ℓ matrix is a block-diagonal rotation matrix, the derivatives $\dot{\mathbf{T}}_i^\ell$ and $\ddot{\mathbf{T}}_i^\ell$ can be computed exploiting the formulations above deduced for the derivatives of the rotation matrices.

Equation (25) can be rearranged into the form

$$\begin{aligned} \sum_k \delta \mathbf{u}_k^{iT} \mathbf{M}_k (\ddot{\mathbf{r}}_k + \ddot{\mathbf{u}}_k) + 2 \sum_k \delta \mathbf{u}_k^{iT} (\mathbf{M}_{G1k} + \mathbf{M}_{G2k}) \ddot{\mathbf{u}}_k^i \\ + \sum_k \delta \mathbf{u}_k^{iT} (\mathbf{M}_{C1k} + 2\mathbf{M}_{C2k} + \mathbf{M}_{C3k}) \mathbf{u}_k^i + \sum_k \delta \mathbf{u}_k^{iT} \mathbf{K}_k \mathbf{u}_k^i \\ = \sum_k \delta \mathbf{u}_k^T \mathbf{f}_{gk} + \delta \mathbf{u}^T \mathbf{f} \end{aligned} \quad (38)$$

3.3. Global equilibrium

A second set of equilibrium equations, i.e. global equilibrium, can be obtained by considering

$$\begin{aligned} \delta \mathbf{q} \neq 0 \Rightarrow \delta \mathbf{r} \neq 0 \Rightarrow \delta \mathbf{R} \neq 0; \delta \mathbf{T} \neq 0; \\ \delta \mathbf{u} = \mathbf{0} \end{aligned} \quad (39)$$

So, equation (12) results in

$$\begin{aligned} \delta \mathbf{p}_\chi &= \mathbf{R}_\ell(\mathbf{q}) \mathbf{N}_\ell(x_\chi, y_\chi, z_\chi) \mathbf{T}_i^\ell(\mathbf{q}) \delta \mathbf{r}_k^i \\ &+ \delta \mathbf{R}_\ell(\mathbf{q}) \mathbf{N}_\ell(x_\chi, y_\chi, z_\chi) \mathbf{T}_i^\ell(\mathbf{q}) \mathbf{u}_k^i \\ &+ \mathbf{R}_\ell(\mathbf{q}) \mathbf{N}_\ell(x_\chi, y_\chi, z_\chi) \delta \mathbf{T}_i^\ell(\mathbf{q}) \mathbf{u}_k^i \end{aligned} \quad (40)$$

The $\delta \mathbf{R}_\ell$, $\delta \mathbf{T}_i^\ell$ and $\delta \mathbf{r}_k^i$ terms can be expressed as

$$\begin{aligned} \delta \mathbf{R}_\ell &= \sum_j (\partial \mathbf{R}_\ell / \partial q_j) \delta q_j = \mathbf{R}'_\ell \delta \mathbf{q} \neq \mathbf{0}; \\ \delta \mathbf{T}_i^\ell &= \sum_j (\partial \mathbf{T}_i^\ell / \partial q_j) \delta q_j = \mathbf{T}_i^\ell \delta \mathbf{q} \neq \mathbf{0}; \\ \delta \mathbf{r}_k^i &= \sum_j (\partial \mathbf{r}_k^i / \partial q_j) \delta q_j = \mathbf{J}_k^i \delta \mathbf{q} \neq \mathbf{0} \end{aligned} \quad (41)$$

Thus, by substituting the equalities in equation (41) into equation (40),

$$\begin{aligned} \delta \mathbf{p}_\chi &= \mathbf{R}_\ell(\mathbf{q}) \mathbf{N}_\ell(x_\chi, y_\chi, z_\chi) \mathbf{T}_i^\ell(\mathbf{q}) (\mathbf{J}_k^i(\mathbf{q}) \delta \mathbf{q}) \\ &+ (\mathbf{R}'_\ell(\mathbf{q}) \delta \mathbf{q}) \mathbf{N}_\ell(x_\chi, y_\chi, z_\chi) \mathbf{T}_i^\ell(\mathbf{q}) \mathbf{u}_k^i \\ &+ \mathbf{R}_\ell(\mathbf{q}) \mathbf{N}_\ell(x_\chi, y_\chi, z_\chi) (\mathbf{T}_i^\ell(\mathbf{q}) \delta \mathbf{q}) \mathbf{u}_k^i \end{aligned} \quad (42)$$

Now, if the orders of magnitude of the three terms in equation (42) are compared, it can be said that all the terms contain the \mathbf{q} virtual displacement and matrices of the same order of magnitude. The second and third terms contain the \mathbf{u} vector that is small since we are in the small-displacement condition of the Euler–Bernoulli beam theory. Thus, the second and third terms are here neglected as their order of magnitude is lower with respect to the first term. Equation (42) becomes

$$\delta \mathbf{p}_\chi = \mathbf{R}_\ell(\mathbf{q}) \mathbf{N}_\ell(x_\chi, y_\chi, z_\chi) \mathbf{T}_i^\ell(\mathbf{q}) \mathbf{J}_k^i(\mathbf{q}) \delta \mathbf{q} \quad (43)$$

If equations (14), (24) and (43) are considered, the following expression can be obtained

$$\begin{aligned} \sum_k \int_{v_k(\ell)} [\delta \mathbf{q}^T \mathbf{J}_k^{iT} \mathbf{T}_i^{\ell T} \mathbf{N}_\ell^T \mathbf{R}_\ell^T] [\mathbf{R}_\ell \mathbf{N}_\ell \mathbf{T}_i^\ell \ddot{\mathbf{r}}_k^i + \mathbf{R}_\ell \mathbf{N}_\ell \mathbf{T}_i^\ell \ddot{\mathbf{u}}_k^i \\ + 2(\dot{\mathbf{R}}_\ell \mathbf{N}_\ell \mathbf{T}_i^\ell + \mathbf{R}_\ell \mathbf{N}_\ell \dot{\mathbf{T}}_i^\ell) \dot{\mathbf{u}}_k^i + (\ddot{\mathbf{R}}_\ell \mathbf{N}_\ell \mathbf{T}_i^\ell + 2\dot{\mathbf{R}}_\ell \mathbf{N}_\ell \dot{\mathbf{T}}_i^\ell \\ + \mathbf{R}_\ell \mathbf{N}_\ell \ddot{\mathbf{T}}_i^\ell) \mathbf{u}_k^i] \rho_k dv \\ + \sum_k \int_{v_k(\ell)} (\mathbf{u}_k^{iT} \delta \mathbf{T}_i^{\ell T} \mathbf{B}_k^T \mathbf{D}_k \mathbf{B}_k \mathbf{T}_i^\ell \mathbf{u}_k^i) dv \\ = \sum_k \int_{v_k(\ell)} (\delta \mathbf{q}^T \mathbf{J}_k^{iT} \mathbf{T}_i^{\ell T} \mathbf{N}_\ell^T \mathbf{R}_\ell^T) \mathbf{g} \rho_k dv + \delta \mathbf{r}^T \mathbf{f} \end{aligned} \quad (44)$$

The integrals that rise from the inertia virtual work term are the same as those previously computed (equations (26), (29), (30) to (33)). The $\delta \mathbf{T}_i^{\ell T}$ terms in the elastic virtual work term in equation (44) can be transformed into an equivalent form by taking into account equation (41)

$$\begin{aligned} \sum_k \int_{v_k(\ell)} \mathbf{u}_k^{iT} \delta \mathbf{T}_i^{\ell T} \mathbf{B}_k^T \mathbf{D}_k \mathbf{B}_k \mathbf{T}_i^\ell \mathbf{u}_k^i dv \\ = \sum_k \int_{v_k(\ell)} \mathbf{u}_k^{iT} (\delta \mathbf{q}^T \mathbf{T}_i^{\ell T}) \mathbf{B}_k^T \mathbf{D}_k \mathbf{B}_k \mathbf{T}_i^\ell \mathbf{u}_k^i dv \\ = \sum_k \mathbf{u}_k^{iT} \delta \mathbf{q}^T \left(\int_{v_k(\ell)} \mathbf{T}_i^{\ell T} \mathbf{B}_k^T \mathbf{D}_k \mathbf{B}_k \mathbf{T}_i^\ell dv \right) \mathbf{u}_k^i \\ = \sum_k \mathbf{u}_k^T \delta \mathbf{q}^T \mathbf{K}_{1,k} \mathbf{u}_k \end{aligned} \quad (45)$$

Finally, equation (44) can be rearranged into the form

$$\begin{aligned} \delta\mathbf{q}^T \mathbf{J}^T [\mathbf{M}(\ddot{\mathbf{r}} + \ddot{\mathbf{u}}) + 2(\mathbf{M}_{G1} + \mathbf{M}_{G2})\dot{\mathbf{u}} \\ + (\mathbf{M}_{C1} + 2\mathbf{M}_{C2} + \mathbf{M}_{C3})\mathbf{u}] \\ + \sum_k \mathbf{u}_k^T \delta\mathbf{q}^T \mathbf{K}_{1,k} \mathbf{u}_k = \delta\mathbf{q}^T \mathbf{J}^T (\mathbf{f}_g + \mathbf{f}) \end{aligned} \quad (46)$$

3.4. Differential equations of motion

By considering the equilibrium of the elastic forces with respect to all others in equation (38), putting on the right-hand side of the equation all the terms except the one related to the elastic forces and substituting it in equation (46), the latter can be rewritten as

$$\sum_k \mathbf{u}_k^T \delta\mathbf{q}^T \mathbf{K}_{1,k} \mathbf{u}_k - \sum_k \delta\mathbf{q}^T \mathbf{J}_k^T \mathbf{K}_k \mathbf{u}_k = 0 \quad (47)$$

This equation shows that the first term can reasonably be neglected because the small-displacement assumption ensures that $\mathbf{u}^T \delta\mathbf{q}^T \mathbf{K}_{1,k} \mathbf{u}$ is negligible with respect to $\delta\mathbf{q}^T \mathbf{J}_k^T \mathbf{K}_k \mathbf{u}_k$. Indeed, nodal elastic displacements, small since we are in a small-displacement hypothesis, appear twice in the first term and once in the second term.

Now, computing the sums for all the elements of the mechanism, the following system of differential equations, which contains local nodal and global equilibrium equations, is obtained

$$\begin{aligned} \delta\mathbf{u}^T [\mathbf{M}(\ddot{\mathbf{r}} + \ddot{\mathbf{u}}) + 2(\mathbf{M}_{G1} + \mathbf{M}_{G2})\dot{\mathbf{u}} \\ + (\mathbf{M}_{C1} + 2\mathbf{M}_{C2} + \mathbf{M}_{C3})\mathbf{u}] + \delta\mathbf{u}^T \mathbf{K}\mathbf{u} = \delta\mathbf{u}^T (\mathbf{f}_g + \mathbf{f}) \end{aligned} \quad (48)$$

$$\begin{aligned} \delta\mathbf{q}^T \mathbf{J}^T [\mathbf{M}(\ddot{\mathbf{r}} + \ddot{\mathbf{u}}) + 2(\mathbf{M}_{G1} + \mathbf{M}_{G2})\dot{\mathbf{u}} \\ + (\mathbf{M}_{C1} + 2\mathbf{M}_{C2} + \mathbf{M}_{C3})\mathbf{u}] = \delta\mathbf{q}^T \mathbf{J}^T (\mathbf{f}_g + \mathbf{f}) \end{aligned} \quad (49)$$

The infinitesimal displacements of the ERLS can be expressed by means of the Jacobian matrix, as in equation (5), so that the $\delta\mathbf{u}$'s and the $\delta\mathbf{q}$'s can be eliminated from equation (48) and equation (49). Hence, the following system of differential equations is obtained

$$\begin{aligned} \mathbf{M}(\ddot{\mathbf{r}} + \ddot{\mathbf{u}}) + 2(\mathbf{M}_{G1} + \mathbf{M}_{G2})\dot{\mathbf{u}} + (\mathbf{M}_{C1} + 2\mathbf{M}_{C2} + \mathbf{M}_{C3})\mathbf{u} \\ + \mathbf{K}\mathbf{u} = \mathbf{f}_g + \mathbf{f} \end{aligned} \quad (50)$$

$$\begin{aligned} \mathbf{J}^T \mathbf{M}(\ddot{\mathbf{r}} + \ddot{\mathbf{u}}) + 2\mathbf{J}^T (\mathbf{M}_{G1} + \mathbf{M}_{G2})\dot{\mathbf{u}} \\ + \mathbf{J}^T (\mathbf{M}_{C1} + 2\mathbf{M}_{C2} + \mathbf{M}_{C3})\mathbf{u} = \mathbf{J}^T (\mathbf{f}_g + \mathbf{f}) \end{aligned} \quad (51)$$

where, again, equation (50) is a statement of nodal equilibrium, i.e. equivalent loads applied to each node must be in equilibrium, whereas equation (51) is a statement of overall equilibrium, i.e. all equivalent nodal loads applied to the linkage produce no work for a virtual displacement of the ERLS.

This novel method presents a coupled approach for the analysis of a chain of spatial flexible bodies where the secondary inertia terms are neglected if general type finite elements are employed.

In a realistic situation dealing with flexible manipulator systems, damping is usually present. Despite significant research, the characterization of damping in vibrating structures and mechanisms, and a thorough understanding of damping mechanisms, have not been attained. Indeed, the damping mechanisms turn out to be locally nonlinear, the variables upon which damping depends are generally not as clear as for inertia and stiffness. Hence, no existing mathematical model can give an accurate and detailed representation of the damping; therefore, approximate models must be employed. The most common approach is to use a Rayleigh model of damping, thus it is proportional to the stiffness and mass of the system. In this way, it is also possible to take into account the damping in the mechanism joints.

Thus, equations (50) and (51) become

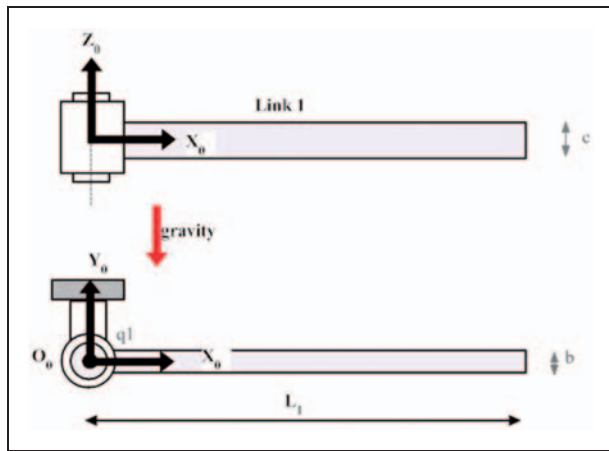
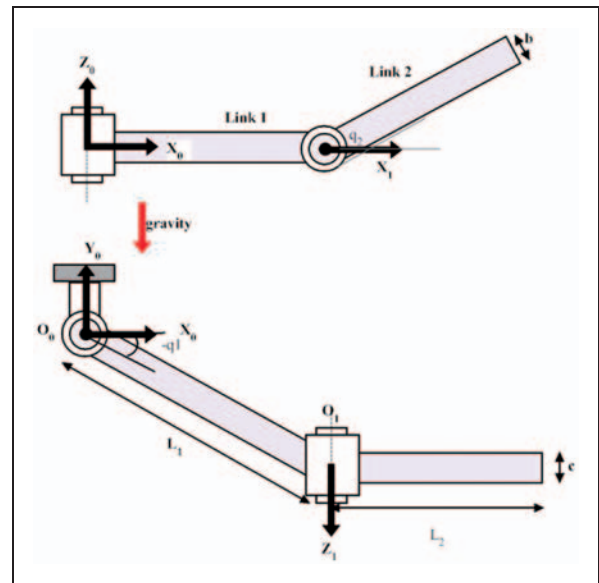
$$\begin{aligned} \mathbf{M}(\ddot{\mathbf{r}} + \ddot{\mathbf{u}}) + 2(\mathbf{M}_{G1} + \mathbf{M}_{G2})\dot{\mathbf{u}} + \alpha\mathbf{M}\dot{\mathbf{u}} + \beta\mathbf{K}\mathbf{u} \\ + (\mathbf{M}_{C1} + 2\mathbf{M}_{C2} + \mathbf{M}_{C3})\mathbf{u} + \mathbf{K}\mathbf{u} = \mathbf{f}_g + \mathbf{f} \end{aligned} \quad (52)$$

$$\begin{aligned} \mathbf{J}^T \mathbf{M}(\ddot{\mathbf{r}} + \ddot{\mathbf{u}}) + 2\mathbf{J}^T (\mathbf{M}_{G1} + \mathbf{M}_{G2})\dot{\mathbf{u}} + \alpha\mathbf{J}^T \mathbf{M}\dot{\mathbf{u}} \\ + \mathbf{J}^T (\mathbf{M}_{C1} + 2\mathbf{M}_{C2} + \mathbf{M}_{C3})\mathbf{u} = \mathbf{J}^T (\mathbf{f}_g + \mathbf{f}) \end{aligned} \quad (53)$$

By means of the second-order differential kinematics equation it is possible to rewrite the ERLS nodes accelerations obtaining

$$\begin{aligned} \mathbf{M}(\ddot{\mathbf{J}\mathbf{q}} + \mathbf{J}\dot{\mathbf{q}} + \ddot{\mathbf{u}}) + 2(\mathbf{M}_{G1} + \mathbf{M}_{G2})\dot{\mathbf{u}} + \alpha\mathbf{M}\dot{\mathbf{u}} + \beta\mathbf{K}\mathbf{u} \\ + (\mathbf{M}_{C1} + 2\mathbf{M}_{C2} + \mathbf{M}_{C3})\mathbf{u} + \mathbf{K}\mathbf{u} = \mathbf{f}_g + \mathbf{f} \end{aligned} \quad (54)$$

$$\begin{aligned} \mathbf{J}^T \mathbf{M}(\ddot{\mathbf{J}\mathbf{q}} + \mathbf{J}\dot{\mathbf{q}} + \ddot{\mathbf{u}}) + 2\mathbf{J}^T (\mathbf{M}_{G1} + \mathbf{M}_{G2})\dot{\mathbf{u}} + \alpha\mathbf{J}^T \mathbf{M}\dot{\mathbf{u}} \\ + \mathbf{J}^T (\mathbf{M}_{C1} + 2\mathbf{M}_{C2} + \mathbf{M}_{C3})\mathbf{u} = \mathbf{J}^T (\mathbf{f}_g + \mathbf{f}) \end{aligned} \quad (55)$$

**Figure 3.** Pendulum.**Figure 4.** Double spatial pendulum.**Table 1.** Mechanical parameters

Link:	Length (m)	Width (m)	Depth (m)	Density ρ (kg/m ³)	Poisson's ratio ν	Young's modulus (N/m ²)
Pendulum	l	0.05	0.0025	7800	0.3	2.1×10^8
Double Pendulum						
1	0.5	0.03	0.01	7800	0.3	2×10^{11} (9×10^9)
2	0.5	0.03	0.01	7800	0.3	2×10^{11} (9×10^9)

Equations 54 and 55 can be grouped together and rearranged in matrix form after discarding the equations for the elastic DOFs that have been zeroed

In this way, the values of the accelerations can be computed at each step by solving the system in (56), while the values of velocities and displacements can be

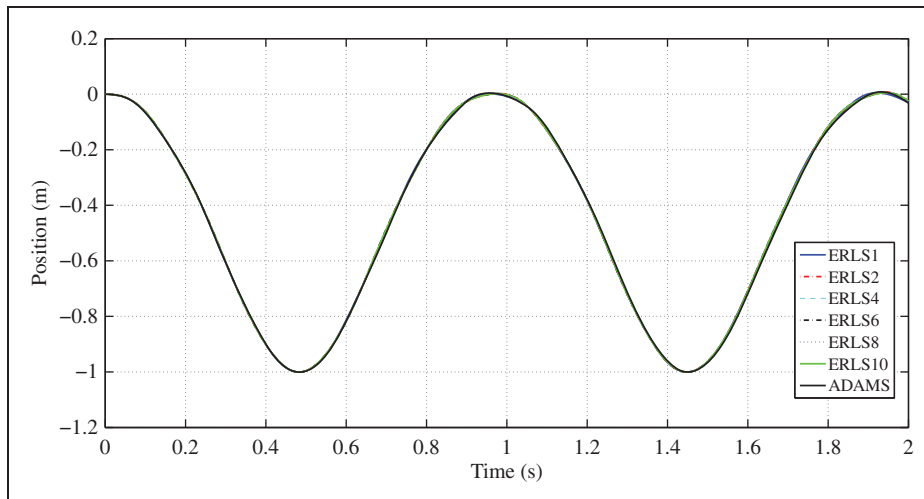
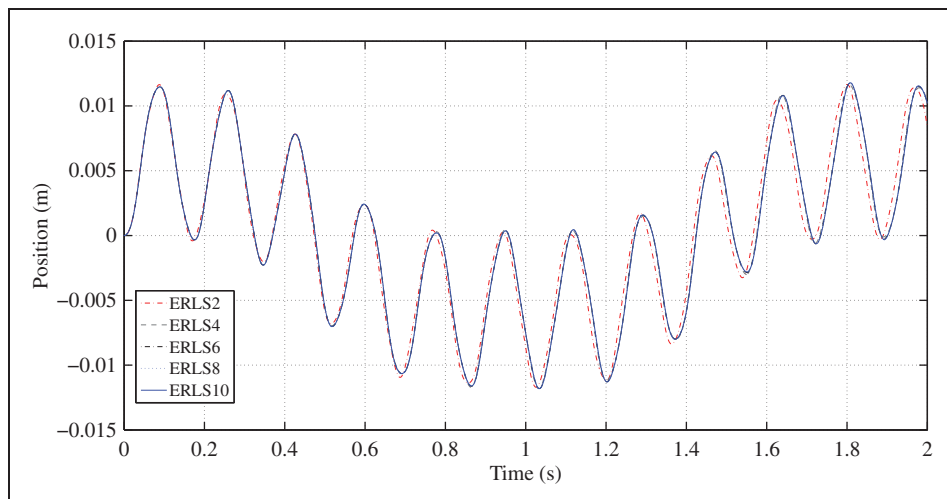
$$\begin{aligned}
 & \begin{bmatrix} \mathbf{M} & \mathbf{MJ} \\ \mathbf{J}^T \mathbf{M} & \mathbf{J}^T \mathbf{MJ} \end{bmatrix} \begin{bmatrix} \ddot{\mathbf{u}} \\ \ddot{\mathbf{q}} \end{bmatrix} \\
 &= \begin{bmatrix} -2(\mathbf{M}_{G1} + \mathbf{M}_{G2}) - \alpha \mathbf{M} - \beta \mathbf{K} & -\mathbf{MJ} & -(\mathbf{M}_{C1} + 2\mathbf{M}_{C2} + \mathbf{M}_{C3}) - \mathbf{K} \\ \mathbf{J}^T(-2(\mathbf{M}_{g1} + \mathbf{M}_{g2}) - \alpha \mathbf{M}) & -\mathbf{J}^T \mathbf{MJ} & -\mathbf{J}^T(\mathbf{M}_{C1} + 2\mathbf{M}_{C2} + \mathbf{M}_{C3}) \end{bmatrix} \begin{bmatrix} \dot{\mathbf{u}} \\ \dot{\mathbf{q}} \\ \mathbf{q} \end{bmatrix} \\
 &+ \begin{bmatrix} \mathbf{M} & \mathbf{I} \\ \mathbf{J}^T \mathbf{M} & \mathbf{J}^T \end{bmatrix} \begin{bmatrix} \mathbf{f}_g \\ \mathbf{f} \end{bmatrix}
 \end{aligned} \tag{56}$$

Table 2. DH parameters

Link:	a_i	α_i	d_i	θ_i
Pendulum	L_1	0	0	q_1
Double pendulum				
1	L_1	$-\pi/2$	0	q_1
2	L_2	0	0	q_2

Table 3. Mid-span deflection of the pendulum with respect to the ERLS at $t = 1.638$ s

Beam elements	Deflection (m)
2	0.09948
4	0.01083
6	0.01078
8	0.01077
10	0.01076

**Figure 5.** Y-coordinate comparison of the pendulum tip.**Figure 6.** Y-coordinate local deformation of the pendulum mid-span with respect to the ERLS.

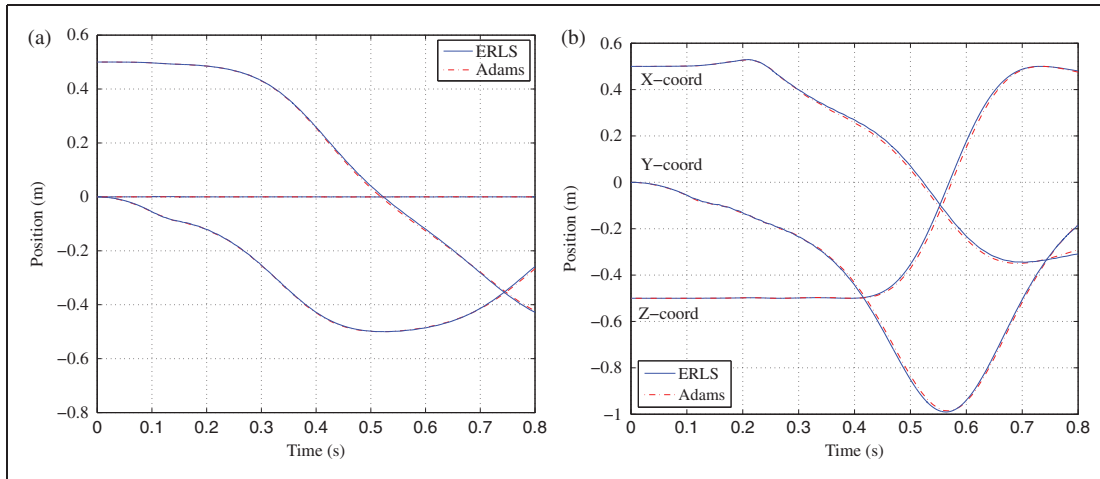


Figure 7. Stiff double spatial pendulum under gravity – two beam elements per link: (a) Tip of the first link and (b) Tip of the second link.

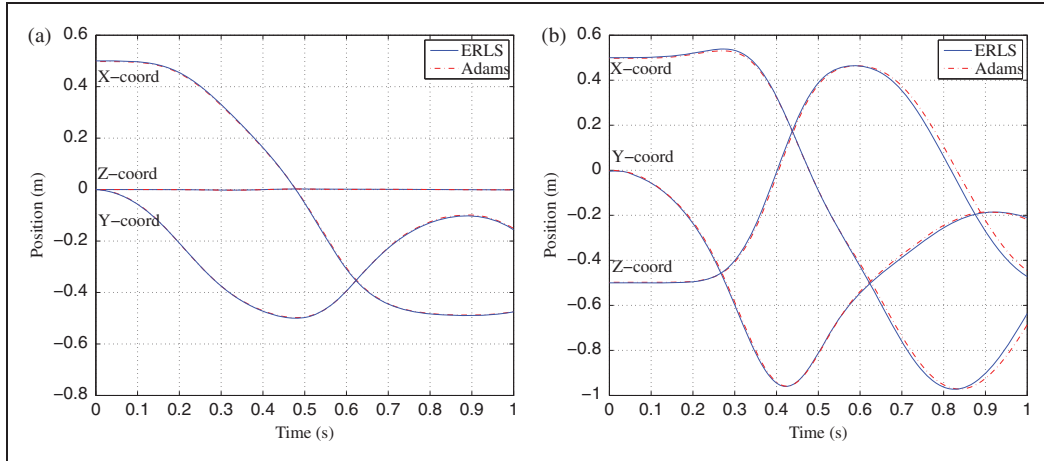


Figure 8. Simulation 2: (a) Tip of the first link and (b) Tip of the second link.

obtained by an appropriate integration scheme (e.g. the Runge–Kutta algorithm).

The coupling between elastic accelerations and accelerations of generalized coordinates of the ERLS is due to the off-diagonal sub-matrices in equation (56) that result from the product of the mass matrix and the Jacobian.

4. Numerical results

The model presented in the previous section is valid for whatever spatial mechanism with any number of free coordinates. In order to give a first proof of the effectiveness of the model, it has been applied on two flexible-link mechanisms and the results compared with Adams-FlexTM.

A MatlabTM software program simulating the dynamic behavior of the flexible-link mechanisms has been built, according to the dynamic model presented above. By running the simulator, the most significant values of the mechanism motion (such as accelerations, velocities, positions and displacements at the nodes) can be obtained and evaluated.

The mechanisms considered for simulation are a 3-D pendulum (as in (Gerstmayr and Schoberl, 2006) and (Dibold et al., 2007)), and a double spatial pendulum, featuring two revolute joints with orthogonal axis of rotation (Figures 3 and 4).

Table 1 contains the main geometrical and mechanical parameters of the flexible-link mechanisms under investigation. Table 2 contains the values of the DH parameters.

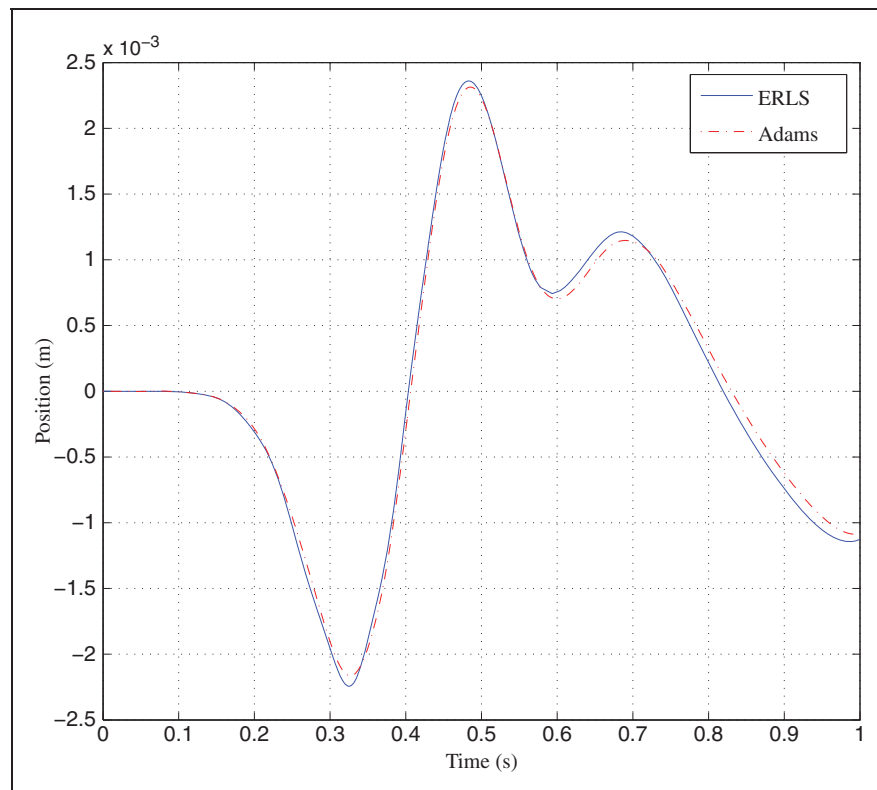


Figure 9. Simulation 2: Z-coordinate of the tip of the first link.

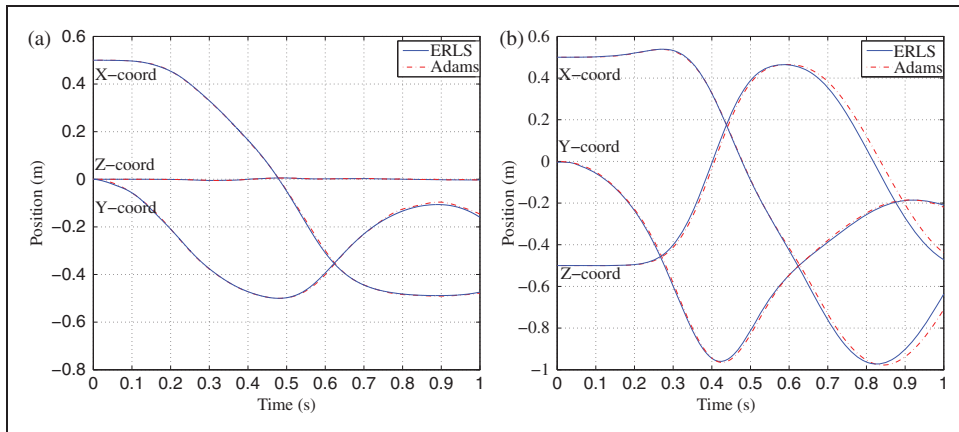


Figure 10. Simulation 3: (a) Tip of the first link and (b) Tip of the second link.

In order to validate the dynamic model presented in this paper, the simulation results were compared with those obtained by means of the Adams-FlexTM software, one of the most popular and widely used multi-body dynamics simulators. Adams-FlexTM uses an assumed mode method of modeling flexible bodies by means of a component mode synthesis technique based on the Craig-Bampton method and an FFR approach (Craig and Bampton, 1968). In this case, the description of a flexible body by means of a modal neutral file in

Adams-FlexTM has been imported from the ANSYS finite-element modeling system where each link has been divided into 128 elements.

4.1. 3-D pendulum

The pendulum can only rotate around its z -axis and, due to the chosen mechanical and geometrical parameters, small deformations but large rotations are taken into account. The pendulum is simulated under gravity

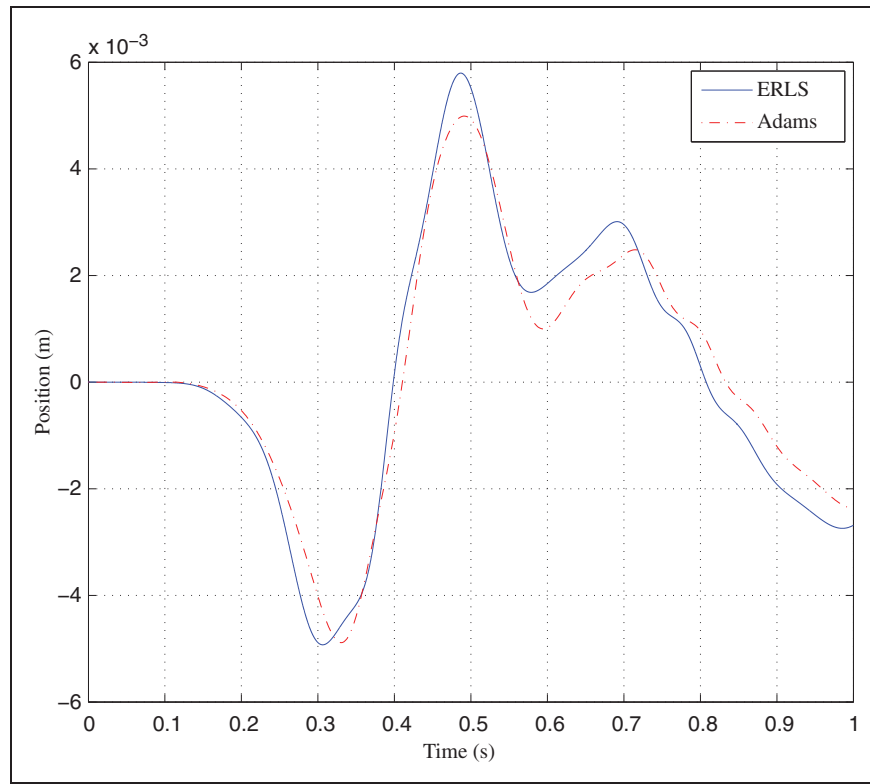


Figure 11. Simulation 3: Z-coordinate of the tip of the first link.

Table 4. Simulation 2: minimum and maximum deformation

	Time min. (s)	Def. min (m)	Time max. (s)	Def. max. (m)
ERLS	0.324	-2.244×10^{-3}	0.482	2.361×10^{-3}
Adams	0.324	-2.162×10^{-3}	0.482	2.309×10^{-3}

($g=9.81 \text{ m/s}^2$) when released from the horizontal position, and different discretizations of the link are taken into account (i.e. 2, 4, 6, 8 and 10 spatial beam elements). Some of the elastic DOFs are fake, e.g. because the translations of the revolute joint connected to the frame are to be zeroed. Moreover, as explained in the previous section, the values of the nodal elastic displacement among the remaining elastic DOFs must be zeroed, so as to be able to correctly define the ERLS. In this case, it was chosen to set to zero the y -translation of the tip of the pendulum. Figure 5 shows a comparison of the Y -coordinate of the tip of the pendulum between the ERLS approach with different mesh refinements and the Adams-Flex™ software. The different plots coincide almost perfectly.

Figure 6 shows a comparison of the mid-span deflection (y -coordinate local deformation) of the pendulum with respect to the chosen ERLS, and in Table 3, the value at a specific time ($t=1.638 \text{ s}$) is compared. The comparison shows the convergence of the solution and

how, also with a small number of beam elements, a good precision can be obtained.

4.2. Double spatial pendulum

In order to show the behavior of the formulation for a spatial problem with joints between two flexible bodies, a spatial double pendulum has been studied.

Two beam elements per link are considered and, thus, the mechanism under investigation has 36 elastic DOFs, given by three translations in the x -, y - and z -directions and three rotations about the x -, y - and z -axes for each of the six nodes, as well as two ‘rigid’ DOFs (the revolute pair angles) of the associated ERLS (represented in Figure 4 as ‘ q_1 ’ and ‘ q_2 ’).

Some of the elastic DOFs are ‘fake’, e.g. because the translations of the revolute joint connected to the frame are to be zeroed, and the constrained elastic DOFs of the nodes lying at the same revolute joint should be set equal. This is due to the fact that two links connected

Table 5. Simulation 3: minimum and maximum deformation

	Time min. (s)	Def. min. (m)	Time max. (s)	Def. max. (m)
ERLS	0.309	-4.921×10^{-3}	0.487	5.796×10^{-3}
Adams	0.330	-4.888×10^{-3}	0.487	4.988×10^{-3}

by a revolute joint have independent z -rotations, while their x -, y -, z -translations and x -, y -rotations about a common frame having the z -axis parallel to the joint rotation axis must be the same.

Moreover, the values of the nodal elastic displacements of two of the remaining elastic DOFs must be zeroed, so as to be able to correctly define the ERLS. In the computed simulations, it was chosen to set to zero the z - and y -translations of extreme points of the links, respectively.

Considering, for instance, two beam elements per link, the following equations must hold

$$\begin{aligned} u_1^{\ell_1}(1) &= u_1^{\ell_1}(2) = u_1^{\ell_1}(3) = u_1^{\ell_1}(4) = u_1^{\ell_1}(4) = 0 \\ u_2^{\ell_2}(7) &= u_2^{\ell_2}(1) \\ u_2^{\ell_2}(8) &= u_2^{\ell_2}(2) \\ u_2^{\ell_2}(9) &= u_2^{\ell_2}(3) \\ u_2^{\ell_2}(10) &= u_2^{\ell_2}(4) \\ u_2^{\ell_2}(11) &= u_2^{\ell_2}(5) \\ u_2^{\ell_2}(9) &= 0 \\ u_4^{\ell_2}(8) &= 0 \end{aligned}$$

where the superscript refers to the common local frame.

The mechanism can then be modeled and simulated according to the dynamic model presented previously.

Several simulations were carried out, and the results were compared and discussed.

4.3. Stiff mechanism subject to gravity

In this simulation, the mechanism is considered stiff due to the high value of Young's modulus of the links: $E=2 \times 10^{11}$ (N/m²).

The initial conditions are $q_1=0$ (rad) and $q_2=\pi/2$ (rad), the Rayleigh damping coefficients are $\alpha=7.00 \times 10^{-2}$ (s⁻¹) and $\beta=2.13 \times 10^{-5}$ (s). A stiff solver has been used for integration.

Figure 7(a) and 7(b) shows the position of the tip of the first and second link of the double spatial pendulum, respectively.

The results based on the dynamic model proposed here are in excellent agreement with those provided by the Adams-FlexTM software: the curves overlap almost

perfectly, thus confirming the effectiveness of the model for rigid-multibody mechanisms.

4.4. Flexible mechanism subject to gravity

In order to evaluate the novel approach for flexible-link mechanisms, the links have been modified in order to introduce flexibility. This has been done by lowering Young's modulus of each link firstly to $E=2 \times 10^{10}$ (N/m²), *simulation 2*, and secondly to $E=9 \times 10^9$ (N/m²), *simulation 3*. The chosen initial conditions are $q_1=0$ (rad) and $q_2=\pi/2$ (rad), the damping coefficients have been zeroed and the solver is a modified Runge-Kutta algorithm.

In Figures 8 and 10, the tips of the two links are depicted for *simulation 2* and *simulation 3*, respectively. In Figures 9 and 11, only the Z -coordinate of the tip of the first link is shown for both cases.

By comparing the results related to the *simulation 2* shown in Figure 8, it can be seen that the curves are in excellent agreement. Figure 9 shows a zoomed representation of the Z -coordinate of the tip of the first link. The mechanism is flexible, indeed the maximum deformation is about 2.5×10^{-3} (m), and both the amplitude and the frequency of oscillations for this coordinate are in excellent agreement between Adams-FlexTM and the simulator described in this paper. Indeed, by evaluating the results in Figure 9, as can be seen in Table 4, the minimum and maximum deflections occur at the same instant, and their difference is of the order of 10^{-4} m or less.

If *simulation 3* is considered, i.e. Figures 10 and 11, it can be seen that the plotted curves are in very good agreement. Figure 11 shows a zoomed representation of the Z -coordinate of the tip of the first link that corresponds to the z -axis nodal elastic displacement. The mechanism is very flexible, indeed the maximum deformation is about 6×10^{-3} (m), and both the amplitude and the frequency of oscillations for this coordinate are in excellent agreement between Adams-FlexTM and the simulator described in this paper. Again, as can be seen in Table 5, where the results of Figure 11 are evaluated, the minimum deflection occurs at slightly different instants while their difference is of the order of 10^{-4} m. It should be remarked that the Z -coordinate is the one that is most affected by gravitational effects, hence its behavior is quite hard

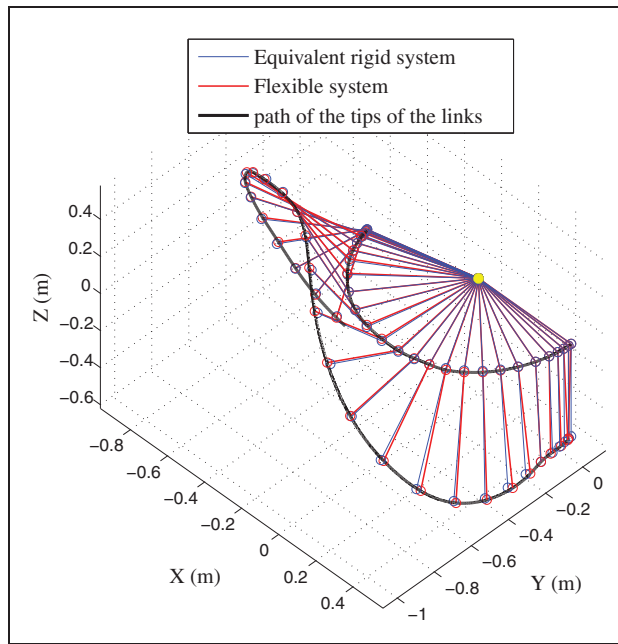


Figure 12. Spatial path followed by the chosen equivalent rigid link and the real mechanism.

to reproduce because the elastic deformations are significant with respect to the rigid motion. In order to show the relation between the chosen ERLS and the real mechanism, in Figure 12 the path covered by both the mechanisms has been plotted. By looking at the overall magnitude of the deformation, it can be pointed out that, if the stiffness of the links is lowered, the discrepancies between ERLS and Adams-FlexTM will increase due to the fact that we are moving away with respect to the beam theory hypothesis.

5. Conclusions

In this work, a novel method for modeling the dynamics of flexible spatial multibody systems is presented. The basic idea is to decompose the overall motion of the mechanism into the rigid motion of a suitably defined ERLS and an overlapped elastic motion. The main concepts of 3-D kinematics, namely DH formulation, first- and second-order differential kinematics, are exploited in order to accurately model the ERLS and the elastic motions. The proposed methodology is general, so the ERLS motion can be computed once the DH frames and parameters, as well as the mechanical properties of the mechanism under investigation, have been set. After the kinematic formulation, the equations of motion for the flexible mechanism can be obtained by direct application of the virtual work principle. In comparison with other flexible-link multibody models (e.g. FFR) where the constraint equations depend on the elastic deformations as well as the

reference motion of the deformable bodies, this novel ERLS-based approach allows us to write and include compatibility equations at the joints involving only the elastic displacements. Moreover, these equations are never used explicitly as they are automatically taken into account when assembling the system matrices. In order to validate the model, a 3-D flexible mechanism has been simulated, and the results have been compared with the Adams-FlexTM multibody dynamic software. The results are in good agreement, thus proving the effectiveness of the dynamic model. Future work will cover experimental validation of the model and improvement of the ERLS formulation for 3-D mechanisms in order to allow the use of component mode synthesis techniques. Moreover, the computational cost of the proposed method will be evaluated and compared with respect to other dynamic models found in the literature.

Funding

This work was supported by the Free University of Bolzano internal research funds project TN5043 Development and validation of dynamic models for high-performance manipulators.

References

- Bauchau O (2011) *Flexible Multibody Dynamics*. New York: Springer.
- Benosman M and Vey G (2004) Control of flexible manipulators: A survey. *Robotica* 22(5): 533–545.

- Boscaroli P, Gasparetto A and Zanotto V (2011) Simultaneous position and vibration control system for flexible link mechanisms. *Meccanica* 46(4): 723–737.
- Boschetti G, Richiedei D and Trevisani A (2011) Delayed reference control for multi-degree-of-freedom elastic systems: Theory and experimentation. *Control Engineering Practice* 19(9): 10441055.
- Boschetti G, Richiedei D and Trevisani A (2012) Delayed reference control applied to flexible link mechanisms: A scheme for effective and stable control. *Journal of Dynamic Systems, Measurement, and Control* 134(1): 011003 (9 pages).
- Caracciolo R, Richiedei D and Trevisani A (2006) Design and experimental validation of piecewise-linear state observers for flexible link mechanisms. *Meccanica* 41: 623–637.
- Caracciolo R, Richiedei D and Trevisani A (2008) Experimental validation of a model-based robust controller for multi-body mechanisms with flexible links. *Multibody System Dynamics* 41(2): 129–145.
- Chang L and Hamilton J (1991) The kinematics of robotic manipulators with flexible links using an equivalent rigid link system (ERLS) model. *ASME Journal of Dynamic Systems, Measurement and Control* 113: 48–53.
- Craig R and Bampton M (1968) Coupling of substructures for dynamics analyses. *AIAA Journal* 6(7): 1313–1319.
- Denavit J and Hartenberg R (1955) A kinematic notation for lower-pair mechanisms based on matrices. *ASME Journal of Applied Mechanics* 23: 215–221.
- Dibold M, Gerstmayr J and Irschik H (2007) On the accuracy and computational costs of the absolute nodal coordinate and the floating frame of reference formulation in deformable multibody systems. In: *Proceedings of the ASME 2007 IDETC/CIE 2007*, Las Vegas, Nevada, USA.
- Dwivedy S and Eberhard P (2006) Dynamic analysis of flexible manipulators, a literature review. *Mechanism and Machine Theory* 41: 749–777.
- Garca-Vallejo D, Mayo J, Escalona J, et al (2008) Three-dimensional formulation of rigid-flexible multibody systems with flexible beam elements. *Multibody Systems Dynamics* 20: 1–28.
- Gasparetto A (2001) Accurate modelling of a flexible-link planar mechanism by means of a linearized model in the state-space form for design of a vibration controller. *Journal of Sound and Vibration* 240(2): 241–262.
- Gasparetto A, Lanzutti A, Vidoni R, et al (2012) Experimental validation and comparative analysis of optimal time-jerk algorithms for trajectory planning. *Robotics and Computer-Integrated Manufacturing* 28: 164–181.
- Ge S, Lee T and Zhu G (1997) Nonlinear feedback controller for a single-link flexible manipulator based on finite element model. *Journal of Robotic Systems* 14(3): 165–178.
- Gerstmayr J and Schoberl J (2006) A 3D finite element method for flexible multibody systems. *Multibody System Dynamics* 15(4): 305–320.
- Giovagnoni M (1994) A numerical and experimental analysis of a chain of flexible bodies. *ASME Journal of Dynamic Systems, Measurement and Control* 116: 73–80.
- Martins J, Mohamed Z, Tokhi M, et al (2003) Approaches for dynamic modelling of flexible manipulator systems. In: *Proceedings of the IEEE Conference on Control Theory Applications*, Vol. 150.
- Nagarajan S and Turcic D (1990) Lagrangian formulation of the equations of motion for elastic mechanisms with mutual dependence between rigid body and elastic motions. Part I: Element level equations. *ASME Journal of Dynamic Systems, Measurements, and Control* 112: 203–214.
- Schwab A and Meijaard J (2005) Comparison of the three-dimensional flexible beam elements for dynamic analysis: finite element method and absolute nodal coordinate formulation. In: *Proceedings of the ASME IDETC/CIE 2005*, California (USA).
- Shabana A (1997) Flexible multibody dynamics: Review of past and recent developments. *Multibody System Dynamics* 1: 189–222.
- Shabana A (2005) *Dynamics of Multibody Systems*, 3rd edn. Cambridge: Cambridge University Press.
- Sugiyama H, Gerstmayr J and Shabana A (2006) Deformation modes in the finite element absolute nodal coordinate formulation. *Journal of Sound and Vibration* 298: 1129–1149.
- Theodore R and Ghosal A (1995) Comparison of the assumed modes method and finite element models for flexible multilink manipulators. *International Journal of Robotics Research* 14(2): 91–111.
- Tokhi M and Azad A (2008) *Flexible Robot Manipulators: Modeling, Simulation and Control*. Control Engineering Series, The Institution of Engineering and Technology (IET).
- Turcic D and Midha A (1984a) Dynamic analysis of elastic mechanism systems. Part I: Applications. *ASME Journal of Dynamic Systems, Measurement and Control* 106: 249–254.
- Turcic D and Midha A (1984b) Generalized equations of motion for the dynamic analysis of elastic mechanism systems. *ASME Journal of Dynamic Systems, Measurement and Control* 106: 242–248.
- Turcic D, Midha A and Bosnik J (1984) Dynamic analysis of elastic mechanism systems. Part II: Experiment results. *ASME Journal of Dynamic Systems, Measurement and Control* 106: 255–260.
- Wang D, Lu Y, Liu Y and Li X (1996) Dynamic model and tip trajectory tracking control for a two-link flexible robotic manipulator. In: *Proceedings of the IEEE Conference on System, Man and Cybernetics*, Beijing, pp. 1020–1024.
- Wasfy T and Noor A (2003) Computational strategies for flexible multibody systems. *ASME Applied Mechanics Reviews* 56(6): 553–613.
- Zanotto V, Gasparetto A, Lanzutti A, et al (2011) Experimental validation of minimum time-jerk algorithms for industrial robots. *Journal of Intelligent and Robotics Systems* 64(2): 197–219.